ABSTRACT

Title of Document: THIN-FILM PHOTOVOLTAICS UNDER EXTREME WIND LOADING DUE TO DOWNBURSTS IN THE WASHINGTON D.C. AREA

**Kristen Sara Markham, M.S., 2010**

Directed By: Associate Professor, Yunfeng Zhang, Department of Civil and Environmental Engineering

Extreme wind loading on buildings can be caused by a variety of different weather phenomenon, including straight-line wind-inducing events known as downbursts. With maximum wind gusts up to 168 mph, downbursts have the potential to cause significant damage to modern infrastructure, comparable to that of the more commonly-known tornado or hurricane. Among the many variables that affect the extent of damage to infrastructure from such events, the performance of a building is largely dependent on two factors – (a) the magnitude of the loads induced on a building, and (b) the strength of the building components resisting these loads. The goal of this research is to characterize the downburst-induced horizontal wind loads on a building façade of a given region, as well as the strength and behavior of a green building material used in the façade of buildings – known as thin-film building integrated photovoltaics (BIPVs). With downburst data collected from the Washington D.C.-Baltimore metropolitan area (WBMA), a failure probability model is derived for BIPVs specific to this region.

# THIN-FILM PHOTOVOLTAIC PANELS UNDER EXTREME WIND LOADING DUE TO DOWNBURSTS IN THE WASHINGTON D.C. AREA

By

Kristen Sara Markham

Thesis submitted to the Faculty of the Graduate School of the
University of Maryland, College Park, in partial fulfillment
of the requirements for the degree of
Masters of Science
2010

Advisory Committee:
Associate Professor Yunfeng Zhang, Chair
Professor Bilal Ayyub
Senior Research Professor Ed Link

# ACKNOWLEDGEMENTS

I would like to first gratefully acknowledge Dr. Yunfeng Zhang, my advisor, for his guidance, support, advice and extensive patience during my graduate career at the University of Maryland. I thank him for showing me and helping me learn how to conduct research, write technical papers, give presentations, and for the opportunities he provided to me while working together. I would also like to thank Dr. Deborah Goodings, Alan Santos, and Dr. Dimitrios Goulias for encouraging me to attend graduate school, and making me realize the importance of an engineering graduate degree. Without your encouragement, I would not be where I am today.

I also thank Dr. Dimitrious Goulias for allowing me the opportunity to do what I love, teach and work with students, while completing my masters degree. I thank Maggie Sharkey and Ehsan Aramoon, my fellow TAs, for their help and support, and for working with me over the years. To the organization Engineers Without Borders, I thank you for giving my engineering career meaning and motivation for the past nearly 6 years, and for the opportunity to lead the organization as it grows and expands. Both teaching and EWB have been instrumental in shaping my engineering career. I thank Dr. William Fourney and Kevin Calabro for encouraging me to do what makes me happy.

I also deeply appreciate Dr. Bilal Ayyub and Dr. Ed Link for serving on the examination committee at the defense of my thesis. My appreciation also extends to the Civil Engineering department administration staff; without their support, none of this would have been possible.

My love and appreciation extends to my wonderful family – my mom, dad and sister who have provided motivation, support and encouragement when I needed it most. Also I would like to express my thanks to my wonderful friends, roommates, and boyfriend for their moral support, understanding, and encouragement.

# TABLE OF CONTENTS

# LIST OF TABLES

# LIST OF FIGURES

# EXECUTIVE SUMMARY

Extreme wind loading on buildings can be caused by a variety of different weather phenomenon, including straight-line wind inducing events known as downbursts. With maximum wind gusts up to 168 mph, downbursts have the potential to cause significant damage to modern infrastructure, comparable to that of the more commonly-known tornado or hurricane. Among the many variables that affect the extent of damage to infrastructure from such events, the performance of a building is largely dependent on two factors – (a) the magnitude of the loads induced on a building, and (b) the strength of the building components resisting these loads.

The first goal of this research is to define a region-specific probabilistic load model of downburst winds for Washington D.C.-Baltimore metropolitan area (WBMA). Currently the occurrence of downbursts is not systematically documented in the United States due to relatively short history of data recording and lack of a sufficiently dense sensor network, making it difficult to characterize their behavior to account for them in design wind loads of buildings. The model presented, based on data collected from several sources and a modified downburst wind load model developed by others, represents the first effort in quantifying the design wind speed for downbursts in the WBMA region.

The second goal of this research is to characterize the behavior of building integrated photovoltic (BIPV) panels used in building façades when subjected to wind loading. Infrastructure today continues to progress towards more “green” construction techniques, promoting the use of energy-saving materials that are integrated into the many systems that make up a functioning building. One method that has quickly gained attention in recent years is that of BIPVs, in which glass-protected thin-film photovoltaic panels are used in the façade and roof of buildings. These

panels simultaneously act as both a generator of clean energy from the sun's light, as well as the protective building envelope of the structure. A variety of dimensions, thicknesses of glass, and layering techniques are used by manufacturers of BIPVs, thus a survey of manufacturers' data of thin-film BIPV models was first conducted to determine the range of properties of these panels on the market today. Then, by assuming that the thin-film layer of the BIPV panels can be neglected due to its negligible thickness, high stiffness and material strength associated with metal oxides, the BIPV panels behavior are modeled using a failure model for similarly constructed laminated glass under uniform loading.

Ultimately the design wind loads determined from the probabilistic downbursts wind model are compared with the probabilistic strength distribution of the BIPVs used in building facades. Based on these, a failure probability model is derived for BIPVs specific to the Washington D.C.-Baltimore metropolitan region.

New building designs that integrate more costly green technologies should be sustainable and resource-efficient, but also still be safe and reliable. Currently the United States lacks a set of standard performance criteria which BIPV panels must pass in order to be widely accepted for use in modern infrastructure. Understanding the general behavior and reliability of BIPVs under extreme wind loading using this model can help provide guidance as these standards are being developed.

# CHAPTER 1: INTRODUCTION AND MOTIVATION

Today, buildings in the United States (U.S.) account for approximately 39% of total energy use and 72% of electricity use according to the U.S. Department of Energy (EPA 2009). As energy demands in the U.S. continue to remain high, a growing need for more environmentally-responsible, "green" design and construction is increasingly apparent. These new building designs should be safe and reliable, and also sustainable and resource-efficient. In 2007, 26 states had passed some form of green building legislation, most mandating high-efficiency standards for government buildings and encouraging the private building sector through tax incentives (King and King 2004; Nitkin 2007). The State of California became the first state to adopt a mandatory, state-wide green building code in January of 2010.

One of the emerging methods of decreasing energy consumption is through the use of a more energy-efficient building envelope, the outer structure of a building, including the facade, windows and doors, and roof (Chuwieduk 2003; Arnold 2009). In recent years a new class of renewable energy technologies known as BIPVs (Building Integrated Photovoltaics) have been developed which function simultaneously as the building envelope and as photovoltaic (PV) power generators (Dougherty et al. 2005) (Figure 1.1). For tall buildings in particular with large surface areas exposed to sunlight, the potential amount of energy generated from the use of this technology in building facades is significant. As an example, one of the largest façade BIPV applications is in Ulm, Germany stands 355 ft (102 m) tall and produces 70 megawatt hours each year.

Today many different BIPV technologies are available on the market. While mono and polycrystalline silicon (c-Si) PV technologies currently hold 80-90% of the total market share of building-installed PVs in the U.S., thin-film PVs (TFPVs) have several distinct advantages over

c-Si PVs, and are favored over c-Si for future BIPV applications. For PVs of similar efficiency – approximately a 100 times thinner layer of PV material is needed for TFPV than for c-Si panels. Today, a growing number of companies produce TFPV units designed to replace more common glass façade panels and have integrated them into the design of buildings throughout the world. While in Germany, the world's largest solar market, BIPV only represents 2% of all installed PV products (Runyon 2010), these multi-functional panels, if reliable, can be an integral part of the increasing number of environmentally-friendly buildings for a less energy-dependent future. A recently published study by GTM Research found that products based on the concept of BIPVs are beginning to emerge in the marketplace after more than 20 years of research and development (GTM 2010). While markets in Europe are larger and more well-established, the U.S. market is developing quickly (GTM 2010).

A failure state that threatens the reliability of TFPVs used in building façades is the structural failure of the glass elements due to excess loading or stress concentrations. Extreme wind events such as downbursts, tornados or hurricanes can cause high winds that can damage these façade elements rendering them unusable (Figure 1.2). The focus of this research is centered on TFPVs in building facades when subjected to extreme wind loading, specifically concentrating on the Washington D.C.- Baltimore Metropolitan area (WBMA). Determining the behavior of this system requires two parts. First, the determination of the design wind pressure subjected on the thin-film BIPV, and second, a resistance probability distribution of the TFPV panel. Where the TFPVs fail is where the tail of the strength distribution is less than the design wind pressure.

To determine the design wind pressure on the façade of a building, a case of extreme weather know as downbursts is considered. Downbursts cause strong lateral winds for a short period of time in a concentrated area on the surface of the earth. Historically these extreme weather events

have been known to cause severe damage to building facades despite current building code requirements because of their high-intensity winds. Downburst events have been recorded in all regions of the United States, yet their characteristics, intensity and occurrence rates are not systematically recorded today (as compared to tornados or hurricanes), and vary substantially by location. When determining wind loads, the American Society of Civil Engineering (ASCE) 7-05 wind load specifications (2005) indicate different design wind speeds depending on the location of construction. To limit the scope of this research to an area of relatively uniform wind loading conditions, specifically the Washington D.C.-Baltimore Metropolitan area (WBMA) of the United States was chosen to study. The data collected on downbursts in this region is used to develop a wind load distribution curve, which is used in a stochastic model to determine the design wind speeds. These wind speeds are converted to design wind pressures using the procedure in ASCE 7-05.

To determine the probabilistic distribution curve of the TFPVs' strength, an understanding of the components and their behavior under loading is required. A TFPV panel is considered to have failed when the glass has fractured. A review of all TFPV technologies available on the market was conducted first to determine the most common materials used and method of construction. Similar in structure and construction to laminated glass, a failure model of laminated glass under uniform loading is used to construct the resistance distribution curve of TFPVs in BIPV applications. By calculating the area where the resistance distribution is less than the design wind pressure, the reliability of this system is determined from the corresponding failure probability.

This thesis is organized into six chapters. Chapter 1 provides the motivation for this research and overview of the work done in this study. Chapter 2 offers a general discussion of the weather phenomenon of a downburst as well as the different methodologies used in previous studies to

categorize and characterize these high-wind producing storms. The data available in the WBMA on the occurrence of downbursts and the methodology followed in this research to establish this dataset are also discussed. Chapter 3 provides details on the conversion process for the downburst data into a distribution curve, and a stochastic model used to determine the design wind speed and wind pressure. The second part of this thesis focuses on BIPVs. Chapter 4 discusses a brief history on PVs, the different types of TFPVs and their layers, and introduces BIPVs and façade applications. The modeling of TFPVs behavior from a laminated glass model is discussed as well as the creation of a distribution curve of resistance. Chapter 5 compares the design wind pressures determined for downbursts in the WBMA and the façade-installed TFPVs resistance. Current building design specifications are discussed. Chapter 6 summarizes the major finding from this research as well as provides a discussion of future work.

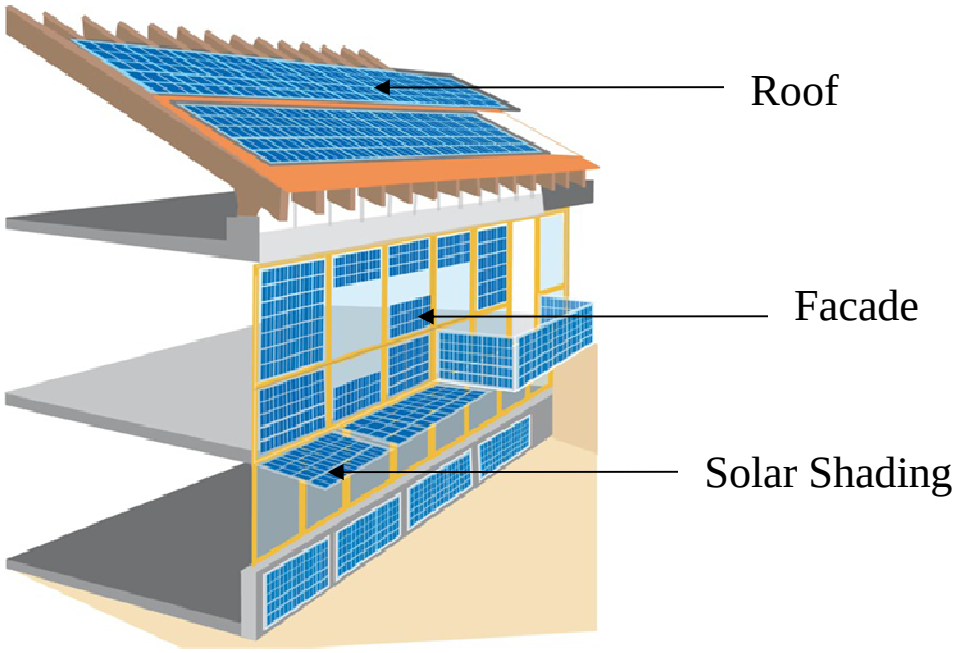


**Figure 1.1: BIPV Applications on a Typical Building (adapted from Shaybani, 2010)**

**Figure 1.2: Façade Failure Due to Hurricane Alicia in 1983, Houston, TX (USACE 2010)**

# CHAPTER 2: DOWNBURSTS

Extreme wind loading on buildings can be caused by a variety of different weather phenomenon. Since 1950 two of these well-know causes of damages, hurricanes and tornados, have been reported to the National Weather Service (NWS) approximately 4 to 5 times per year in Maryland (MD) and 11 times per year in Virginia (VA) (NCDC 2010). In the coastal regions of MD and VA, hurricane events are frequent enough to merit higher design wind speeds in the wind load design charts of ASCE-7-05 design load standards in the United States (ASCE 2005). In this area, as well as throughout the U.S., a less-known yet equally damaging weather phenomenon known as a downburst (wind speed up to 168 mph (75 m/s) ), is estimated to occur approximately ten times as frequently as tornados according to the National Weather Service (NWS 2010). This extreme weather event, however, is not considered in the ASCE-7-05 design standards. Current lack of reliable information on the occurrence of downbursts would make this difficult to do so.

A downburst is created by a column of sinking air that, after hitting the earth's surface, spreads out in all directions, producing damaging straight-line winds, similar, but distinguishable from that of tornados. The reason, in part, why this phenomenon is not well-known or documented today is that their relatively small size (less than 10 km across) and short duration (lasting only 2 to 20 minutes) make them difficult to reliably detect and track. Downburst can occur anywhere, and the Washington D.C.-Baltimore Metropolitan area (WBMA) (northern VA, MD, and Washington D.C.), similar to other metropolitan areas in the U.S., has experienced downburst wind gusts of 130 mph (58 m/s) (Fujita 1985). Maximum horizontal winds of a downburst can be 168 mph (76 m/s), winds comparable to that of a Category 5 hurricane or an F3 tornado.

Downbursts, while originally studied because of the significant threat they pose to airborne planes during take-off and landing, can also be a threat to structures. In May of 2009 the Dallas Cowboys Football practice facility collapsed due to a downburst, injuring 12 people (Gross et al. 2010). With a roughly estimated occurrence rate higher than hurricanes and tornados and with winds comparable to other extreme wind events, it is reasonable to justify this weather phenomenon as one that merits further study, particularly for buildings with façade elements susceptible to breakage from high wind loading.

In the WBMA, in order to determine the reliability of Building Integrated Photovoltaics (BIPVs) and more specifically thin-film photovoltaic (TFPV) panels installed in building façades, the wind loading distribution curve of downburst winds must first be established for the WBMA. To determine this distribution this chapter discusses how a downburst is defined and what features characterize this extreme-wind causing event. In addition, the methodologies previous studies have followed to determine downburst wind speeds for a particular region and the methodologies used in this research are discussed.

## 2.1 DEFINITION AND ORIGIN OF DOWNBURST CONCEPT

Downbursts are a weather phenomenon first discovered by Fujita in 1976-1977 after a detailed study of two severe-weather related airplane crashes in the U.S. (Fujita 1976; Fujita and Byers 1977). Downbursts can be defined as strong, concentrated downdrafts from convective storms (i.e. thunderstorms) that can cause damaging divergent winds on or near the ground surface of the earth. The “jet-like” downdraft that caused two plane crashes in 1975 was first identified in 1976 and soon after Fujita (1976) and Fujita and Byers (1977) proposed using the term “downburst” for this extreme weather event.

To further study downbursts, the Northern Illinois Meteorological Research on Downbursts (NIMROD) field program was established in 1978, which used Doppler radars to successfully identify downbursts, verifying their existence. Since then an increasing focus on observational and theoretical studies of downbursts has been pursued.

## 2.2 DOWNBURST FORMATION

During a thunderstorm, differences in temperature on the surface of the earth create instability in the air, sometimes driving warm, moist air to higher elevations in the atmosphere. This warm, dry air rises from the earth's surface and enters the thunderstorm causing rain to evaporate, cooling the dry air rapidly. The cooled air then becomes too heavy to be supported mid-air and subsequently falls back towards the Earth's surface, creating a downdraft. As the air falls it accelerated downwards and finally hits the earth's surface to create the phenomenon of a downburst (Yuh-Lang 2007).

At touchdown, the downburst is characterized by a shaft of strong downward velocity at its center and strong divergence upon impact. Once the air downdraft has hit the ground, it flows outward from the center of the downburst in the form of straight-line horizontal winds. Figure 2.1 is a conceptual drawing of how this process occurs (Fujita 1985).

## 2.3 MICROBURSTS AND MACROBURSTS

Wakimoto (1985) further divided downbursts into two categories based primarily on size – macrobursts and microbursts. Macrobursts are defined as downbursts with diameters of more than 2.5 miles (4 km), duration of 5-20 minutes, and wind speeds up to F3 intensity, or 134 mph (60 m/s). Microbursts are smaller downbursts of less than 2.5 miles (4 km) in diameter, 2-5 minutes in duration, with winds as high as 168 mph (75 m/s). A Chicago study yielded

microburst durations of 3.4 minutes on average, and a second study in Denver (1982) found average microburst lasted 2.8 min (Fujita 1985).

Due to the nature of the dataset used in this study, reported downburst events could not be confidently classified as “microbursts” or “macrobursts” in many cases, thus the general term “downbursts” is used instead. Both microbursts and macrobursts are capable of producing extreme winds, and the greatest importance of the downbursts in this research is the wind speed produced as a result of these events.

## 2.4 WET AND DRY DOWNBURSTS

**Results of an extensive project named JAWS (Joint Airport Weather Studies) completed in 1982 revealed that there are not just one, but two main conditions in which downbursts can occur. Some downbursts are accompanied by heavy rains from thunderstorms, while others are caused by virga shafts - observable streaks or shafts of precipitation that fall from a cloud but evaporate before reaching the ground (Brown et al. 1982). This observation further divided downbursts into “wet” and “dry” categories, which others confirmed in years following (Wolfsen 1983; Caracena et al. 1983; Wilson et al. 1984; Fujita 1985; Caracena and Flueck 1988). A summary of the characteristics of wet and dry downbursts and corresponding diagrams can be found in Table** 2.1 **and** Figure 2.3.

Wet downbursts occur in conditions of simultaneous heavy rains and high winds, relying on the downward acceleration of the precipitation to form (Fujita 1983, Doswell 1994). Much less is known, however, about how wet downbursts originate compared to dry downbursts, and thus they are correspondingly more difficult to forecast (Doswell 1994). They can be easily identified by doppler radar reflectivity data, however, because they have a high reflectivity compared to other parts of convective storms (Wilson et al. 1984). The formation of a bow echo, a specific

bow-like shaped storm cell as shown in Figure 2.2 has been associated with the occurrence of downbursts (Fujita 1978).

Dry downbursts can also occur in the presence of rain, however little or no rain is most common. They are created by evaporation in relatively dry conditions which produces a downward force, named negative buoyancy, that propels the air downward (Doswell 1994). They can be identified by a virga, or shaft of precipitation that falls from a cloud then evaporates before reaching the ground. For further information readers are referred to Wakimoto (1985).

Little published information is available on the type of downburst that are most characteristic in the WBMA, however an unpublished study by Pryor (2009) suggests that wet downbursts are more common than dry downbursts in this region. Atkins and Wakimoto (1991) suggest that wet downbursts are most characteristic of the southeastern U.S.

It should be noted that because of the different characteristics of downbursts depending on the region of study, a discussion on the frequency of occurrence of downbursts in a large area (e.g. the Unites States) is too large an area of study. The WBMA was chosen for two reasons. First, there has been relatively little research on downburst occurrences in this area of the U.S., thus studying this region can lead to a better characterization of the threat of downbursts in this region. Second, downburst horizontal straight-line winds produce high-velocity gusts between approximately 33-164 ft (10-50 m), similar to the height of high-rise buildings characteristic of city centers (Holmes 2002; Kim and Hangan 2007). It is the medium to high rise buildings where Building Integrated Photovoltaics (BIPV) in facades are most commonly installed. The WBMA contains two major city centers with medium to high rise buildings, one of which is the U.S. national's capitol.

**Table 2.1: Dry and Wet Downburst Characteristics (adapted from Rose 2010)**

| Characteristics | Dry Downburst | Wet Downburst |
|---|---|---|
| ***Location of Highest Probability (within the U.S.)*** | Dry Climates (Midwest/West) | Moist or temperate climates (Southeast) |
| ***Precipitation*** | Little/None | Moderate/Heavy |
| ***Features Below Cloud Base*** | Virga | Shafts of strong precipitation reaching the ground |

## 2.5 WASHINGTON D.C.-BALTIMORE METROPOLITAN AREA (WBMA) DOWNBURSTS

The varying features of a climate of a particular region can cause it to be more or less conducive to downburst occurrences of different types. Downbursts in the eastern U.S. are most likely wet downbursts, which originate within convective storms (thunderstorms). In a recent unpublished analysis of the downburst occurrences in the eastern part of the U.S., among the areas of the most frequent occurrences was the WBMA (Pryor 2009). The low-level northward flow of warm air and moisture from the Atlantic Ocean creates pressure instability, then storm fronts combined with the orographic lift (raising the elevation of air mass) caused by the Appalachian Mountains produce good conditions for convective thunderstorms, and thus downbursts.

Further published evidence of downbursts in the WBMA is supported by Fujita (1985). Fujita studied a microburst event at Andrews Airforce Base near Washington D.C. that occurred on August 1, 1983. The peak wind speeds caused by the downdraft were clocked at approximately 158 mph (70 m/s), one of the highest speeds recorded in downburst history. A graph of wind speed vs. time of this downburst is shown in Figure 2.4.

### 2.5.1 WBMA Data Coverage Limits

The WBMA in this research is defined by the coverage area of the National Weather Service (NWS) Forecast Office for the Baltimore/Washington area. This area includes most of Maryland, District of Columbia, Northern Virginia, parts of Eastern West Virginia. Figure 2.5 shows the coverage area of the main doppler radar for this region and Figure 2.6 shows all the counties

within the coverage area. This figure also includes the number of Skywarn[1] participants, or trained citizens who report weather conditions such as downbursts, convective storms, tornados, etc. to the NWS. The areas of green are the counties which have the most densely populated areas of Skywarn-trained citizens, which also correspond to the cities of Washington D.C. and Baltimore. Doswell (2005) points out severe storm event (such as a downburst) reporting quality and methodologies can be inconsistent among different NWS offices, thus in an effort to obtain consistent data, only one NWS office was chosen.

### 2.5.2 The Convective Season of the WBMA

Downbursts in the WBMA occur with convective storms. In this area, and throughout the United States, convective storms are more frequent in the warm summer months than in the colder months of the year (Kelly et al. 1985). In this research, data on the occurrence of downbursts is thus restricted to May-August. According to Kelly et al. (1985) these four months account for 69% of damaging wind storms, 74% of strong wind gusts, and 76% of violent windstorms for weather throughout the U.S.

## 2.6 METHODOLOGY OF DOWNBURST DATA COLLECTION AND ANALYSIS

Unlike other extreme-wind weather events such as tornados or hurricanes, no comprehensive database of occurrences currently exists that officially tracks downbursts, where they occur, their strength, wind speed, and other pertinent details. Thus in order to best predict the probability of occurrence of a downburst in the WBMA, a review of previous studies and research was

[1] Skywarn website - http://www.weather.gov/skywarn/

conducted to assess methods of obtaining data for this research. The chosen methodology is a reflection of the culmination of the knowledge obtained from these studies as it is relevant to this research.

### 2.6.1 A Review of Downburst Studies Conducted in the United States

The methodologies of studying downburst occurrences throughout the United States can be divided into three categories: (1) long-term, sensor network studies, (2) retroactive surface data studies, and (3) computer modeling based studies. Of each of these methodologies used to study downbursts, the second methodology, retroactive surface data collection, is most relevant for the datasets available for the WBMA of the United States.

#### 2.6.1.1 Long-term, Sensor Network Studies

One methodology used to study downburst behavior and count occurrences can be classified as a long-term sensor network study. These types of studies, while they have been conducted in a variety of environments studying different types of downbursts, follow the same general methodology of obtaining microburst data on wind speeds, size and counts. This methodology requires an extended period of time in which to actively observe the occurrence of downbursts in a finite area. In these studies a network of sensors and data recorders such as a Portable Automated Mesonet (PAM) is first set up, then the downbursts are identified using the wind speed and direction data collected. A PAM consists of a base station connected to a network of remote sampling stations. The base station logs all data (wind speed, wind direction, pressure, humidity, etc…) obtained from each of the stations (Brock 1977).

From these studies using a high-density network of sensors much has been learned about the characteristics and behaviors of downbursts. Compared to relying on already existing, more sporadically placed sensors of varying quality, or relying on trained citizen observers to report

such events, the generated data from this type of network is much more consistent. Understandably, however this methodology also requires a significant amount of resources, time and funding to complete. Several detailed studies throughout the United States of this type have been conducted in effort to better characterize downburst behaviors. These include the following:

- Northern Illinois Meteorological Research on Downburst (NIMROD) (1978)
- Joint Airport Weather Studies (JAWS) (1982)
- Classify, Locate and Avoid Wind Shear (CLAWS) (1984)
- FAA/Lincoln Laboratory Operational Weather Studies (FLOWS) (1984-85)
- Microburst and Severe Thunderstorm (MIST) (1986)
- Convection Initiation and Downburst Experiment (CINDE) (1988)
- Thunderstorm Outflow Project (2002)

Information and conclusions from these studies can be found in more detail in other papers (e.g. McCarthy et al. 1982; Fujita 1985; Rinehart et al. 1987; Wilson 1988; Hjelmfelt 1988; Gast and Schroeder 2003). Figure 2.7 indicates the location of several of these studies. The general detection methods of each of these studies is similar. The MIST study is explained in more detail below.

During the MIST experiments several observation methods were employed for the detection of downbursts. Held in Northern Alabama in 1986, the most important meteorological data to this study was surface weather data. Surface data was provided by a dense PAM network of 41 observation stations and 30 FLOWS (FAA-Lincoln Laboratory Observational Weather Studies) stations (Atkins and Wakimoto 1991). The average spacing between stations was approximately 1.25 miles (2 km) and data was recorded every 1 minute, with the hopes that all but the smallest microburst (< 1.25 miles (2 km)) would be identified by the sensors. PAM data was analyzed

using a computer algorithm first suggested by Fujita (1985) and Wakimoto (1985) to identify downburst occurrences. NCAR (National Center for Atmospheric Research) Doppler radars were also spaced out to provide full coverage of the area. The interested reader is referred to these studies for specifics on the set of standard conditions required of surface data observations used to identify the characteristic wind speeds over short periods of times.

Studies such as the MIST project have the advantage of a dense network of frequent wind observations, a condition that is very advantageous when attempting to observe all downbursts events for a given area. For the purposes of this research these studies such as the MIST study provide a better understanding of the formation and proper identification of downbursts, but are less useful as a methodology to follow. Unfortunately no such network exists or has been set up for the WBMA, meaning that an extensive network of sensors would need to be set up in this region and subsequently monitored. Therefore, the data used here must be collected from previously recorded sources. Ideally, a network of sensors set up in a large area for an extended period of time would present more reliable data and more information on the downbursts that occur beyond an estimated or measured wind speed and is the subject of future work.

#### 2.6.1.2 Retroactive Surface Data Studies

More pertinent to this research are the downburst studies that have been conducted retroactively. These studies must combine a variety of already-recorded data sources to identify and verify the severe weather occurrences such as downbursts. All the data that could be used to identify these events already exists, though not typically for the sole purpose of downburst identification. A more detailed description of this type of methodology can be found in the closely related field of research on tornado occurrences (e.g. Kelly et al. 1978; Brooks et al. 2003; Doswell et al. 2005).

In this methodology the initial tally of a specific weather occurrences is gathered from published storm reports that are available in two different formats online from the Storm Prediction Center (SPC) and National Climatic Data Center (NCDC), both part of the National Oceanic and Atmospheric Administration (NOAA)[2]. This data originates from surface weather observation stations on rivers and coast areas, at airports, from human observers, as well as other methodologies. And while errors associated with this database are possible due to the variety of data sources and methods used to collect the data, since 1972 a concerted effort has been made to ensure complete and accurate data (Schaefer and Edwards 1999).

Within this database, downburst occurrences are typically reported under the category of high wind events. For each event the characteristics of the event, including location, date, time, duration and estimated or measured wind speed are typically included. Examples of these data entries are found in Figure 2.11,Figure 2.12 and Figure 2.13.

Several methods of checking the validity of these reports are available. Radar reflectivity imagery from Next-Generation Radar (NEXRAD) can be used to verify the existence of a convective system (in the shape of bow or crescent shaped echos at the location of the downburst) (Fujita 1978). Additionally, the daily infrared satellite imagery and 850-mb theta-e data, where available, can be collectively used to identify if conditions for convective activity are favorable (Atkins and Wakimoto 1991).

Figure 2.8 displays the results from Pryor's unpublished study (2009) of downburst occurrences in the eastern U.S. This data is limited to the timeframe of years 2001-2003, thus more data

[2] The NOAA websites for storm report data: http://www.spc.noaa.gov/climo/ (preliminary data), and http://www4.ncdc.noaa.gov/cgi-win/wwcgi.dll?wwEvent~Storms (final data)

beyond these three years would be better for characterization of downburst occurrence in the WBMA.

#### 2.6.1.3 Computer Modeling Based Studies

Some of the more recent studies of downburst occurrences have utilized computer based data and software to collect information on downbursts (e.g. Ellrod et al. 2000; Pryor et al. 2002; Pryor et al. 2003). GOES (Geostationary Operational Environmental Satellite) satellites provide continuous monitoring of weather patterns through imager and sounder data. Each GOES satellite monitors one area on the surface of the Earth by circling it at speeds matching its rotation. GOES Microburst Product is a software program that uses GOES sounder image data to generate a map showing areas of elevated likelihood that a microburst could occur (Figure 2.9). The closer to red the color, the higher likelihood of occurrence is predicted.

GOES microburst prediction methods and other computer generated models such as WINDEX (McCann 1994) and GUSTEX (Geerts 2001) derived from the GOES data are recent and still under evaluation and are thus not used in this research. As an example of their application, in a study by Walter (2007) a variety of data, including GOES-derived WINDEX data was collected for a 30-year period to determine the number of days in which downbursts were likely to occur annually. Figure 2.10 shows the predicted peak wind speeds of downbursts.

## 2.7 WBMA DOWNBURST DATA COLLECTION METHODOLOGY

### 2.7.1 Datasets Used for Downburst Information Collection

Compiling a dataset of downburst occurrences for a specific region is ultimately limited to the time period in which the downburst weather phenomenon has been recognized as a type of severe weather event (i.e., from 1970s to present). Since there has been no formal and consistent

mechanism for reporting this type of severe weather throughout the years, developing a sufficiently large dataset to characterize the downburst activity for the WBMA multiple approaches are used. This section outlines the approach for compiling such a dataset of downburst occurrences in the WBMA.

#### 2.7.1.1 Storm Event Database – Data Collection Methodology:

Data was collected using two different approaches. The primary data source originates from the NCDC. The searchable and publicly accessible online database of severe weather events called the Storm Event Database[3] is the same database used in previous studies (e.g. Kelly et al. 1978; Brooks et al. 2003; Doswell et al. 2005). It contains official records of all reported severe weather events that have been observed and recorded across the United States from 1950 to the present day. The data published in this database is also published on NOAA's SPC website[4] but this data is considered preliminary only.

In order to merit an entry in the Storm Event Database, the reported weather must be classified as "severe" weather. Severe weather, as defined by the NWS, is weather that produce one or more of the following events (NWS 1995):

- large hail of at least 0.75 in (1.9 cm) diameter
- damaging winds of at least 58 mph (26 m/s)
- tornados

In addition to these, any storm event that causes structural damage is typically considered to be severe, even if its intensity was not recorded (Doswell et al. 2005). Since strong wind speeds, typically above 58 mph (26 m/s), are one of downbursts' most defining characteristics, it is

[3] Storm Event Database - *http://www4.ncdc.noaa.gov/cgi-win/wwcgi.dll?wwEvent~Storms*
[4] Storm Prediction Center *http://www.spc.ncep.noaa.gov/climo/*

determined in this research to search this database for severe and damaging wind events caused by downbursts. Information for this database comes from a variety of human and automated sources – the NWS, Military Services, Federal Aviation Administration, as well as data from trained civilian volunteers.

The Baltimore/Washington section of the NWS publishes monthly summaries of severe weather taken from the Storm Event Database, compiling all of the severe weather reports that pertain only to the WBMA into one document. Thus to obtain all existing records of downbursts in this region, the files containing data for the months in the convective season (May – August) published on the Baltimore/Washington NWS website[5] were compiled. This data was then searched using the keywords "downburst," "microburst," and "macroburst," for occurrences of downburst occurrences within the severe wind events in all available years (1996-2009). Each record identified in this compiled set of data was recorded, totaling 78 records identified as downburst events.

The data for each record varied greatly in the amount of detail reported. Where possible the following information was recorded for each downburst occurrence:

- Date of occurrence
- Time of downburst
- City and state where the observation was made
- Latitude and longitude coordinates
- Maximum estimated or measured wind speed
- Any further textual details pertaining to the downburst occurrence given in the storm report

[5] NWS Baltimore/Washington Storm Data - *http://www.erh.noaa.gov/lwx/Storms/Strmdata/*

To ensure that all reported cases within the WBMA were consistent with the NOAA's nationwide Storm Event Database from which the data was extracted, all records were cross checked with this database. In all cases records of the same information were found. Additionally in many cases where the Baltimore/Washington compiled data had missing information – particularly the latitude/longitude coordinates of the location of the touchdown of the downburst – the national database entry contained that piece of information.

Several examples of the Storm Event Database records from the WBMA are shown in Figure 2.11, Figure 2.12 and Figure 2.13, illustrating the variance in the detail of reports. A month's worth of Storm Data includes many of these entries separated by both region (e.g. Central Maryland) and by type of report (strong wind, tornado or hail). The database entries shown from the NWS Baltimore/Washington section's compiled data include the title at the top of each page, the region of the particular report of interest and all of the details it gives. Also included are the records from the national Storm Event Database of the same events to show the similarities and differences between the two types of entries and compare the amount of detail in each.

Of the records reviewed, all indicated a date, time and location. In many cases the entries also listed the estimated or measured wind gust speed, however especially in the earlier entries, the wind gust speed was not noted in the weather reports. 45 of the 78 entries reported an estimated or measured wind speed of a downburst of 50 knots (58 mph, 26 m/s) or larger. The other 33 had either a numerical measurement of the wind speed of the downburst of "50+ knots" or no wind speed estimate at all.

Due to the small size of downbursts and the lack of densely placed wind speed measuring anemometers throughout the WBMA, it is understandable that a wind speed value may not be available for downbursts from ground surface data. It is assumed, however, that if the event is

placed in the Severe Storm Database, then the NWS approved the event's reporting as fitting the criteria of a "severe" wind event – that is one over 58 mph (26 m/s). Thus for each record with wind data marked as "50+" or as nothing, an estimated 58 mph (26 m/s) speed was assumed. This assumption is consistent with the assumptions used by McDonald and Abbey (1979) who applied this idea to tornado datasets. In their dataset, 8.1% of tornados were missing intensity estimates, 39.4% lacked adequate information. Thus they assigned a minimum value of intensity to any missing data, assuming that if the tornado was reported, it likely existed, but also if it had been more noteworthy, more information would have been reported on it (Schaefer et al. 1986). In addition to the assumption that all unreported downburst wind speeds are 58 mph (26 m/s), the downburst dataset was also considered in which only the downbursts with reported wind speeds (estimated or measured) were included for purposes of comparison and analysis.

In a number of cases the Storm Event Database records indicated the exact wind speed measured for the downburst, however in most cases either a range of winds speeds or an estimated wind gust is presented. Given the range of values of wind speeds (e.g 60-80 mph), the low (e.g 60 mph), average (e.g. 70 mph) and high (e.g. 80 mph) estimates were evaluated when creating the model of the downburst occurrences in this area in an attempt to encompass the full range of possible wind speeds that may have occurred.

For an understanding of where the estimated wind speeds originate on the Storm Event entries, a common way that wind speed is estimated, if exact measurements are not available, is by using the Beauford Scale. The scale uses the end product of a damaging wind event – damage to buildings, trees, etc… to estimate the wind gust speed. Table 2.2 shows the different severity estimates, relating wind speed and resulting damage to each other. Based on the categories in this estimation system, winds above approximately 55 mph (24.6 m/s) can cause significant

structural damage including snapping of trees and structural damage. In many of the reports listed in the Storm Event Database, both building damage and snapped trees were reported. Taking the storm reports presented in Figure 2.11 wind speeds were estimated at 61 knots (70 mph, 31.2 m/s). At this speed the scale indicates that trees can be broken and structural damage can occur. The text in this severe storm report indicates that over 100 trees were knocked down and structural damage occurred in a commercial district in Bowie, MD, which seems to align with the wind estimates presented on the database entry.

Many of the estimates that are given in this database come from citizen reporters trained through a program known as Skywarn[6]. This program sponsored by the NWS teaches citizens about the different types of weather and how to report severe weather observed to NWS. For reporting estimated wind speeds such as those associated with a downburst, a Skywarn training manual suggests observing damage to trees and the environment in an effort to use the Beauford scale to measure the estimated wind speed.

[6] *Skywarn* - http://www.weather.gov/skywarn/

**Table 2.2: The Beaufort Scale - Wind Speed Estimates (adapted from SPC 2010)**

| Beaufort Number | Wind Speed in mph (m/s) | Description | Effect on Land |
|---|---|---|---|
| **0** | < 1 ( 0.4) | Calm | Calm; smoke rises vertically. |
| **1** | 1-3 (0.4-1) | Light Air | Smoke drift indicates wind direction, vanes still. |
| **2** | 4-7 (1-3) | Light Breeze | Wind felt on face; leaves rustle; vanes begin to move. |
| **3** | 8-12 (3-5) | Gentle Breeze | Leaves, small twigs in constant motion; light flags extended. |
| **4** | 13-18 (5-8 | Moderate Breeze | Dust, leaves and loose paper raised up small branches move. |
| **5** | 19-24 (8-11) | Fresh Breeze | Small trees begin to sway. |
| **6** | 25-31 (11-14) | Strong Breeze | Large branches of trees in motion; whistling heard in wires. |
| **7** | 32-38 (14-17) | Moderate Gale | Whole trees in motion; resistance felt in walking against the wind. |
| **8** | 39-46 (17-21) | Fresh Gale | Twigs and small branches broken off trees. |
| **9** | 47-54 (21-24) | Strong Gale | Slight structural damages occur; slate/shingles blown off roofs. |
| **10** | 55-63 (24-28) | Whole Gale | Seldom experienced on land; trees broken; structural damage occurs. |
| **11** | 64-72 (28-32) | Storm | Very rarely experienced on land; usually causes widespread damage. |
| **12** | > 72 (32) | Hurricane Force | Violent and destructive winds. |

#### 2.7.1.2 News Search via Lexis Nexis – Data Collection Methodology:

Considering the gaps and inherent inaccuracies in the data of the Storm Data, a search was also performed using the database LexisNexis to search all publications of the major newspapers and newsfeeds in the WBMA between the same years of 1996 to 2009. The goal in performing this search was to increase the probability of detection of at least the strongest wind events. It is these events that are of greatest interested to the structural design of buildings as they have a higher potential to damage infrastructure. Through the news database Lexis Nexis the sources searched including the major newspapers within the coverage area of the Baltimore/Washington NWS - The Washington Post, The Washington Times and The Baltimore Sun among others as well as the newsfeeds/newswires for the area – were searched. This search resulted in 15 total reports of downbursts using the keywords "downburst", "microburst" and "macroburst". Comparing the events with the events recorded in the Storm Event Database found that 2 of the 15 records were consistent. The two overlapping records from both databases were counted only once, the other 13 records were added to the first dataset to create a total of 93 records, representing 91 downburst events.

It is of some cause for concern that there was not more overlap found between the Storm Event Database and the news search performed. Throughout this paper it is recognized that there are unavoidable flaws in the dataset, and the data is treated in such a manner.

#### 2.7.1.3 Accuracy of Data Sources

Since the diameter of downbursts can be much smaller than the distance between wind data collectors or trained civilians in the WBMA, it is highly likely downburst events are not included in the dataset, even when multiple data sources are consulted. However the assumption is made

that if the downburst is strong enough to cause major damage, it is highly likely that it will be reported to either a news source or to the NWS. Since the values of the high speed winds (rather than the lower speeds) caused by downbursts are of most importance it is reasonable to assume that a high percentage of the strong downbursts have been identified in one of the two sources. The Storm Event Database entries are only as accurate as the tools and resources used to report the event. In some cases the data is collected from an automated weather station – here the winds are measured with an anemometer and are highly accurate. However in other cases the event is reported by a trained civilian with little to no equipment, and thus relies on visual clues or the Beauford scale (Table 2.2) for an estimated wind speed.

#### 2.7.1.4 Methodology Comparison to ASCE 7-05

In the design of infrastructure in the United States, ASCE (American Society of Civil Engineers) 7-05 – "Minimum Design Loads for Buildings and Other Structures" (2005) is followed in the determination of the loads on buildings. ASCE 7-05 provides a means for determining required wind loads which a building must withstand (Peterka and Sohban 1998). While the methodology used to create the wind map involved the collection of wind speed data as opposed to just downburst data, the similarities to the methodology in this research are listed as follows:

- The data used in the determination of the design wind speeds for the United States were obtained by combining wind data from multiple meteorological stations into one "superstation" for a given region (methodology described in Peterka 1992). This is similar to the compilation of data from multiple sources across the WBMA obtained for the downbursts in this study.

- These “superstations” were generally the size of a “typical state,” particularly in the eastern United States because sufficient data existed at multiple stations in the region, which is similar to the size of the WBMA region of study.
- The typical length of record over which correlations were calculated was 15-25 years depending on the length of the time period of data available when this map was first developed (1998). In this study the length of time is 14 years.

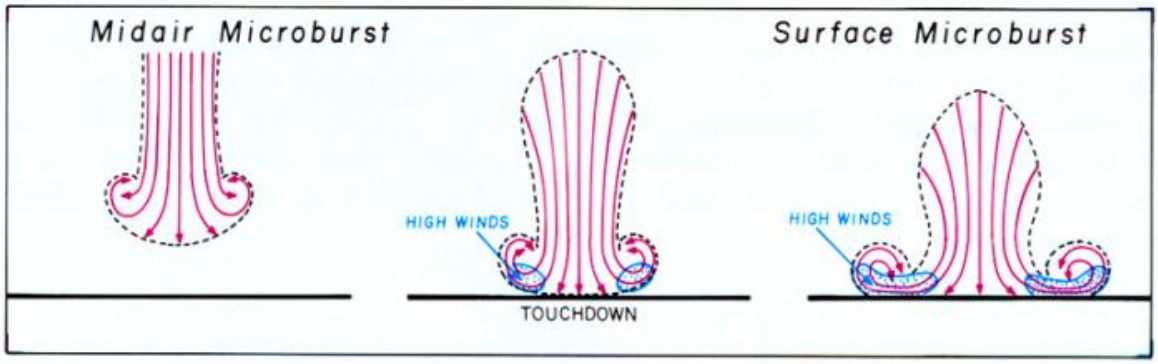


**Figure 2.1: First Downburst Conceptual Model (Fujita 1985)**

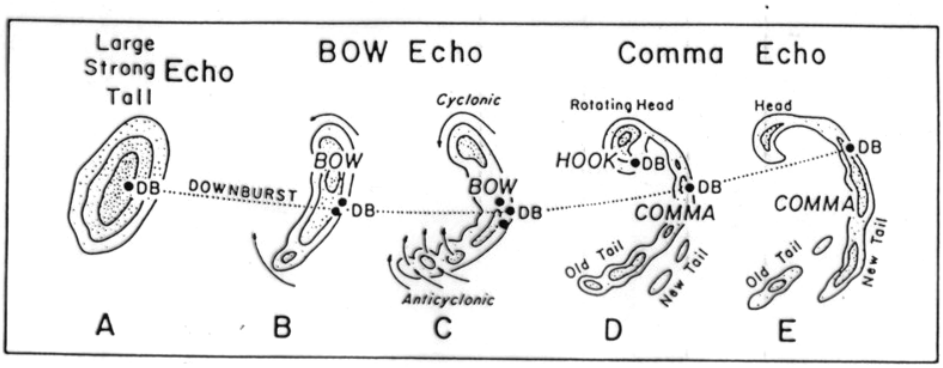


**Figure 2.2: Bow Echo Formation and Downburst Locations (Fujita 1978)**

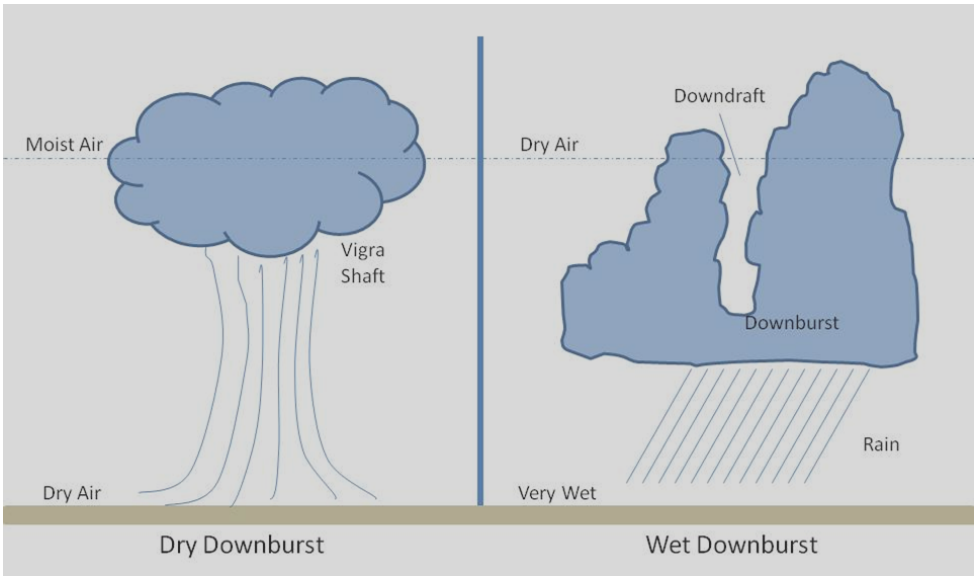


**Figure 2.3: Dry and Wet Microburst Diagrams (adapted from Caracena and Flueck 1988)**

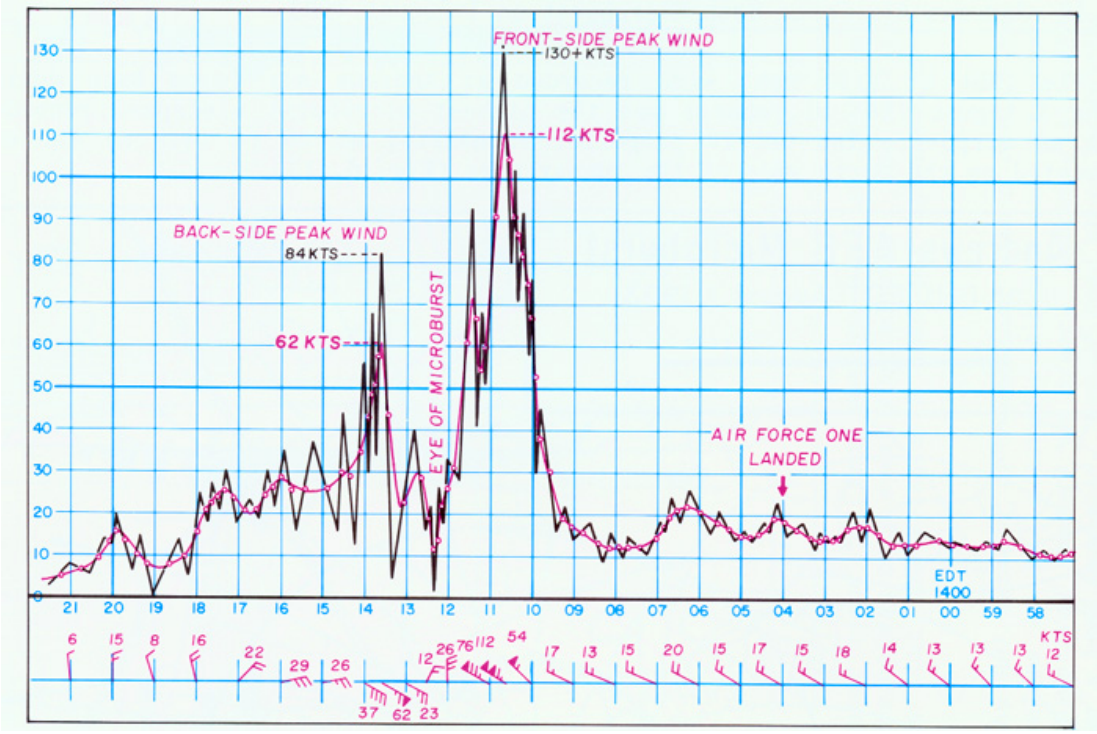


**Figure 2.4: Andrews Airforce Base Downburst - August 1, 1983 (Fujita 1985)**

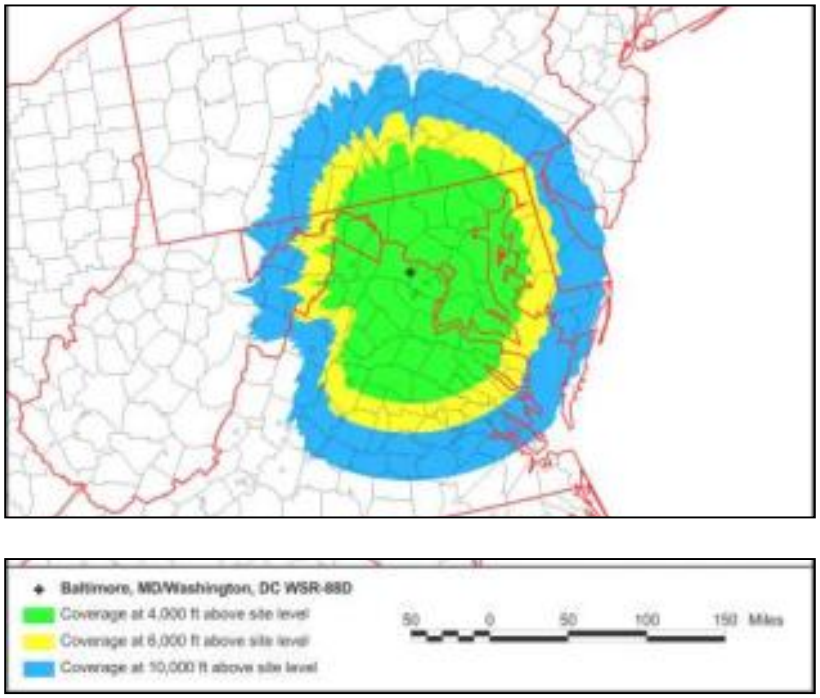


**Figure 2.5: Doppler Radar Coverage for the Baltimore/Washington NWS (NWS 2010)**

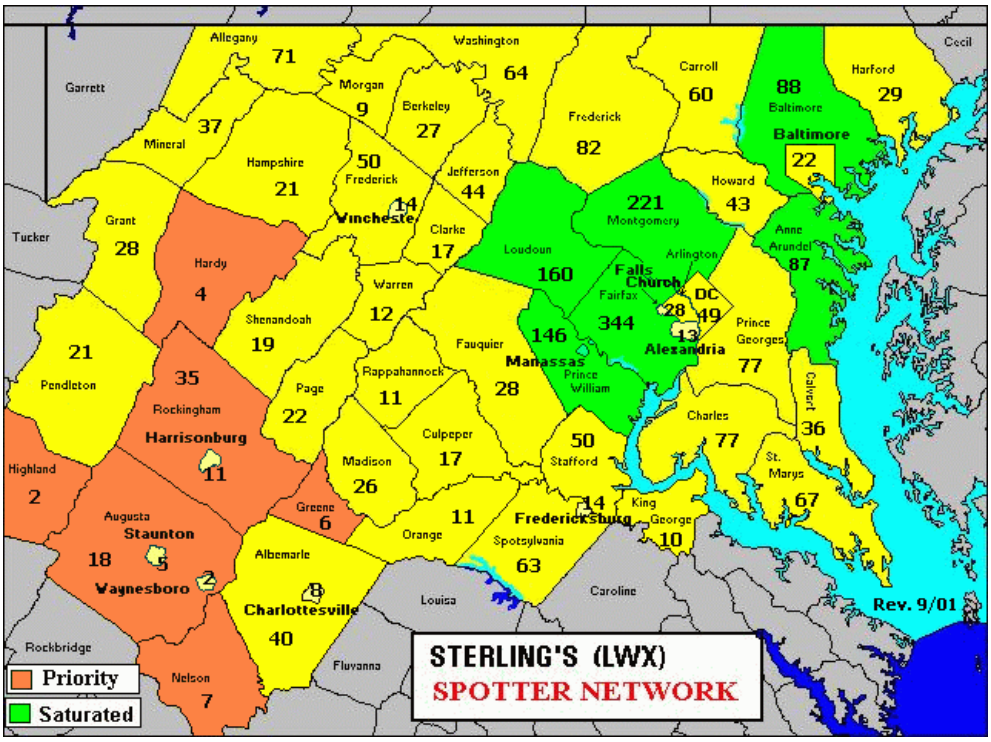


**Figure 2.6: Coverage Area of Baltimore/Washington NWS by County (NWS 2010)**

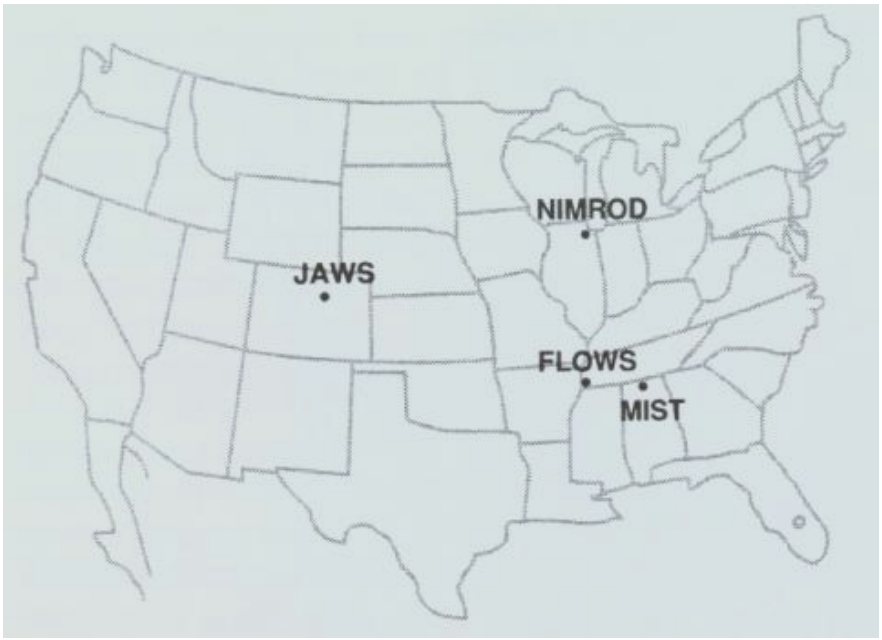


**Figure 2.7: Location of Extensive Downburst Studies in the United States (Wakimoto 2002)**

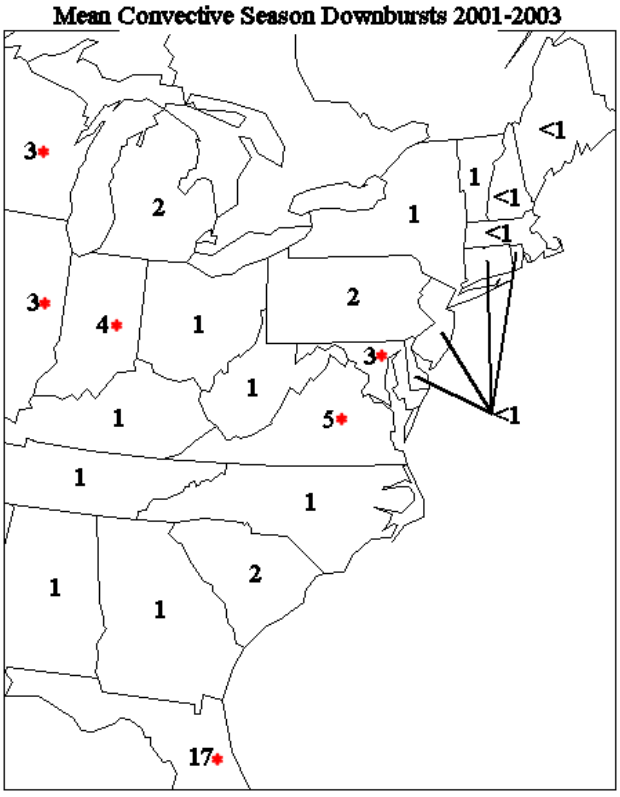


**Figure 2.8: Downburst Occurrences by State 2001-2003 (Pryor 2009)**

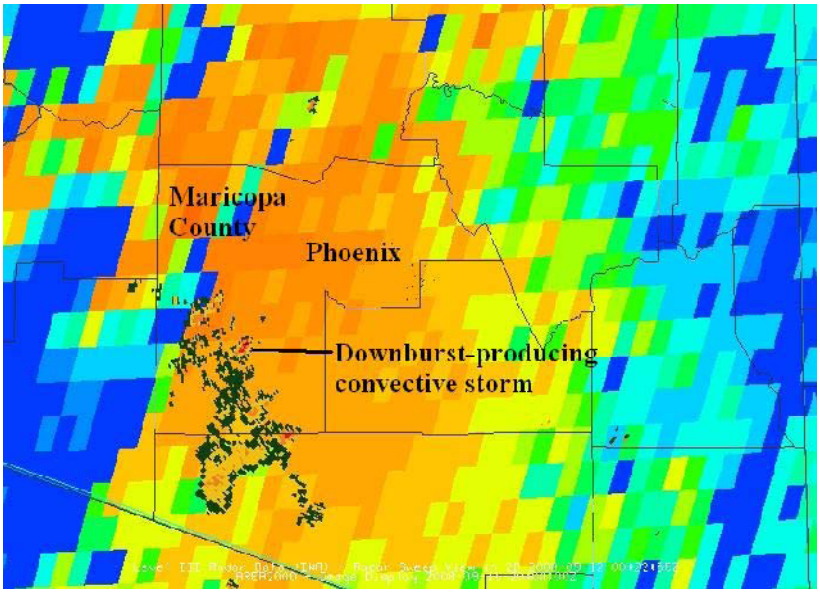


**Figure 2.9: GOES Microburst Product overlaid with Radar data (Pryor 2009)**

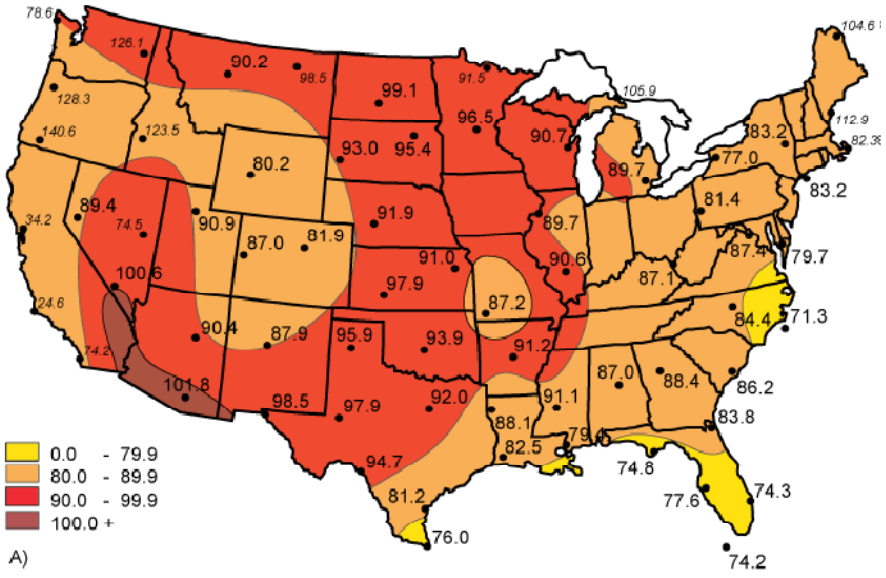


**Figure 2.10: 50-year Recurrence Interval for Microburst Peak Wind Speeds (mph) (Walter 2007)**

**National Weather Service**
**Storm Data and Unusual Weather Phenomena**

August 1996

| Location | Date | Time Local/ Standard | Path Length (Miles) | Path Width (Yards) | Number of Persons Killed | Number of Persons Injured | Estimated Damage Property | Estimated Damage Crops | Character of Storm |
|---|---|---|---|---|---|---|---|---|---|
| **MARYLAND, Central** | | | | | | | | | |
| **Prince George'S County** | | | | | | | | | |
| **Bowie** | **16** | **1550EST 1552EST** | | | **0** | **0** | **75K** | | **Thunderstorm Wind (G61)** |

A wet microburst knocked down over 100 trees, several power lines, and caused minor structural damage along a 1 3/4 mile, 300-yard wide path through a commercial/residential section of Bowie. Hail averaging the size of quarters (1 inch diameter) piled up between 1 and 2 inches deep at several residences prior to and during the microburst.

**Figure 2.11: Baltimore/Washington Storm Event Report - Early Format**

**Storm Data and Unusual Weather Phenomena - July 2008**

| Location | Date/Time | Deaths & Injuries | Property & Crop Dmg | Event Type and Details |
|---|---|---|---|---|
| FAUQUIER COUNTY --- 1.2 E BETHEL [38.77, -77.80] | | | | |
| | 07/23/08 18:11 EST | | 25K | Thunderstorm Wind (EG 74 kt) |
| | 07/23/08 18:11 EST | | 0 | Source: NWS Storm Survey |

Damage from a microburst was surveyed in the Airlie-Bethel area. Extensive tree damage in the form of topped and uprooted large trees occurred in the community of Bethel Academy. Portions of some uprooted trees damaged roofing of nearby homes. All damage was consistent with a microburst, with maximum winds estimated at 85 MPH.

**Figure 2.12: Baltimore/Washington Storm Event Report – Recent Format**

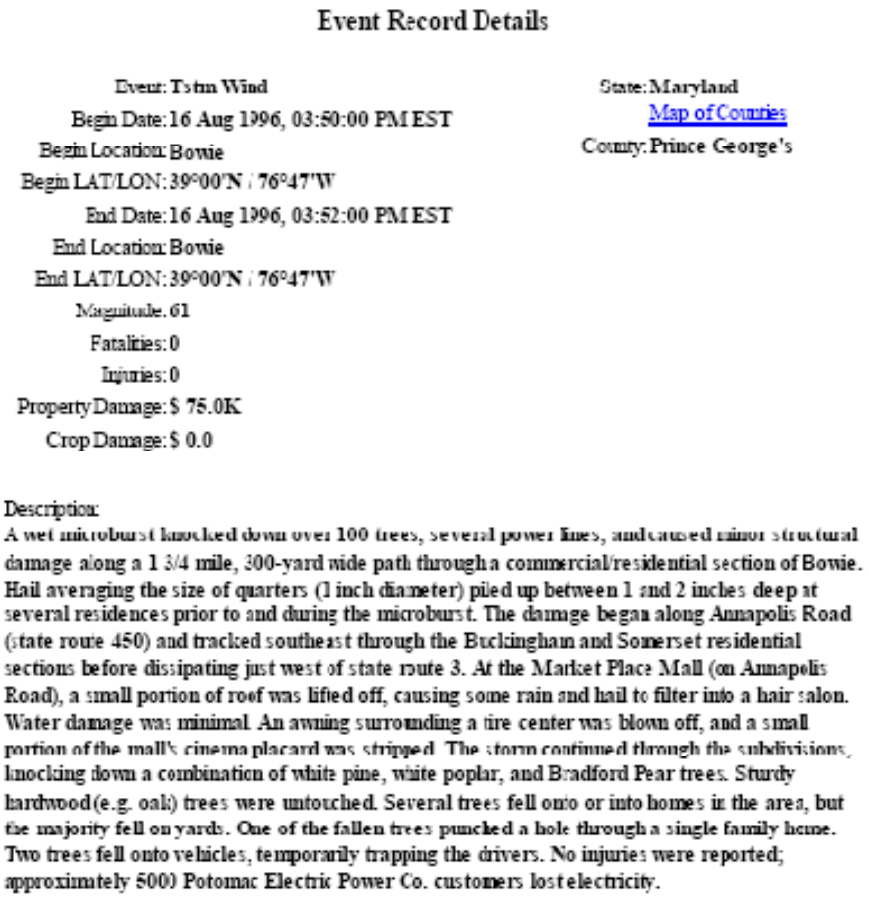

Event Record Details

Event: Tstm Wind
Begin Date: 16 Aug 1996, 03:50:00 PM EST
Begin Location: Bowie
Begin LAT/LON: 39°00'N / 76°47'W
End Date: 16 Aug 1996, 03:52:00 PM EST
End Location: Bowie
End LAT/LON: 39°00'N / 76°47'W
Magnitude: 61
Fatalities: 0
Injuries: 0
Property Damage: $ 75.0K
Crop Damage: $ 0.0

State: Maryland
Map of Counties
County: Prince George's

Description:
A wet microburst knocked down over 100 trees, several power lines, and caused minor structural damage along a 1 3/4 mile, 300-yard wide path through a commercial/residential section of Bowie. Hail averaging the size of quarters (1 inch diameter) piled up between 1 and 2 inches deep at several residences prior to and during the microburst. The damage began along Annapolis Road (state route 450) and tracked southeast through the Buckingham and Somerset residential sections before dissipating just west of state route 3. At the Market Place Mall (on Annapolis Road), a small portion of roof was lifted off, causing some rain and hail to filter into a hair salon. Water damage was minimal. An awning surrounding a tire center was blown off, and a small portion of the mall's cinema placard was stripped. The storm continued through the subdivisions, knocking down a combination of white pine, white poplar, and Bradford Pear trees. Sturdy hardwood (e.g. oak) trees were untouched. Several trees fell onto or into homes in the area, but the majority fell on yards. One of the fallen trees punched a hole through a single family home. Two trees fell onto vehicles, temporarily trapping the drivers. No injuries were reported; approximately 5000 Potomac Electric Power Co. customers lost electricity.

**Figure 2.13: National Storm Event Report (same date as Figure 2.11)**

# CHAPTER 3: DOWNBURST DATA AND DISTRIBUTION

## 3.1 SUMMARY OF DATA:

Over the 14 year period of records from 1996 - 2009 in the WBMA, 93 total downburst events were reported during the convective season (May - August) - 78 were reported in the Storm Event Database, and 15 were reported in the Lexis Nexis database, with 2 overlapping.

## 3.2 ELIMINATION OF EXTRANEOUS DATA ENTRIES:

Several of the 93 records were eliminated or combined to create a more meaningful and useful dataset. Two of the events had records from both the Storm Event and Lexis Nexis databases, thus the information from both sources was combined to create one event to represent each downburst occurrence.

Several of downbursts reports occurred on the same day at similar times but in different locations, likely meaning one convective storm produced multiple downbursts. Previous climatology studies have chosen to count the number of days, rather than the total number of downburst (e.g. Brooks 2003). The use of "downburst days" as opposed to the inclusion of all downbursts in the dataset is consistent with the approach taken by Brooks et al. (2003). Brooks argues that this approach takes advantage of the best aspects of the limited dataset. The location of the touchdown point and date of occurrence are taken as the most reliable factors and thus it is explained that using tornado (or in this case downburst) days gives the estimate of the threat of 1+ downbursts touching down at any location during a 24 hour period. Using this methodology the occurrence of one major convective storm that produced several sightings of downburst does not skew the dataset. One problem that this presents is what downburst, of the several that may

occur on a given day, should be chosen to represent that day's downburst occurrences. In this research the downburst with the highest wind speed value was chosen to represent the worst case scenario.

Eliminating the extraneous data from the original dataset, a total of 58 downbursts remain. A list of each of these events, including date, location and wind speed are listed in Table 3.1. In this table the average wind speed values are reported. In the cases where a range of wind speed values was listed (rather than a single value), an average of the minimum and maximum estimates was taken to determine the average wind speed. In Figure 3.1 each downburst occurrence is represented by a marker. White and green markers indicated unknown or average wind speeds from 58 – 74 mph (26 - 33 m/s), yellow is wind speeds of 75 – 89 mph (34 - 40 m/s), and red is 90 mph (40 m/s) and above.

Of the total 58 downbursts in the final dataset listed in Table 3.1, 46 of these downbursts events reported wind speed estimates or measurements and the remaining 12 did not. This supplementary dataset without the assumed "50+ knot" winds was also analyzed using the procedures that follow to fit the distribution curves and find the design wind speed and pressure for purposes of comparison with the final dataset.

**Table 3.1: Downbursts in the WBMA (in order by date) 1996-2009**

| Date | Average Wind Speed | | Approx. Location |
|---|---|---|---|
| | m/s | mph | |
| 5/4/1996 | 31.3 | 70 | New Market, VA |
| 6/4/1996 | 26.8 | 60 | Green Hill, MD |
| 6/14/1996 | 35.8 | 80 | Mannassas City, VA |
| 6/24/1996 | 26.8 | 60 | DC |
| 7/13/1996 | 26.8 | 60 | Charlotte Hall, MD |
| 7/14/1996 | 40.2 | 90 | Lovettsville, VA |
| 7/15/1996 | 26.8 | 60 | Benedict, MD |
| 7/19/1996 | 26.8 | 60 | Rosemont, MD |
| 7/30/1996 | 26.8 | 60 | Paw Paw, WV |
| 8/16/1996 | 31.3 | 70 | Bowie, MD |
| 8/27/1996 | 26.8 | 60 | La Plata, MD |
| 6/18/1997 | 26.8 | 60 | DC |
| 6/26/1997 | 40.2 | 90 | Welltown, VA |
| 8/17/1997 | 40.2 | 90 | Deale, MD |
| 5/31/1998 | 26.8 | 60 | Flinstone, MD |
| 6/2/1998 | 26.8 | 60 | Annapolis MD |
| 6/13/1998 | 26.8 | 60 | Scottsville, VA |
| 6/16/1998 | 26.8 | 60 | Jefferson, MD |
| 6/30/1998 | 25.9 | 58 | Ownings Mills, MA |
| 7/21/1998 | 35.8 | 80 | Berkeley |
| 6/14/1999 | 31.3 | 70 | Oakton, VA |
| 7/24/1999 | 26.8 | 60 | Spotslyvania, VA |
| 8/14/1999 | 35.8 | 80 | Leesburg, VA |
| 5/13/2000 | 35.8 | 80 | Middleburg, VA |
| 5/19/2000 | 26.8 | 60 | Greene, VA |
| 8/7/2000 | 29.1 | 65 | DC |
| 8/8/2000 | 24.1 | 54 | N VA |
| 5/27/2001 | 31.3 | 70 | Sterling, VA |
| 6/6/2001 | 29.1 | 65 | Shenandoah, VA |
| 6/12/2001 | 29.1 | 65 | NE Carrol, MD |
| 6/29/2001 | 26.8 | 60 | Severna Park, MD |
| 8/10/2001 | 31.3 | 70 | New Baltimore, VA |
| 8/11/2001 | 29.1 | 65 | Edgewood, MD |
| 5/13/2002 | 33.5 | 75 | Ellicott City, MD |
| 5/31/2002 | 24.6 | 55 | NW Spotsyvania, VA |
| 6/6/2002 | 31.3 | 70 | Wilderness Corner, VA |
| 6/27/2002 | 36.2 | 81 | Sunderland, MD |
| 8/23/2002 | 29.1 | 65 | Urbana, MD |
| 5/7/2003 | 31.3 | 70 | Warrenton, VA |
| 5/9/2003 | 26.8 | 60 | Albernarle, VA |
| 6/9/2003 | 34.0 | 76 | DC |
| 6/13/2003 | 24.6 | 55 | SE DC |
| 6/30/2003 | 35.8 | 80 | Potomac |
| 7/4/2003 | 35.8 | 80 | Glenelg, MD |
| 7/6/2003 | 31.3 | 70 | Anne Arundel, MD |
| 7/9/2003 | 26.8 | 60 | PG County, MD |
| 8/22/2003 | 33.5 | 75 | Culpeper, VA |
| 8/27/2003 | 31.3 | 70 | Sterling, VA |
| 7/14/2004 | 35.8 | 80 | Solomons Island, MD |
| 7/23/2005 | 26.8 | 60 | DC/MD |
| 7/2/2006 | 31.3 | 70 | Annandale, VA |
| 7/19/2006 | 29.1 | 65 | Roanoke, VA |
| 7/29/2007 | 31.3 | 70 | Bel Air, MD |
| 6/3/2008 | 35.8 | 80 | Potomac, MD |
| 6/4/2008 | 40.2 | 90 | Luray, VA |
| 7/23/2008 | 38.0 | 85 | Bethel, VA |
| 6/9/2009 | 25.5 | 57 | Annapolis, MD |
| 7/25/2009 | 31.3 | 70 | New Market, VA |
| 7/27/2009 | 35.8 | 80 | Reistertown, MD |

## 3.3 METHOD OF VERIFICATION

To provide some means of verification of accuracy of this dataset this data is compared to a Pryor (2009) who compiled a dataset for downburst activity for the eastern United States for the years 2001-2003. Comparing the two datasets for this time period for the WBMA, the average number of events was 7 days or 9 events, which is similar to the 9 average downburst events for Virginia, West Virginia and Maryland found by Pryor. Considering the coverage area of the WBMA does not encompass all of MD, VA or WV, this is determined to be an acceptable number.

In some cases, recorded surface wind data is used to verify a downburst occurrence. As an example, on July 2nd, 2006 a downburst occurrence was reported in Annandale, VA. The closest airport that records wind data is Ronald Reagan Washington National Airport (DCA) approximately 9 miles from Annandale. A time versus wind speed graph is shown in Figure 3.2 showing the effects of this downburst by the spike in the peak wind speed and rapid change in wind direction. The reported wind speeds of this downburst were 70 mph. DCA anemometers report a maximum wind speed of 65 mph. This is determined to be reasonable due to the distance from the airport to the downburst location.

## 3.4 DOWNBURSTS CATEGORIZED BY WIND SPEED

The downbursts of major concern are those with wind speeds above 90 mph (40 m/s) – the design wind speed for buildings in the WBMA (ASCE 2005). The NWS defines a severe weather wind event as one with winds above 50 knots (58 mph, 23 m/s), thus wind reports from the Storm Event Database are above this first threshold. Figure 3.3 shows a histogram of the

frequency of occurrence of downbursts in the WBMA by wind speed from 1996-2009. In this figure the average wind speed values are used if a range of wind speed values is reported.

## 3.5 FREQUENCY OF OCCURRENCE OF DOWNBURSTS

With a dataset of 14 years of downburst occurrences and each of their measured or estimated wind speeds, it is now useful to fit a distribution curve to this data in order to model the occurrence rate of downbursts. Several methods are used in this study and their results were compared to determine the best distribution parameters.

### 3.5.1 Downburst Wind Distribution Functions

#### 3.5.1.1 Extreme Value Distributions

The family of Extreme Value Distributions (EVD) is good candidates for extreme wind frequency analysis (Rohan and Dale 1987). Li (2000) and Oliver et al. (2000) proposed models for downburst winds for transmission line design, recommending the use of an EVD to model the meteorological data. Studies have found that the Gumbel distribution (Type I EVD) in particular models extreme wind distributions well (Cook 1982; Simiu et al. 2001; Rajabi 2008). Holmes and Moriarty (1999) analysis of downburst winds in Australia used the Generalized Extreme Value Distribution (GEVD) to conclude the Type I EVD was good fit, but conservative. The Weibull distribution (Type III EVD) and Generalized Pareto distribution have also been used to model extreme winds (Simiu and Heckert 1996; Holmes and Moriarty 1999; Pandey et. al 2003). The basis of the ASCE 7-05 design wind speed maps for the United States is wind speed data fitted with a Type I EVD (Peterka and Shahid 1998). In an effort to compare the design wind speeds of ASCE-7-05 with the values determined from the downburst wind speeds the same

distribution curve is determined. The Type III EVD is also evaluated for comparison of fit to the dataset. The Appendix includes further information on these two distributions.

**Downburst Sample Mean and Standard Deviation**

The sample mean and standard deviation must be computed before the EVD data fitting. To determine the sample mean $\bar{x}$ and standard deviation $\sigma_{\bar{x}}$, the following equations are used, where m is the total number of downbursts:

$$\bar{x} = \frac{1}{m}\sum_{i=1}^{m} x_i \tag{3.1}$$

$$\sigma_{\bar{x}} = \sqrt{\frac{1}{m}\left(\frac{1}{(m-1)}\right)\sum_{i=1}^{m}(x_i - \bar{x})^2} \tag{3.2}$$

The sample mean and standard deviation for the minimum, average, and maximum wind speed estimates are included in Table 3.2.

The difference in mean values between the dataset using minimum, average, and maximum wind speed respectively is not large because only several of the downburst occurrences were reported as a range of wind speed estimates. Most downburst occurrence reports only include one wind speed estimate, meaning that this number is used in the computation of the minimum, average and maximum wind speed values.

### 3.5.2 Determination of Parameters to Fit Data to Distribution

To fit the downburst wind speed data to Type I and III EVDs, parameter estimation is necessary. In the creation of the wind map of the ASCE 7-05, wind data was fitted using the Method of Moments (MOM), described by Simiu and Scanlan (1986). The MOM and Maximum Likelihood Estimation (MLE) methods are used in this research. The Appendix includes more detailed information on these two methods.

The MOM calculations were computed by hand, and the MLE parameters were calculated using the computer software program EasyFit (MathWave 2010). These values are summarized in Table 3.3 and Table 3.4. A graph of the average wind speed PDFs is shown in Figure 3.4.

### 3.5.3 Goodness-of-Fit

The Anderson-Darling (A-D) test (Stephens, 1974) is used to test whether the sample data comes from a population of a specific statistical distribution. It is a modification of the Kolmogorov-Smirnov (K-S) test, and uses a specific distribution to calculate its critical values. The K-S test is an alternative to the A-D test, but cannot be used if the distribution being tested has parameters estimated from the sample data. The Appendix includes more detailed information on the A-D and K-S tests.

The A-D test shows that the Type III EVD provides a better fit for the data because the difference between the critical value and the $A^2$ statistic is less for the Type III EVD than the Type I EVD. The A-D test also indicated that in both cases the MLE method provided better fitting data. Thus the Type III EVD is chosen using the parameters estimated from the MLE methodology.

When the distributions are fit to the data limited only to only the events with measured or estimated wind speed values (rather than “50+ knots”), the distributions provided better fits to the data than when the unreported wind speed values are included. The parameters estimated using MOM and MLE for Type I and III EVD, however, are not very different between the two datasets. Like the dataset that includes the 12 downburst events with wind speeds that were not reported, the MLE method for the Type III EVD provides the best fit for the data.

**Table 3.2: Mean and Standard Deviation of Downburst Wind Speeds**

| | Low | Average | High |
|---|---|---|---|
| **Mean ($\bar{x}$)** (mph) | 68.05 | 68.83 | 69.86 |
| **Standard Deviation ($\sigma_{\bar{x}}$)** | 9.83 | 10.02 | 10.79 |

**Table 3.3: Type I Extreme Value Distribution Parameters by Method of Moments**

| Wind Speed Estimate | $\alpha$ | $\mu$ |
|---|---|---|
| **Low** | 0.130 | 72.474 |
| **Average** | 0.128 | 73.337 |
| **High** | 0.119 | 74.717 |

**Table 3.4: Type I Extreme Value Distribution Parameters by Maximum Likelihood Estimation**

| Wind Speed Estimate | $\alpha$ | $\mu$ |
|---|---|---|
| **Low** | 0.130 | 73.63 |
| **Average** | 0.128 | 74.33 |
| **High** | 0.119 | 75.01 |

**Table 3.5: Type III Extreme Value Distribution Parameters by Method of Moments**

| Wind Speed Estimate | $\alpha$ | $\gamma$ |
|---|---|---|
| **Low** | 8.23 | 72.16 |
| **Average** | 8.17 | 73.02 |
| **High** | 7.67 | 74.34 |

**Table 3.6: Type III Extreme Value Distribution Parameters by Maximum Likelihood Estimation**

| Wind Speed Estimate | $\alpha$ | $\gamma$ |
|---|---|---|
| **Low** | 7.13 | 72.42 |
| **Average** | 7.12 | 73.27 |
| **High** | 6.62 | 74.59 |

### 3.5.4 Final Downburst Distribution

Given the parameters of the Type I and III EVD that are estimated, the following functions represents the probability density and cumulative distribution functions (PDF and CDF respectively) for the average wind speed values using the values determined by MLE:

Type I EVD:

$$f(v) = 0.128\, e^{-(v-74.33)0.128} e^{-e^{-(x-74.33)0.128}} \tag{3.3}$$

$$F(v) = 1 - e^{-e^{(v-73.337)0.13}} \tag{3.4}$$

Type III EVD:

$$f(v) = \frac{7.12}{73.27^{7.12}}\,(v)^{(7.12-1)} e^{-\left(\frac{v}{73.27}\right)^{7.12}} \tag{3.5}$$

$$F(v) = 1 - e^{-\left(\frac{v}{73.27}\right)^{7.12}} \tag{3.6}$$

Where *f(v)* is the PDF of downburst wind speeds and *v* is the wind speed in mph. *F(v)* is the CDF of downburst wind speeds, which provides the probability that a downburst wind speed is less than or equal to a given *v*.

These functions are now used in a stochastic model to determine the design wind speed for the WBMA due to downburst wind loading for comparison with the ASCE-7-05 50-year design wind speed.

## 3.6 DOWNBURST DESIGN WIND SPEED MODEL

A value for the design wind speed for downbursts in the WBMA is needed to compare to the wind load capacity of BIPVs in buildings. For the WBMA a 50-year design wind speed of 90 mph (40 m/s) is specified in ASCE 7-05. The goal is to determine where a downburst 50-year design wind speed falls in relation to this value. A stochastic model that includes the CDF of the downburst wind speeds is used.

### 3.6.1 Assumptions:

ASCE 7-05 makes several assumptions when creating the map of the design wind speeds for the U.S. These same assumptions are assumed in this study:

- The wind speeds determined for a particular area are for a 50-year, 2 percent probability of exceedence.
- No corrections to the data are made for terrain roughness upwind of the anemometer site and wind direction is not accounted for (Peterka and Shahid 1998).
- The output values for wind speed represent 3-second gust wind speeds in miles per hour at 33 feet above ground for Exposure C (terrain with scattered obstructions having heights of generally less than 30 ft – e.g. flat open country, grassland).

### 3.6.2 Downburst Model:

A stochastic model for downburst wind speeds is proposed by Li (2000). This model is derived from the Poisson Pulse Process, explained in the Appendix. The final equation for the exceedence probability, $p(t)$, over the threshold wind speed value *v*, of a set of wind data due to downbursts is given as:

$$p(t) = G_{\mathrm{db}}(v)\lambda t \tag{3.7}$$

Where $\lambda$ is the occurrence rate of downbursts per year, $t$ is time, and $v$ is equal to $V_d$, the design wind speed of the structure. $G_{db}(v) = 1 - F(v)\gamma$ , where $F_{db}(v)$ is the CDF of downburst wind speeds (mph), modified by the probability of an affected area being hit ($\gamma$). Thus $F_{db}(v) = F(v)\gamma$, where $F(v)$ is the CDF of the downburst wind speed (mph) determined in the previous section and $\gamma$ is the modifier, or strike factor. When a downburst occurs, it may or may not necessarily strike a building, thus $\gamma$ is included as a way of taking this into account.

### 3.6.3 Discussion on Strike Factor:

The probability that a downburst strikes a building can be determined by using geometrical probability and introducing a reference area (Li 2000). This can be calculated in several different ways; three methods are discusses in this research.

#### 3.6.3.1 Method 1: Point Probability

This methodology considers both the size of the downbursts and the total area which the downbursts can strike (i.e. the reference area). The original model (Thom 1963) of point probability was created to represent the probability of a tornado hitting a certain point within a given area using the formula:

$$P = \frac{\bar{z}}{A}\lambda \tag{3.8}$$

Where $\bar{z}$ is the mean path area of the tornado in square miles, $\lambda$ is the number of tornados per year and $A$ is the reference area and $P$ is the probability of a tornado striking a point in any year. Removing the occurrence rate $\lambda$, the strike factor $\gamma$ in this model can be defined as:

$$\gamma = \frac{\bar{z}}{A} = \frac{\text{mean path area}}{\text{WBMA area}} \tag{3.9}$$

or the mean path area over the total area of interest.

Since 1963, this model has been modified through the incorporation of stochastic models, intensity path area relationships, and the effects of structure size. Twisdale and Dunn (1983) modified this model to account for the size of a tornado relative to the size of a building it could hit. However, since the diameter of a downburst (as compared to a tornado) is typically significantly larger than that of a building, this model is less practical for downbursts. Choosing the size of the building to be infinitesimally small compared to the diameter of the downburst (i.e the building is represented by a point), the Twisdale and Dunn (1983) model becomes the same model of Thom (1963).

To achieve a similar equation for this research all downburst events and approximating the downburst diameters $(W_{db})_{\mathrm{i}}$, and path lengths $(L_{db})_{\mathrm{i}}$ for the *i*th downburst are summed, then divided by the number of total downbursts *n*. and the total reference area *A*. This yields:

$$\gamma = \frac{\sum_{i=1}^{n}((W_{db})_{\mathrm{i}}\,(L_{db})_{\mathrm{i}})}{\mathrm{n}}/\mathrm{A} \tag{3.10}$$

A similar form of the simplified form of the equation above is used in Schaefer et al. (1985) to determine tornado risk. The actual length $(W_{db})_{\mathrm{i}}$ and width $(L_{db})_{\mathrm{i}}$ of the *i*th downburst path is not likely to be known, but if an average value for all downburst lengths and widths is assumed, the above equation is changed to:

$$\gamma = \frac{(\overline{L_{db}})(\overline{W_{db}})}{A} \tag{3.11}$$

$\overline{L_{db}}$ and $\overline{W_{db}}$ represent the average values of the downburst path dimensions. Given a downburst duration $\overline{t_{db}}$ and a speed $\overline{v_{db}}$ an approximation of the path length can be determined. Thus:

$$\gamma = \frac{(\overline{v_{db}}\overline{t_{db}})(\overline{W_{db}})}{A} \tag{3.12}$$

A microburst by definition, last approximately 2-5 minutes (macroburst last longer). The translational velocity of a downburst can be about 3 times that of a thunderstorm (Holmes and Oliver 2000; Savory et al. 2001). A study of dry downburst in Colorado observed speeds of 22 – 45 mph (10-20 m/s) (Hjelmfelt 1988). A speed of 45 mph (20 m/s) was assumed by Holmes and Oliver (2000). The reference area *A* can be determined as the total reference area of the WBMA-18896 mi$^2$ (48940 km$^2$) (NWS 2006) following the assumptions made by Li (2000) and Holmes (2000).

Using this method, and assuming the downburst travels at a speed of 45 mph (20 m/s) and lasts for 3-minutes (average value from previous studies e.g. Fujita 1985), and also assuming the width of the downburst to be 2.5 miles (4 km), $\gamma$ can be calculated as:

$$\gamma = \frac{(\overline{v_d}\overline{t_d})(\overline{W_d})}{A} = \frac{\left(45 \text{ mph} * \frac{3 \text{ min}}{60 \frac{\text{min}}{\text{hr}}}\right)(2.5 \text{ miles})}{18896 \text{ mi}^2} = \mathbf{2.97\ x10^{-4}}$$

This methodology introduces many variables of which the values are not explicitly known in this research. With thorough data that includes information such as the downbursts' translational velocities, diameters, and durations this method could be more accurate than other methods. However, using the limited dataset generated in this research this number may misrepresent the downbursts of the WBMA. This method yields the lowest design wind speeds of the three methods proposed.

#### 3.6.3.2 Method 2: Urban Area Ratio

A second methodology considers the ratio of the urban areas $A_u$ in the WBMA to the reference area $A$, the total area of the WBMA:

$$\gamma = \frac{A_u}{A} = \frac{Urban\ area}{WBMA\ area} \tag{3.13}$$

Urban areas are likely to be the main locations in which medium to high rise buildings are constructed. In the event of a downburst, these areas are likely the only locations where building façade damage would be of concern. The total urban area $A_u$ is determined as:

$$A_u = \sum_{i=1}^{n} (A_u)_i \tag{3.14}$$

Where $(A_u)_i$ is the area of the *i*th urban location in which buildings are located, and *n* is the number of urban locations.

Washington D.C. and Baltimore represent the main urban areas in the WBMA. Taking the areas inside the Washington and Baltimore beltways (I-495 and I-695), approximated from using the total length of each highway (64 miles and 51 miles respectively) as the approximate circumference of a theoretical circle surrounding each urban area (FHA 2010):

$$\gamma = \frac{A_u}{A} = \frac{A_{Baltimore} + A_{Washington\ D.C.}}{A} = \frac{207\ \text{mi}^2 + 326\ \text{mi}^2}{18896\ \text{mi}^2} = \mathbf{2.83x10^{-2}}$$

When used in the wind speed model equation, this method yields the middle range of wind speeds. It is less conservative than Method 3, but yields higher values than Method 1.

#### 3.6.3.3 Method 3: Conservative Assumption

Li (2000) verifies his downburst wind speed model by assuming that if a downburst occurs, it will hit a structure. Design wind codes for transmission lines in Australia assume that this is the

case. Li (2000) showed that with this assumption, the model produces design wind values consistent with the design code. Using this assumption:

$$\gamma = 1$$

This assumption is simple in nature, and is the most conservative. It yields the highest downburst occurrence probabilities because the probability of a downburst occurring is not modified from the raw data.

## 3.7 50-YEAR AND 100-YEAR DOWNBURST DESIGN WIND SPEED

The three methods discussed above provide a lower, middle and upper bound for the possible values of the strike factor. Using these values the 50- and 100-year design values for buildings in the WBMA are computed and summarized in Table 3.8, assuming the values in

**Table 3.7**.

The exceedence probability $p(t)$ over the threshold wind speed value *v* is:

$$p(t) = G_{\mathrm{db}}(v)\lambda t \tag{3.15}$$

Substituting $G_{db}(v) = 1 - F(v)$, modified by $\gamma$, and the design wind speed $\mathrm{V}_d$ for *v*, the final equation for probability of exceedence becomes:

$$p(t) = [1 - F_{db}(\mathrm{V}_d)\gamma]\lambda t \tag{3.16}$$

By definition the return period *R* is equal to the reciprocal of the annual exceedence probability (i.e. $1/\,p(t)$), thus to determine the design wind speeds for a return period of 50 or 100 years, and substituting t=1, the follow equation is derived:

$$R = \frac{1}{[1 - F(\mathrm{V}_d)\gamma]\lambda} = \frac{1}{\left[e^{-\left(\frac{\mathrm{V}_d}{73.27}\right)^{7.12}}\right]\lambda\gamma} \tag{3.17}$$

Solving for $\mathrm{V_d}$, the equation becomes:

$$\mathrm{V}_d = 73.27\left[-\ln\left(\frac{1}{\lambda\gamma R}\right)\right]^{1/7.12} \tag{3.18}$$

The values are substituted in to this equation to yield the equation for the 50-year exceedence probability are summarized in

**Table 3.7**. Using these values the 50- and 100-year design wind speeds are summarized in Table 3.8. Assuming a strike factor of 1 the design wind speeds exceed the ASTM-7-05 design wind speeds. Using the other two strike factors, both are below the 90 mph design wind speed.

**Table 3.7: Parameter Values for Determining Downburst Design Wind Speeds**

| Variable | Value |
|---|---|
| **R** | 50, 100 years |
| $\boldsymbol{F(V_d)}$ | $1 - e^{-\left(\frac{V_d}{73.27}\right)^{7.12}}$ |
| $\boldsymbol{\lambda}$ | $\frac{59\ downburst\ days}{14\ yrs} = 4.21$ |
| $\boldsymbol{t}$ | $1\ year$ |

**Table 3.8: 50- and 100-year Downburst Design Wind Speed (mph) at 33 ft**

| Strike Factor ($\boldsymbol{\gamma}$) | Design Wind Speed (mph) | |
|---|---|---|
| | **50-year** | **100-years** |
| **0.00297** | --[*] | 59.36 |
| **0.0283** | 79.48 | 83.23 |
| **1** | 92.73 | 95.19 |

[*] *The design wind speed with this strike factor is too low to be calculated given the CDF used to calculate it.*

### 3.7.1 Conversion to Wind Pressure

To convert the design wind speeds (mph) to pressure (lb/ft$^2$), the equation from the ASCE-7-05 code (2005) for velocity pressure (Equation 6-15 in the code) is used:

$$q_z = 0.00256 K_z K_{zt} K_d V^2 I \tag{3.19}$$

Where $K_d$ is the wind directionality factor, $K_z$ is the velocity pressure exposure coefficient, $K_{zt}$ is the topographic factor, and *I* is the importance factor. An exposure level of C is chosen here to be consistent with methodology used in the creation of the ASCE 7-05 design wind speed maps (Peterka and Sohban 1998).

$z_g$ and $\alpha$ are values that are dependent on this exposure level. For exposure level C, $\alpha = 9.5$ and $z_g = 900$, based on the values in Table 6-2 of ASCE 7-05 (2005).

$K_z$ varies with height *z* above the ground. To be consistent with the methodology used in the creation of the ASCE 7-05 design wind speed maps (Peterka and Sohban 1998) and the anemometer height at which the wind speed values were obtained in this study, a height of 33 ft (10 m) is used.

Table 3.9 defines the assumed values for the variables in Equation 3.19 for the velocity pressure calculations. The resulting velocity pressures are calculated (Table 3.10). These values will be used later on to calculate failure probability of BIPV panels by comparing to the strength data of façade-installed BIPVs.

**Table 3.9: Assumed ASCE 7-05 Velocity Pressure Variables**

| **Variable** | Value | ASTM 7-05 Reference |
|---|---|---|
| $K_d$ | .85 | Table 6-4 |
| $K_{zt}$ | 1 | Section 6.5.7.2 |
| $K_z$ | $2.10\left(z/z_g\right)^{2/\alpha}$ | Table 6-3 |
| $I$ | 1 | Section 6.5.5 |

**Table 3.10: Design Velocity Pressure (lb/ft$^2$) at 33 ft by Strike Factor**

| **Strike Factor ($\gamma$)** | **Design Velocity Pressures (lb/ft$^2$)** | |
|---|---|---|
| | **50-year** | **100-years** |
| **0.00297** | -- | 8.02 |
| **0.0283** | 14.39 | 15.78 |
| **1** | 19.59 | 20.64 |

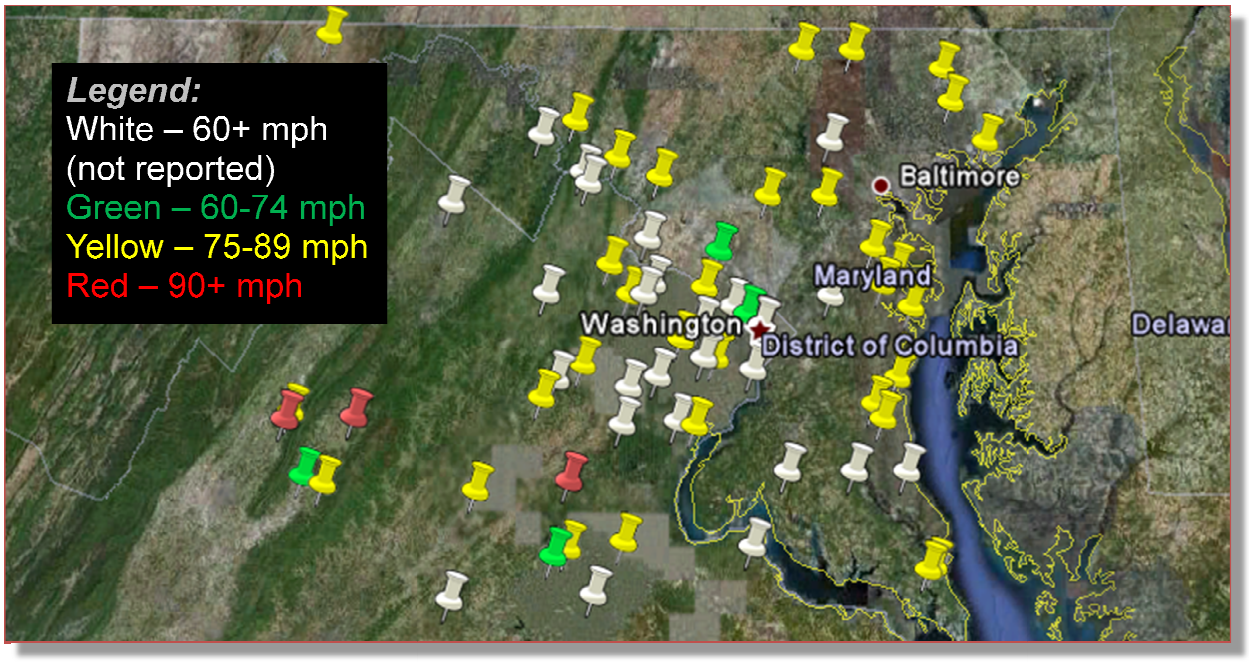


**Figure 3.1: Downbursts in the WBMA, 1996-2009**

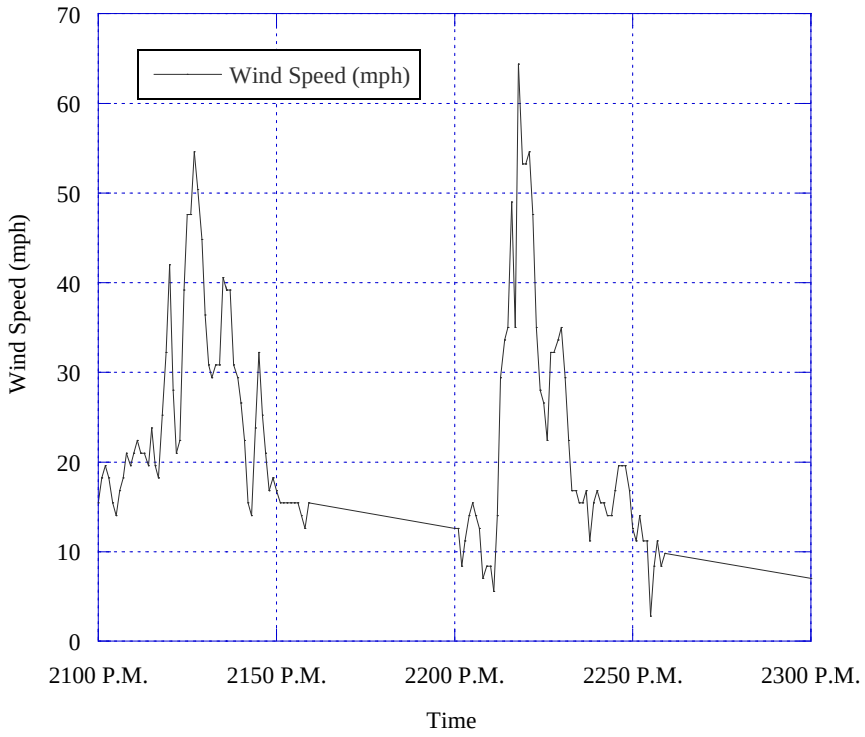


**Figure 3.2: A time history of the July 2nd 2006 Annandale, VA downburst**

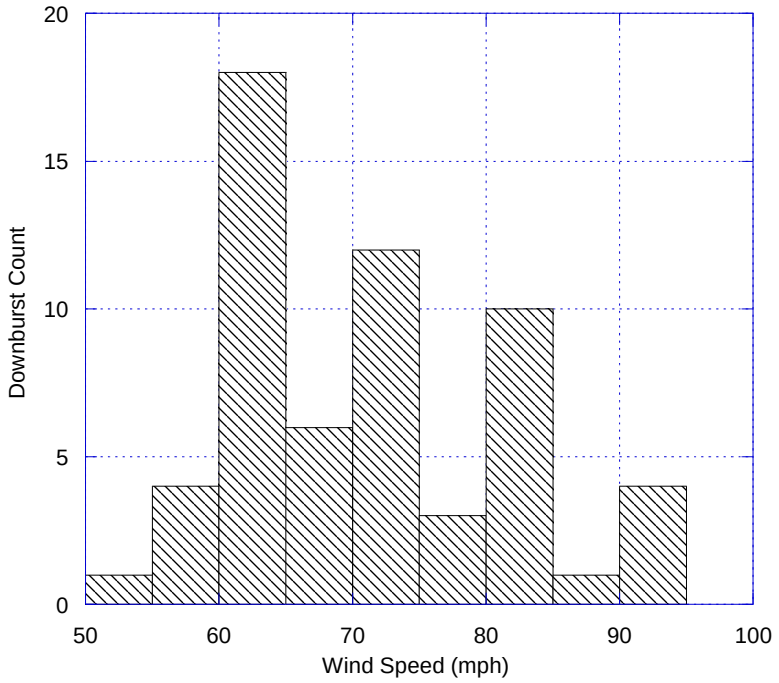


**Figure 3.3: Downbursts by Wind Speed (mph) in WBMA from 1996-2009 (1 mph = 0.45 m/s)**

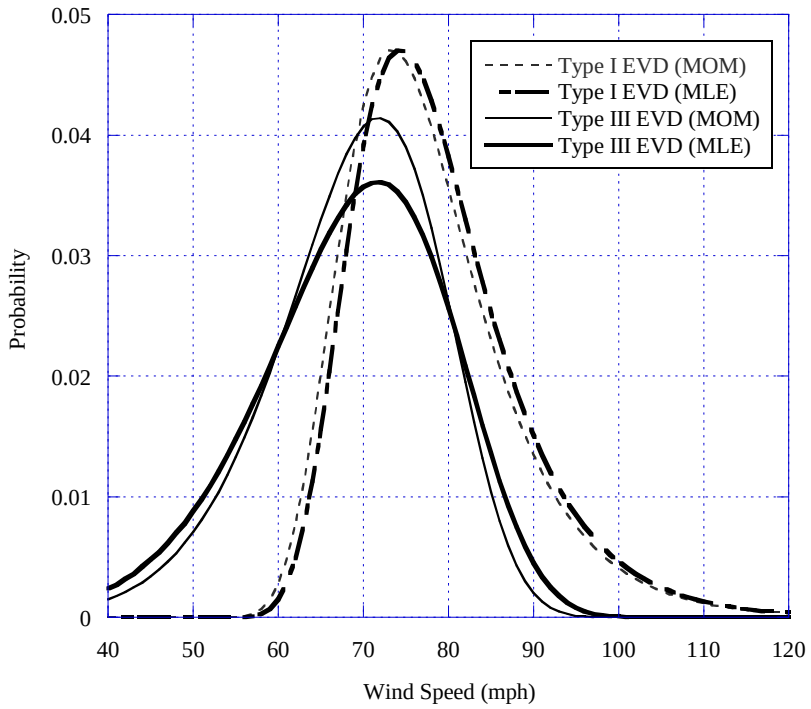

**Figure 3.4: Type I and III PDFs for Downburst Wind Speeds in the WBMA using method of moments (MOM) and maximum likelihood estimation (MLE)**

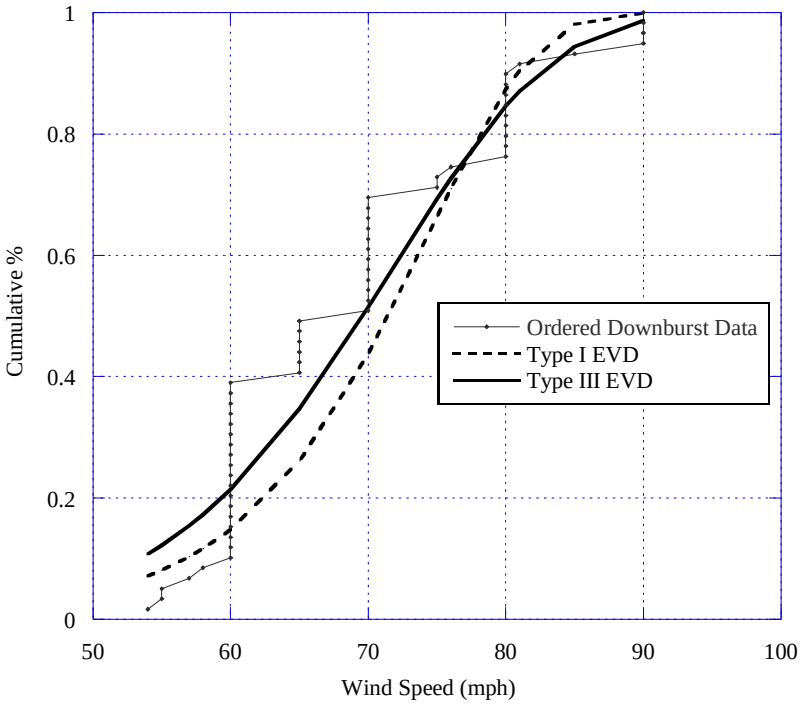


**Figure 3.5: Type I and III EVD CDFs fitted to WBMA Downburst Data from 1996-2009**

# CHAPTER 4: BUILDING INTEGRATED PHOTOVOLTAICS (BIPV) UNDER UNIFORM LOADING

Since the first discovery of a photovoltaic (PV) cell capable of converting sunlight to useable energy in the late 1800s, PV technology has come a long way in terms of efficiency and wide-spread use. Beginning with the development and commercialization of crystalline silicon (c-Si) PVs in the 20$^{th}$ century, research focuses in PV technology today have turned more towards thin-film PVs (TFPVs), which require much less raw materials to produce than c-Si. It is these TFPVs that are being produced and installed in the facades of high-rise buildings to function both as a source of power and the building envelope of the building, an application known as building integrated photovoltaics (BIPVs). As this technology has grown in popularity, various standards have been implemented in different countries to regulate the quality of BIPVs, however the potential effect of strong downburst wind-induced loads has not been assessed for façade-installed BIPVs. To understand this potential impact, a review of the most common TFPV BIPV technologies, their components and material properties is conducted to determine possible ways to assess their behavior under extreme wind loading. Based on this assessment, a model known as the Glass Failure Prediction Model (GFPM) was chosen to use to model the behavior of TFPVs under uniform wind loading and then compared with test data to provide verification of the model.

## 4.1 THE ORIGIN OF PHOTOVOLTAICS

The idea of photovoltaics first originated in the early 1800s when a French physicist, Alexandre-Edmond Becquerel, first observed what he called the photovoltaic (PV) effect. In 1883, Charles Fritts, an American inventor, constructed a 1% efficient fully-functioning solar cell (Fritts 1883). Many years later in 1954 a crystalline silicon (c-Si) p/n junction was accidentally discovered, which generated voltage when exposed to light (Chapin et al. 1954). This new technology was about five times more efficient than Fritts', however at a high cost of production, PVs were not ready for wide-scaled use. By the 1960s key papers such as those published by Prince (1955), Loferski (1956) and Wysocki et al. (1960) among others had developed the basis of design of c-Si solar cell operations. Enough was understood about their design to enable the production of PV cells to provide satellites of the 1950s and 60s with sufficient power to sustain themselves in space.

Two pivotal events occurred in 1973 that helped spur increased interest in PV technologies. First, the discovery of what is called a "violet cell" increased the efficiency of even the most state-of-the-art c-Si technologies of the time by 30% (Lindmayer 1973). Second, the U.S. Department of Energy was formed under President Nixon's direction to, in part, support PV and other renewable energy technologies. This renewable energy support was further fueled by the world's first oil embargo later that year. The decade that followed brought about the maturity of the industry of c-Si PVs. Large solar power companies and manufacturers across the U.S., Japan and Europe were established and the start of "pilot" PV lines to be used for commercial and residential applications. Efficiency of c-Si panels reached 20% in 1985 by researchers in Australia (Green 1995) and has continued to increase in efficiency slowly over the past 20 years

(Figure 4.1**Error! Reference source not found.Error! Reference source not found.**). Today most of solar installations are mono- or poly- c-Si PVs, representing an approximately 80-90% market share. Yet as the market continues to grow, the focus of researchers is turning more towards the development and improved efficiency of thin-film photovoltaic technologies (TFPVs), a potentially lower cost approach for solar power. Further reduction of PV module costs is conditional on the availability of raw materials worldwide, meaning TFPVs which require lesser quantities of the PV materials are more economically favorable. C-Si technologies, while the cornerstone of the establishment of the photovoltaic industry, has been deemed by some more as a technology of today, rather than of the future.

## 4.2 DEVELOPMENT OF THIN-FILM PHOTOVOLTAIC (TFPV) TECHNOLOGIES

TFPVs, the second generation PVs after the more common c-Si PVs, have followed a similar path of development to that of c-Si PVs, only a few decades later in terms of efficiency and use. Research efforts focused on TFPVs began in the 1950s in the U.S. with the publication of results of approximately 6% efficiency by Reynolds et al. (1954). By the 1980s, a-Si (amorphous silicon), CIS/CIGS (copper indium gallium selenide), and CdTe/CdS (cadmium telluride) TFPV technologies had achieved efficiencies of over 10% during small-scale lab testing, but the difficulty of achieving this efficiency for larger areas (larger than approximately 1 $cm^2$) had not been overcome. Complications with the scaling up of TFPVs limited their use to powering small electronics such as calculators at the time. In the early 1990s new technologies were developed and patented that allowed for larger scale TFPV technologies to be implemented. As an

example, BP Solar, a British electric company, acquired patents to electrodeposition of thin-film CdTe in 1989, and 10 years later purchased Solarex who focused on a-Si technology. This established BP Solar as one of the leading TFPV solar companies until 2002 when BP Solar drew out of all but the c-Si market. The Japanese PV industry became large contenders throughout the 1990s as intensive research on TFPVs led to new device designs, and improved material processing (Hegedus and Luque 2002).

Research and development in TFPVs has continued (Figure 4.1), in part, because it has been recognized that the silicon (Si) crystals required to for c-Si technologies are expensive and slow to grow compared to thin-film technologies. Si wafers are nearly 100 times thicker than TFPVs (~1-3µm vs 100 µm). Today the solar industry continues to develop, but at a faster pace. Many start-up companies have established themselves within the past decade in the U.S. in attempt to take advantage of the growing market for PVs, many in c-Si, and others in TFPVs. While still relatively few companies in the United States market TFPVs for commercial applications, the thin-film industry continues to take shape through BIPV applications world-wide.

## 4.3 BIPV: COMBINING TFPVS AND ARCHITECTURE

BIPVs, a relatively new area of increased research interest in the field of PVs in recent years, can be defined in a broad sense as PV components that replace the look and function of a primary building material (Strong 1996). BIPV products, such as TFPVs, act as a weather resistant skin of the building, placed often times on the facades or roofs of a building. The advantage of this system over that of more traditional applications of PVs is that no additional land area is needed, and the PVs are integrated into the building itself rather installed separately. By simultaneously acting as the building envelope material and a power generator, the system provides savings in

material and electricity costs. BIPVs do not always come in the form of solar panels, for example some companies now produce solar shingles – or flexible PVs that are shaped like traditional shingles. However for façade applications framed solar panels are more common.

### 4.3.1 Placement of BIPVs on Buildings:

BIPVs can function as a building material of several different parts of a building including:

- Façade
- Roof
- Solar shade (for windows or doors)
- Skylights and windows

In the case of extreme horizontal wind loading, the façade of building will experience these wind forces directly, thus façade applications only are considered in this research. For facades, there are two distinct applications in which PVs are integrated into a building – these are (Figure 4.2):

- Curtain walls
- Rain screens

Rain screens are a double layered building envelope which includes an outer layer that sheds most precipitation and an inner layer which handles the rest. The water that does penetrate the outer layer of this open-joint system is drained through a cavity behind it. In this system the PV panels are installed as a part of the outer layer (Figure 4.2a), however this is a less common method of utilizing PVs in facades. The focus of this research is on curtain wall applications of BIPVs, thus while rain screen application of BIPVs exist, they are not discussed in detail.

A curtain wall is typically a single layer, aluminum framed wall constructed of in-fills of glass or other materials. The BIPV components are usually installed as in-fills between the vertical and horizontal aluminum members (Figure 4.2b). A curtain wall does not act as a structural support

for a building – thus all its components must only support their own dead load and any external forces that are placed on it.

Understanding how the PV panels are most commonly installed in building facades is important in understanding the boundary conditions of the PV panels being subjected to horizontal downburst winds. In traditional curtain wall as well as in BIPV curtain walls most in-fill panels are supported by the horizontal and vertical aluminum mullions, creating 4-sided, continuous support conditions.

## 4.4 TYPES OF TFPV PANELS USED IN BIPV APPLICATIONS AND THEIR MATERIAL PROPERTIES

To better characterize BIPV behavior in façade applications under wind loading, an understanding of the construction and material properties of different types of TFPVs used in BIPV façade applications is needed. This section discusses the basics of TFPV technologies, specifically three TFPVs available on the market for use in BIPV applications:

(a) Amorphous Silicon (a-Si)

(b) Copper-Indium-(Gallium)-Selenide (CI(G)S)

(c) Cadmium Telleride (CdTe)

A-Si being the most common technology, with CI(G)S and CdTe in second and third respectively (Table 4.1**Error! Reference source not found.Error! Reference source not found.**). These three technologies are available most commonly as single layer PV panels. Laboratory testing has also shown that increased efficiency can be obtained using tandem and triple cells, in which multiple layers of TFPV are applied on top of one another, yet their large

scale use is still in development. Similarly other PV materials such as organic cells, metamorphic Ga(In)As, GaInP, and other multi-junction TFPVs have had success in research laboratories but have not yet been fabricated into large-scale PV panels. Those technologies that have succeeded in the PV market thus far can be manufactured with sufficient efficiency in large scale PV applications.

While each PV technology employs slightly different layering structure and thicknesses, the basic elements of a TFPV cell are the same. Sunlight falls on the top surface of the solar cell where it penetrates the front glass substrate to electrical contacts (e.g. typically a type of TCO – transparent conducting oxide). These metal oxides allow light photons to penetrate and be absorbed and converted to electrical charges by several layers of semiconductors (n-, (i-) and p-type). A back layer of TCO forms the second electrical contact, followed by a layer of polyvinyl butyral (PVB), and finally second layer of glass. These layers within a PV panel are important to know and characterize because it is these layers that feel the stresses under high wind loading. .

**Table 4.1: TFPV panel producers in the world market (ENF 2010)**

| ***Solar Technology*** | ***Companies Producing Solar Panels*** |
|---|---|
| a-Si | 131 |
| CI(G)S | 30 |
| CdTe | 4 |

### 4.4.1 Amorphous Silicon (a-Si) (and Micromorphous Silicon)

**Origin:** With advancements in processing and fabrication methodologies of c-Si PVs, and further silicon research, a-Si solar cells were discovered (Chittick 1969) and constructed

(Carlson 1977), using only about 1% of the silicon needed for typical c-Si cells. Today many of the commercial manufacturers and vendors of TFPV panels market a-Si technologies. According to ENF, there are 131 current companies producing a-Si products as of the year 2010. A short list of these manufactures is: Astroenergy, Auria, Bankok Solar, UniSolar, Dupont, ENN, EPV Solar, FlexCell, Global Solar, Inventux, Kaneka, Mistuishi, Polar PV, Sinonar Solar, Solar Plus, Solem, Sunfilm, SunGen, SunStar, TerraSolar, and Tianjin Jinneng Solar. The majority of these companies are not U.S.-based.

**Efficiency:** When a-Si was first discovered, the efficiency was that of only about 1% (Morel 1978), however the overall efficiency of a-Si is higher today, but is still significantly less than c-Si (around 6 - 10%). Tandem and triple-layer cells called micromorph silicon solar cells in which a-Si and very thin layers of crystalline silicon (µc-Si) are deposited on top of one another have shown significantly higher efficiencies.

**Structure and Material Properties:** Unlike c-Si whose atomic arrangements are regular crystals, a-Si has an irregular arrangement of atoms – allowing approximately 2.5 times more light to be absorbed, but less efficiently. Because it is not crystalline in nature and due to its extreme thinness, when flexed it will not break – allowing it to be deposited on to flexible or non-flexible substrates. The substrates used are numerous, including ceramics, metals, steel or plastics, however for façade applications of TFPVs, a-Si is typically deposited on to glass. As pointed out by Madou (2002), very little is known about the mechanical properties of a-Si itself. Its modulus of elasticity is estimated to be 80 +/- 20 GPa (Freund and Suresh 2003).

To improve efficiency some manufacturers of a-Si products have begun to manufacture micromorphous silicon module technologies using multiple layers of silicon such as amorphous

and a thin layer of crystalline silicon. Several manufacturers' diagrams of their a-Si solar cells are shown in Figure 4.3 – 4.5.

### 4.4.2 Copper-Indium-(Gallium)-Diselenide (CI(G)S)

**Origin:** The first thin-film CI(G)S PV was fabricated by Kazmerski et al. (1976) around the same time as a-Si technologies were being developed. The first large-scale production of CI(G)S PV modules began in 2006 by the Germany company Wurth Solar. Among some of the CI(G)S PV panel manufacturers today are: Ascent Solar, Avancis, Dupont, Global Solar, ICP Solar, Nanosolar, SoloPower, Solar Frontier, Global Solar and Wurth Solar. Of these many market thin-film flexible laminates rather than CIGS solar panels.

**Efficiency:** Similar to other TFPV, CI(G)S is far more efficient per unit of material than c-Si – a CI(G)S film approximately 1 micron thick has the potential to generate a similar power to that of a c-Si with a 200 - 300 microns thickness. The maximum efficiency achieved in small area PV laboratory testing as of August 2010 is 20.3% (Stuar 2010). The efficiency of larger scale solar panels currently average around 13%. This large discrepancy between lab-scale cells and full-scale modules is largely due to the difficulties in the development of new and complex manufacturing processes that produce CI(G)S cells.

**Structure and Material Properties:** Unlike a-Si, CI(G)S TFPVs are crystalline in structure. Of the research published concerning CI(G)S under stresses, a study by Chen (1992) discusses that substrates of similar thermal expansion coefficients to CI(G)S should be chosen so that when the two layers cool from about 500°C, the thin-film will not experience increased tensile or compressive stress. Stressed thin-films can exhibit voids and microcracking under tension or adhesion failure under compression (Chen 1992). When searching for material properties of

CI(G)S panels, the most common results for the properties listed below were not for the CI(G)S itself, but for the glass specifically designed to be used in the CI(G)S PV panels. As an example, AGC Solar, give properties of its glass that is specifically designed for CI(G)S applications (AGC 2010). Several manufacturers' diagrams of their CI(G)S panels are shown in Figure 4.6 and Figure 4.7.

### 4.4.3 Cadmium Telleride (CdTe)

**Origin:** The first CdTe crystals were synthesized in 1947 by Frerichs (1947), then proposed as a possible PV technology in 1956 (Jenny 1954; Kruger 1955; Loferski 1956; de Nobel 1959). Two types of CdTe cells emerged, homojunctions (single layer) and heterojunctions (multiple layers), however nearly all research focus has concentrated on heterojunction PV cells since the 1960s. CdTe has been used in both the p- and n- layers of this TFPV technology, however CdTe as the p-layer with stable oxides such as ITO, ZnO, $SnO_2$ and CdS as the n-type layer (e.g. CdTe/ZnO) has emerged as most popular. All CdTe cells, CdTe/CdS, which can be manufactured by deposition onto either the glass superstrate or substrate, have similar efficiencies. A brief list of CdTe TFPV manufacturers are: Abound Solar, Calyxo, First Solar, MiaSole, Q-cell and Primestar.

**Efficiency:** Present day small CdTe modules are approximately .5 to 1 $m^2$ in area with efficiency being around 10-15%. CdTe cells by MiaSole were recently confirmed to produce efficiencies of 13.8% in 1 $m^2$ panel, and Solibro achieved an efficiency of 13% (Cheyney 2010). NREL has achieved efficiencies of 19.9% in laboratory testing of small CdTe cells (McMahon 2008). One of the main difficulties that manufacturers face with CdTe PV is similar to other TFPV technologies, namely, maintaining efficiency on module-sized scales.

**Structure and Material Properties:** Flexible CdTe solar cells on polymer substrates have been successfully produced at reasonable efficiencies, indicating that flexibility is possible (Romeo et al. 2005). Several manufacturers' diagrams of their CdTe solar cells are shown in Figure 4.8 and Figure 4.9.

In summary, each of the three aforementioned TFPV technologies used for BIPV applications represents a unique technology discovered and developed for the commercial market to convert photons of light from the sun into useable power. In order for these modules to be available in Europe each module must pass a set of standard tests, include one for wind loading (IEC 61646 - Thin-film terrestrial photovoltaic (PV) modules – Design qualification and type approval), however in the U.S. solar PV panels, modules, and components are not currently required to undergo third-party testing to back up manufacturer claims of durability, quality, or reliability. ASTM, however, is working towards a similar standard to that of IEC 61646 in Europe. As a part of the qualifications of IEC 61646, TFPV panels must pass a mechanical load test requiring the panels to withstand 50.2 psf (2400 Pa) of uniform pressure applied on the front and back for 1 hour duration each (IEC 2008). However, even with these qualification standards, there are very few published studies on the behavior and properties of TFPV panels under uniform loading conditions. Instead in several cases the strength and behavior of the glass used on the front and back parts of the panels as a way to characterize the TFPV panel strength (Webb 2010). Thus in an effort to characterize the behavior of TFPVs, the properties and behavior of glass lites of similar structure and dimensions are reviewed and used in this study.

## 4.5 MATERIAL LAYERS WITHIN PV PANELS:

Each of the TFPVs has a similar construction of layers, primarily comprising of two glass lites, adhesive (e.g. PVB, EVA), front and back contacts (TCO or metal), and the PV layer(s) (see Figure 4.3, Figure 4.6, Figure 4.8). In modeling the behavior of TFPV panels under wind loading it is important to review the behavior of these, most importantly the glass superstrate and substrate since these are subject to the most compressive and tensile forces under flexural loading due to their location on the exterior surfaces of the PV panels. Below is a discussion on the types and properties of glass used in TFPV panels, as well as a review of the most common types of glass used in PV panels based on data collected from leading BIPV manufacturers' published data sheets or product specification.

### 4.5.1 Glass

The role of glass in a TFPV panel is primarily to protect the TFPVs from the elements while still allowing light to pass through to allow the TFPV to function properly and efficiently. Thin lites of glass can act as both the substrate and superstrate (front and back) of a PV module. According to the National Institute of Standards and Technology (NIST) glass has a high theoretical strength (approximately 17 GPa), however, the theoretical strength of glass is a property that has yet to be taken advantage of due to its highly brittle nature and its susceptibility to tiny surface flaws known as Griffith Flaws, that act as stress concentrators in the glass under loading conditions (Griffith 1921). Glass cannot deform plastically and thus it can break without early warning due to high surface tension. This also makes glass highly susceptible to localized over-

stressing. There are a number approaches to strengthen glass to increase its load capacity which are discussed in the next section. These methods help avoid its failure due to surface flaws.

Glass used in TFPV panels is typically soda lime glass formed mainly from three raw materials: soda, lime and silica (AMMA 1984). Heat strengthened (HS) and fully tempered (FT) glass are both made from soda lime glass, but have undergone treatment to increase their load capacity. The general properties of glass are commonly agreed upon within the building industry, however due to its brittle nature and susceptibility to fracture due to surface flaws, the coefficient of variation (as high as 25%) of these values is quite high compared to that of other common engineering materials (Beason et al. 1998; Pilkington 2010).

#### 4.5.1.1 Annealed/Float Glass

Float glass is the most basic form of flat glass used in TFPV panels. Its name originates from the manufacturing process developed by Pilkington Brothers Ltd. in 1959. In this process the ingredients are heated in a 1500°C furnace to form molten glass, which is then poured across a surface of molten tin. The liquid glass spreads out and flattens as it cools. The glass is then transported horizontally on rollers in one continuous sheet into a long oven to form a uniform thickness sheet. A slow and controlled cooling process is necessary to prevent any residual stresses in the glass that result from more rapid cooling. Once completed the final glass product is typically termed “annealed” glass, distinguishing it from float glass that has received further treatment such as heat strengthening or tempering after the float process. This glass can be cut, machined, drilled, edged and polished after manufacturing.

Of all flat glass products, annealed glass is typically the most inexpensive to manufacture, but is also the weakest. Because no further heat treatment is applied to the glass, it is highly

susceptible to failure in tension. When annealed glass fails it breaks into large pieces that can be a safety hazard if it falls from a building façade. Table 4.2 shows some of the typical values assumed for its behavior.

#### 4.5.1.2 Heat Strengthened (HS) Glass

Heat strengthened (HS) glass is formed by applying further heat treatment to float glass. During this process, the glass sheet is heated to its softening point then rapidly cooled with air jets, causing the surface and edges of the glass to cool rapidly and contract, while the center is still hot and fluid. As the glass sheet cools, to counteract the state of compression of the surface and edges between 3500 and 7500 psi (per ASTM C1048), the center is in a state of tension to maintain equilibrium within the material. This is advantageous to the strength of the glass sheet because the failure of glass almost always occurs at flaws on the tension surface of the glass. HS glass is generally twice as strong as annealed glass of the same thickness and configuration, but it has the disadvantage that is cannot be cut or machined in anyway once the heat strengthening process has been completed. All drilling of holes, cutting or grinding must take place before the HS process is completed. When HS glass breaks, it breaks into large pieces in a similar fashion to annealed glass, however it is preferred due to its strength coupled with good post-breakage behavior. Table 4.2 shows some of the typical values assumed for its behavior.

#### 4.5.1.3 Fully Tempered/Toughened (FT) Glass

Fully tempered (FT) glass, also known as safety glass, is similar to that of HS glass except that the cooling process is faster, creating higher residual compressive stresses on the surface and edges of the glass. To be officially considered FT, the surface compression must be over 10000 psi (per ASTM C1048). Compared to annealed glass, tempered glass can be up to 5 times

stronger. It has the same disadvantage as HS glass in that it cannot be modified once tempered. When this type of glass breaks it shatters into small pieces. Fully tempered glass also has the disadvantages of some loss of flatness due to the increased compressive stress on the glass surfaces, which can be difficult to use in laminated glass. Additionally FT glass has some possibility of spontaneous breakage, i.e. failure internally generated by inherent impurities such as nickel sulfide within the glass. Table 4.2 shows some of the typical values assumed for its behavior.

**Table 4.2: Properties of Monolithic Annealed, Heat Strengthened and Fully Tempered Glass (Button and Pye 1993; GANA 2008; ASTM 2009)**

| Property | Annealed | HS | FT | Source |
|---|---|---|---|---|
| Modulus of Rupture (50% probability of breakage) | 5.95 ksi (41 MPa) | 12.04 ksi (83 MPa) | 23.93 ksi (165 MPa) | Button and Pye 1993 |
| Design Stress (0.8% probability of breakage) | 2.8 ksi (19.3 MPa) | 5.60 ksi (38.6 MPa) | 11.2 ksi (77.2 MPa) | GANA 2008 |
| Residual surface stress | Nearly 0 (0 MPa) | 3.48 ksi (24 MPa) | 10.00 ksi (69 MPa) | ASTM 2009 |

### 4.5.2 Laminated glass (LG)

Laminated glass typically consists of two glass lites bonded together with an elastomeric interlayer, commonly made of polyvinyl butyral (PVB). Unlike monolithic glass, the behavior of this sandwiched glass-PVB-glass laminates is highly dependent on its temperature (Linden et al. 1984; Reznik and Minor 1986). The behavior of this glass is believed by some to fall between that of a monolithic plate of glass and that of two unbounded plates of glass of equivalent thickness (Hooper 1973; Edel 1997; Norville 1998). Because of uncertainties in the exact shear response of the interlayer and its role at varying rates and temperatures, the strength of laminated glass is usually downgraded as compared to equivalent monolithic glass plates (Foss 1994). However, others have found that at room temperature LG of the same geometry and under the same load conditions is equal or stronger in strength than monolithic glass of equivalent thickness (e.g. Beason et al 1998; Van Duser 1999).

### 4.5.3 Laminated glass model for TFPV panels

The importance of LG in this research is that, in an effort to most accurately represent the behavior of TFPV panel under uniform loading conditions, LG offers the closest glass structure to that of a TFPV panel. Because very little detailed information is available on the behavior of TFPV panels under loading, the use of LG is determined to be an acceptable alternate due to its many similarities in material make-up, size and structure. Similar to LG, TFPV are typically composed of two glass lites with an interlayer of PVB or similar. The difference between the two is that in the TFPV panels the interlayer also contains a very thin layer of photovoltaic materials and TCOs (metal oxides with much higher modulus and strength than the elastomeric layer). Since the photovoltaic material is located near the center of the two glass lites, it experiences

only very little of the bending stress compared to the exterior glass lites. In addition it has a high modulus of elasticity and ability to deform (demonstrated by its used in TFPV flexible laminates available on the market today) as compared to glass.

## 4.6 TFPV PANEL MANUFACTUERS DATA

In choosing to make the assumption that LG can be used to model TFPV panels, this implies that the behavior of the TFPV panels is dependent on the material properties of the glass lites used, thus since there are several different types, dimensions and thicknesses of glass that can be used, a limited review of 36 manufacturer's specifications for their TFPV panels was conducted. A total of 23 a-Si, 9 CI(G)S and 4 CdTe manufacturers' TFPV product specifications were reviewed for type of glass used (annealed, HS, FT), glass lite and PVB thickness, and glass size. A list of these manufacturers is listed below. Inconsistencies in the way data was reported were observed in terms of how thickness was reported, and in some cases, data was not available.

TFPV manufacturers surveyed:

Abound Solar
AGC Solar
Ascent Solar
Astronergy
Targray
Auria
Avancis
Energyglass
Bangkok Solar
Calyxo
Canadian Solar
Unisolar
BP Solar
Canon
Canrom
CNPV
DelSolar
Central Electric
Limited
Ditecar
Ditecar
Bosch Solar
Eopply
E-ton Solar
Evergreen Solar
Dupont
ENN
EPV Solar
Ertex Solar
First Solar
FlexCell
Global Solar
ICP Solar
Inventux
Kaneka
MiaSole
Mistubishi
Nanosolar
Polar PV
PowerFilm Solar
Primstar Solar
Q-Cell
Schott
Signet Solar
Sinonar Solar
Solar Plus
SolarPower
SolarFrontier
Solems
Sunfilm
SunGen
SunStar
TerraSolar
Tianjin Jinneng
Solar
Unisolar
Wurth Solar

### Assumed Glass Thickness in TFPV Panels

Of the TFPV panel manufacturers who reported glass thickness, all but one manufacturer used a 1/8 in (3.0-4.0 mm) front and back glass lites, thus this size is assumed, constituting a total thickness of approximately 1/4 inch for all materials.

### 4.6.1 Assumed Glass Type in TFPV Panels

The type of glass used for TFPV panels varied significantly more, however of the manufacturers who reported glass type, 67% used annealed glass, 13% used HS glass, and 20% used FT glass for the front lite. For the back lite, 50% used annealed glass, 8% used HS, and 42% used FT. From these statistics, it appears that the most common type of glass used in LG is annealed glass. However, FT comes in a close second, particularly for the back lite of glass.

For simplicity, annealed glass is chosen as the most representative type of glass used for TFPV panels based on the percentages determined. The other advantage of modeling TFPV panels using annealed glass is that this is the weakest of the three glass types considered, thus the estimate of glass strength determined from laminated glass data using annealed glass provides a lower bound estimate of the strength of TFPVs under wind loading. This adopted approach should lead to a lower estimate of the strength of the TFPV panels.

### 4.6.2 Assumed Geometric Properties

A wide range of sizes of TFPV panels are available based on the manufacturers data. Many manufacturers had multiple sizes of panels available, and others noted they could custom make PV panels to fit the needs of the architect or engineer. In general, sizes ranged from 11 to 236 inches (270 - 6000 mm) per side with varying aspect ratios. The median dimensions fell

approximately within 39 to 47 inches (1000 - 1200 mm) and the mean were 39 to 59 inches (1000 - 1500 mm) depending on which dimension is considered. The aspect ratios ranged from 1 to 7, however the median and mean aspect ratios were 1.95 and 2.28 respectively. An effort is made to match these property values with those of the laminated glass data used to represent TFPV behavior.

## 4.7 LAMINATED GLASS FAILURE MODEL

Many studies have been conducted in an effort to better understand the behavior of glass under loads. A review of published studies on glass failure was conducted to gather information on the failure strengths of glass experimentally determined by others. Monolithic glass failure data is reported and analyzed in many studies (e.g. Orr 1957; Hershey and Higgins 1973; Kanabolo and Norville 1985; Norville et al 1998). Laminated glass failure data is also reported and analyzed (e.g. Linden et al. 1984; Behr et al 1985; Reznik and Minor 1986; Vallabhan et al 1981; Minor and Rezik 1990; King 1996; Norville 1998).

Analysis of glass failure in the 1960s and early 1970s generated the first design charts used in building codes from empirical models by Orr (1957) and Hershey and Higgins (1973). In the late 1970s a new model was developed by PPG Industries (PPG 1979) based on the finite element analysis conducted by Tsai and Stewart (1976) and Krall et al. (1981). However due to significant controversy over the first glass design charts and the PPG methodology, these design charts were not widely adopted into building codes of the time. The current methodology used in building codes today was first presented by Beason 1980, Beason and Morgan (1984), Norville and Minor (1985), and Beason et al. (1998) in an effort to model the failure probability of glass. Termed the Glass Failure Prediction Model (GFPM), this model became the basis of the modern-

day ASTM standard E1300 (Standard Practice for Determining Load Resistance of Glass in Buildings) – that is in use today for the design of glass used in building glass façade elements. This method was initially developed for monolithic glass, and later extended to cover the design of laminated glass in more recent versions. Due to the complexity and number of factors that can affect the strength of a glass under uniform loading, rather than create a new model, the glass failure prediction model (GFPM) adopted by ASTM E1300 (2009) is used in this study.

### 4.7.1 Glass Failure Prediction Model (GFPM)

The GFPM is based on a statistical theory of failure for brittle materials advanced by Weibull (1939). This method allows the probability of failure of a glass plate to be calculated in terms of:

- glass plate geometry (dimensions and thickness)
- load duration
- elastic properties of glass
- magnitude of the applied load

The GFPM model used in this research was intended designed to predict the failure of monolithic glass, and was later extended to encompass laminated glass (LG) by multiplying its output by a constant to obtain the probability of failure value for LG. The original failure probability function proposed by Beason (1980) and explained fully in Beason and Morgan (1984) is expressed as:

$$P_f = 1 - e^{-B} \tag{4.1a}$$

Where:

$$B = \frac{k}{(ab)^{m-1}}(Eh^2)^m \left(\frac{t_d}{60}\right)^{\frac{m}{16}} R\left(m, \hat{q}\frac{a}{b}\right) \tag{4.2b}$$

$$= \frac{k}{(ab)^{m-1}}(Eh^2)^m \left(\frac{t_d}{60}\right)^{\frac{m}{16}} e^J$$

$$J = \ln\left(R\left(m, \hat{q}\frac{a}{b}\right)\right) \tag{4.3c}$$

$$\hat{q} = \frac{q(ab)^2}{Eh^4} \tag{4.4d}$$

*a*, *b* = dimensions of the glass

*k*, *m* = surface flaw parameters (assumed to be m = 7 and k = 1.365 x $10^{-29}$ $in^2$ $lb^{-7}$ ) (Beason 1998)

*E* = elastic modulus of glass (taken to be 10.4 x $10^6$ psi) (Beason 1998)

*h* = thickness of glass lite (for laminated glass this is the total thickness)

$t_d$= load duration

*q* = uniform load applied on the glass

$\hat{q}$ = dimensionless load

*J* is determined by using a chart that relates the aspect ratio and $\hat{q}$ with J. (see Figure 4.11).

To understand why many of these variables are incorporated into this complex equation, each of the effects of the variables is discussed in the following sections.

### 4.7.2 Effect of Plate Geometry on Glass Strength

The dimensions of a glass sheet have been found to affect the maximum load that glass can withstand. The area is important because the larger the sheet of glass, the higher the potential for surface flaws and thus the more likely the glass may fail. Resistance to stress corresponds to the integrity of the surface, and the presence of microflaws can dramatically lower its strength.

The thickness of the glass can also determine the stresses in the glass, thus a thicker glass equates to a greater load resistance. Because glass typically fails on the tension surface due to its brittle nature, the thicker the glass, the smaller the surface stress for a given load.

The PVB layer thickness has also been shown to affect the total strength of laminated glass (Norville 1998; King 1996). PVB typically is available in approximately 0.38 mm (0.02 in) increments (e.g. .38, .76, 1.14, 1.52 mm), the most commonly used being 0.38 mm (0.02 in). A thicker PVB layer at room temperature was shown in these studies to resist higher loads than thinner PVB layers. In the survey conducted by the writer on the commercial TFPV data, most BIPV manufacturers did not report the thickness of the PVB layer in their TFPV panels. Thus since it has been found that thinner PVB layers are weaker under uniform loading than laminated glass with thicker PVB layers, with an intent to be conservative, the lower bound of 0.38 mm thickness is assumed for this study, which is consistent with the assumptions made used in ASTM E1300 (2009).

In the GFPM model $a$ and $b$ are the variables that represent the dimensions of the glass panel under consideration; these values vary based on the size of the TFPV panel. The thickness $h$ is the total thickness of the glass. In the case of LG this would be the sum of the thickness of the two glass lites and the PVB layer. Since the PVB layer thickness is much less than that thickness

of the glass, it can be neglected, and thus the thickness for the LG is assumed to be 1/4 in. (6 mm), which includes a front and back glass of 1/8 in. thick based on the commercially available TFPV data.

### 4.7.3 Glass Strength Dependence on Load Duration

The behavior of glass under loading is highly time-dependent, thus when specifying a design strength of glass, the duration of the load must be specified. Glass can withstand more load for a shorter period of time than for a longer time and its load capacity at fracture decreases at approximately 1/16$^{th}$ power of load duration under constant load. The current ASTM E1300 standard (2009) uses a 3-second load duration to parallel the 3-second loads used in the wind design charts. Since the downburst wind data is based on 3-second wind gust load data, the GFM model used in this research uses a 3-second load duration for consistency among the two data sets in this research. If a load is used that is not a 3-second load, this load can be converted to an equivalent 3-second load using the following equation from ASTM E1300 (ASTM 2009):

$$q_{eq} = q_{d_i}\left[\frac{d_i}{3}\right]^{1/16} \tag{4.2}$$

$q_{eq}$= equivalent 3-second load

$d_i$= load duration of the load being converted into an equivalent 3-second load

$q_{d_i}$= load with duration $d_i$ being converted to an equivalent 3-second load

### 4.7.4 Strength of Weathered Glass

Over time glass strength degrades due to its exposure to weather, thermal and wind induced stresses, among other factors. Thus the strength of newly formed glass is substantially higher than that of weathered, in-service glass (Abiassi 1980; Norville and Minor 1985). The design parameters *m* and *k* used in the above equation are the two parameters that account for this degradation in the behavior of the in-service glass. It has been found by experiment that for weathered glass these two parameters take the following values: $m = 7$ and $k = 1.365 \times 10^{-29}\ in^{12}\ lb^{-7}$ (Beason and Norville 1989). The use of these surface parameters will result in a lower estimation of the strength of glass under loading, thus taking into account the loss it strength due to weathering.

### 4.7.5 Failure Probability of Annealed Laminated Glass

#### 4.7.5.1 Conversion of monolithic glass to laminated glass strength

In order to use the GFPM for LG to model the BIPVs under wind loading, the values for the monolithic glass must be converted to the equivalent LG (per the procedure adopted by ASTM E1300 (2009)). Several studies consider the behavior of LG as being less than that of its monolithic equivalent of equal thickness and dimensions (Hooper 1973; Edel 1997). These studies have mostly focused on LG beams rather than plates. Other studies have indicated that LG has a strength near to their monolithic equivalent in size and thickness (Minor and Reznik 1990; Norville 1990). Initially manufacturers of LG chose to use a conservative estimate of LG strength by multiplying the monolithic strength by a factor less than one. The more recent version of the ASTM E1300 standard (2009) has been modified to eliminate this strength factor and instead adopt similar, but separate methods for monolithic and laminated glass. Comparing

the charts used to determine the strength of LG and monolithic glass, however, the current ASTM E1300 standard (2009) method is nearly the same (Figure 4.14 and Figure 4.15). This is in agreement with the findings of Minor and Reznik (1990) who compared LG failure loads from studies by Linden et al (1984) and Reznik and Minor (1986) with that of the failure loads of monolithic glass of the same size by Kanabolo and Norville (1985).

#### 4.7.5.2 BIPV Panel Sizes Chosen for use in GFPM

Assuming the use of method of GFPM as used in the ASTM E1300 (2009) for predicting the failure probability of a LG panel, five cases with different dimensions were of glass were considered in this study. An effort was made to represent the range of gathered data on the TFPV solar panels available. The glass sizes in these five cases were chosen with different aspect ratios in an attempt to encompass the majority of the façade-installed TFPV panels in use today in the U.S.

Three of the sizes (38 x 76 inch, 66 x 66 inch and 66 x 96 inch) (965 x 1930 mm, 1676 x 1676 mm, 1676 x 2438 mm respectively) were chosen to parallel the sizing of the laminated glass tested in Linden et al. (1984) and Reznik and Minor (1986) for ease of comparison of the model results to actual LG test data. The average and median values of the TFPV panel dimensions were found to be approximately 40 inches and the aspect ratios are around 2.1; the 38 x 76 inch (965 x 1930 mm) size has similar dimensions and an aspect ratio of 2.11. The two other sizes considered have dimensions 39 x 39 inch and 25 x 40.5 inch (1000 x 1000 mm and 629 x 1029 mm respectively). The 39 x 39 inch panel is the size of the a-Si TFPV panels installed on the National Air and Space Museum at Dulles Center in Washington D.C., and was chosen to represent a small aspect ratio (1). The 25 x 40.5 inch dimensions (aspect ratio is 1.62) are from

the Schott ASI solar panel data sheet (Schott 2010). Schott solar panels are installed in at the New York Stillwell Avenue subway station, and were chosen to represent a mid-range aspect ratio.

#### 4.7.5.3 Probability of Failure Calculations

Using these dimensions, the probability of failure curve for each set of dimensions is computed. Table 4.2 shows the variables used in these calculations. The fragility curves are shown in Figures 4.12 and 4.13.

#### 4.7.5.4 Model Verification

To cross-check that these calculations are consistent with those given by the charts used in the ASTM E1300 (2009), using this model the load is evaluated at a probability of failure of 0.008, following that of the ASTM E1300 standard. These loads are indicated in Table 4.3. Using the ASTM E1300 design chart for 6mm, 4-side simply-supported LG (Figure 4.14) each of these sizes are also evaluated. At a probability of failure of 0.008, all of the values calculated are consistent with the design charts commonly used for glass thickness design (ASTM 2009). Because the 36 x 76 in, 66 x 66 in and 66 x 96 in panels used to calculate the probability of failure in this model are the same sizes as those used in previous studies, by calculating the probability of failure at 50%, these values can be compared to the average failure values of the laminated glass lites tested in Linden et al. (1984) and Reznik and Minor (1986) to obtain some measure of accuracy of the model (Table 4.4). Linden et al. (1984) performed testing on 29 laminated glass specimens (60 x 96 in) and Reznik and Minor (1986) used 25 and 26 specimens (38 x 76 in. and 66 x 66 in. respectively). The reported 60-second loads are converted to

equivalent 3-second loads in Table 4.4 by multiplying by a factor of 1.2 per Equation X7.1 in ASTM E1300 (2009) which converts a load of a given duration to an equivalent 3-second load. In all cases laminated glass, the model provides a higher failure strength. This is to be expected since the glass properties chosen for use in this model represent the properties of weather, rather than new glass (new glass is used in Linden et al (1984) and Reznik and Minor (1986)).

**Table 4.3: Parameter values used in determining probability of failure using GFPM**

| | ***36 x 76 in.*** | ***66 x 66 in.*** | ***66 x 96 in.*** | ***39 x 39 in.*** | ***25 x 40.5 in.*** |
|---|---|---|---|---|---|
| *m* | 7 | 7 | 7 | 7 | 7 |
| *k* | $1.365 \times 10^{-29}$ | $1.365 \times 10^{-29}$ | $1.365 \times 10^{-29}$ | $1.365 \times 10^{-29}$ | $1.365 \times 10^{-29}$ |
| $t_d$ | 3 sec. | 3 sec. | 3 sec. | 3 sec. | 3 sec. |
| *E* | $1.04 \times 10^6$ psi | $1.04 \times 10^6$ psi | $1.04 \times 10^6$ psi | $1.04 \times 10^6$ psi | $1.04 \times 10^6$ psi |
| *h* | 1/4 in. | 1/4 in. | 1/4 in. | 1/4 in. | 1/4 in. |
| *a* | 36 in. | 66 in. | 36 in. | 39 in. | 25 in. |
| *b* | 76 in. | 66 in. | 76 in. | 39 in. | 40.5 in. |
| *Aspect ratio* | 2.11 | 1 | 1.45 | 1 | 1.62 |

**Table 4.4: Maximum loads resisted by laminated glass at probability of failures of 0.008 and 0.5 for each set of dimensions considered using the GFPM**

| $P_f$ | ***36 x 76 in.*** | ***66 x 66 in.*** | ***66 x 96 in.*** | ***39 x 39 in.*** | ***25 x 40.5 in.*** |
|---|---|---|---|---|---|
| *0.0008* | 58 | 40 | 30 | 105 | 153 |
| *0.5* | 145 | 100 | 65 | 290 | 330 |

**Table 4.5: Mean failure strengths predicted by GFPM model compared to the equivalent 3-second load strength from laminated glass test data**

| $P_f$ | ***36 x 76 in.*** | ***66 x 66 in.*** | ***66 x 96 in.*** | ***39 x 39 in.*** | ***25 x 40.5 in.*** |
|---|---|---|---|---|---|
| GFPM (equivalent 3-second load) *(50% failure)* | 145 | 100 | 65 | -- | -- |
| Mean Failure Load *(Reznik and Minor (1986) and Linden et al. (1984))* (equivalent 3-second load) | 160 (134)* | 133 (111)* | 92.4 (77)* | -- | -- |

**Note: The numbers in parenthesis are the 60-second loads before conversion to 3-second equivalent loads*

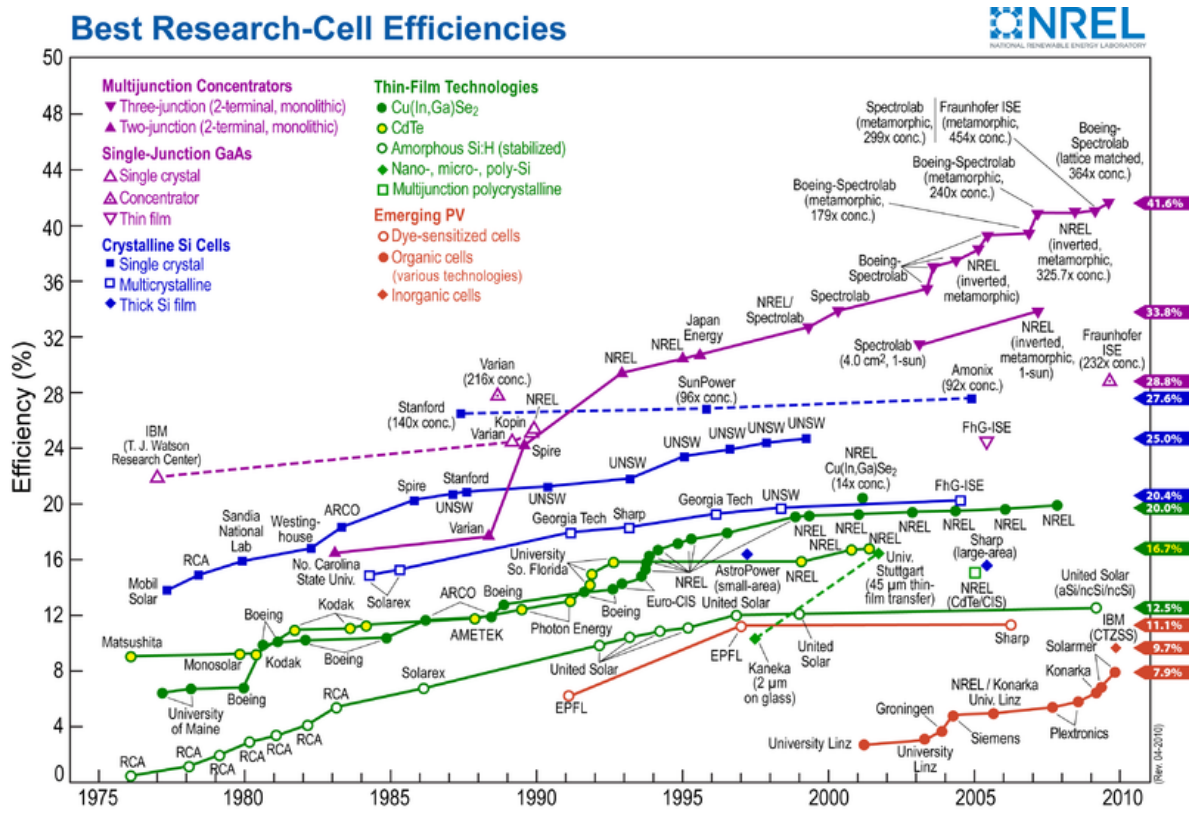


**Figure 4.1: National Renewable Energy Laboratory (NREL) maximum efficiencies of PVs by year**

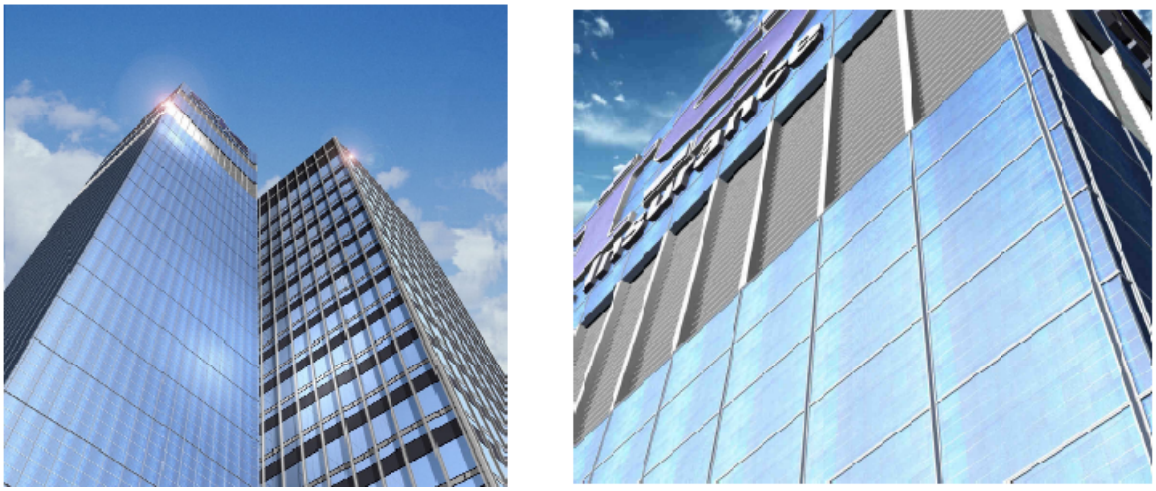

(a) (b)

**Figure 4.2: Examples of façade BIPVs in (a) curtain wall and (b) rain screen applications (Sayigh 2000)**

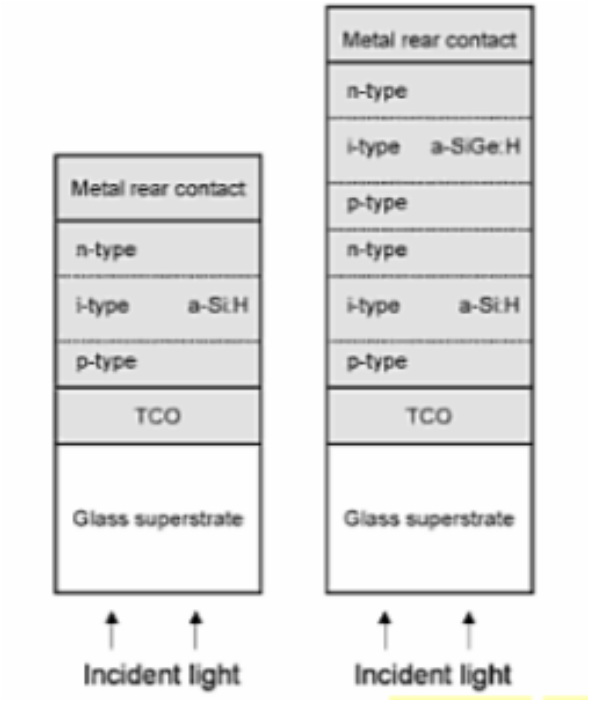


**Figure 4.3: a-Si and micromorphous Si typical layers (Kaltschmitt et al. 2007)**

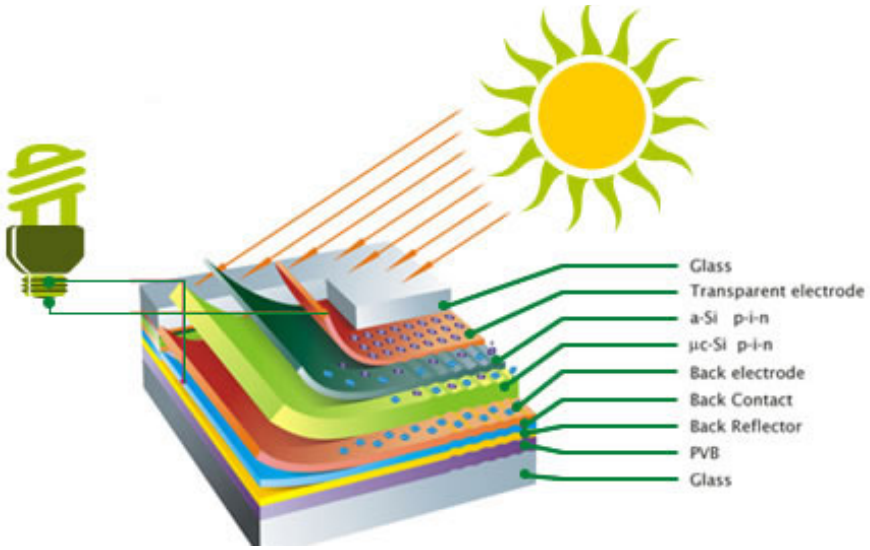


**Figure 4.4: (a) AstroEnergy a-Si/µc-Si micromorphous solar panel construction (AstroEnergy 2010)**

(a) (b)

**Figure 4.5 (a) Schott ASI Thru PV Module, (b) EPV Solar EPV-4X Solar Module (Schott 2010)**

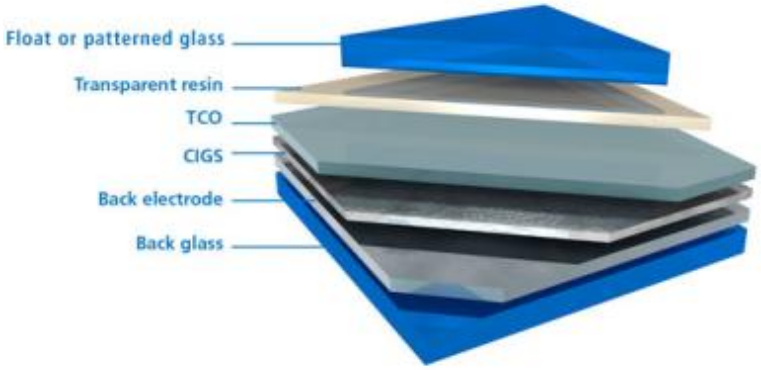


**Figure 4.6: Typical layers of a CI(G)S solar cell (AGC 2010)**

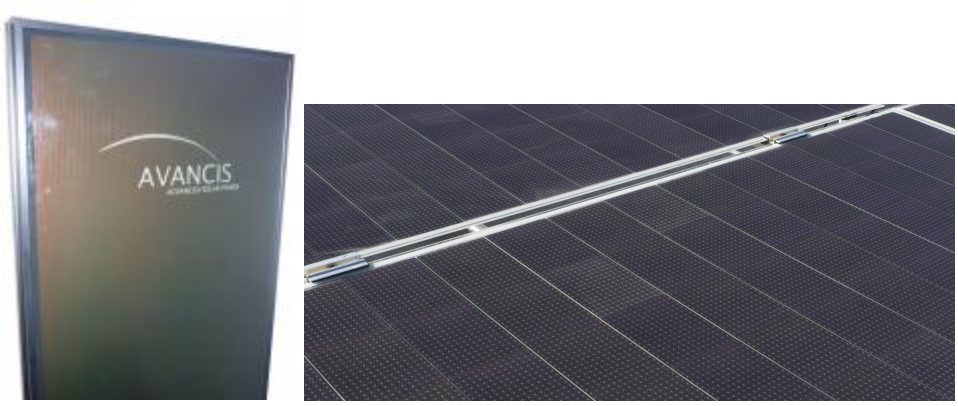


(a) (b)

**Figure 4.7: (a) Avancis Powermax CIS module, (b) Nanosolar Utility CIGS Panels (Avancis 2010; Nanosolar 2010)**

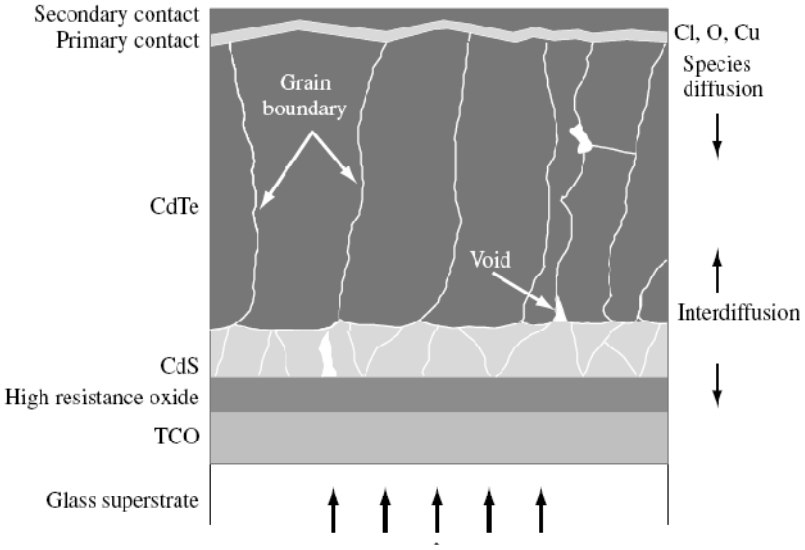


**Figure 4.8: Typical layers of a CdTe solar cell**

(a) (b)

**Figure 4.9: (a) Q-cell CIGS Q.Smart 70-90 PV panel, (b) First Solar CdTe (Q-Cell 2010; First Solar 2010).**

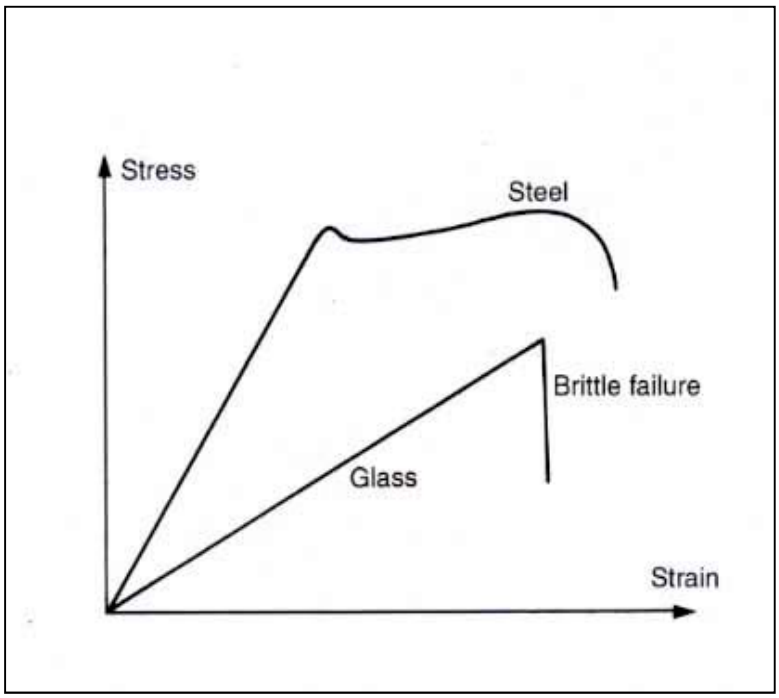


**Figure 4.10: Behavior of glass under loading**

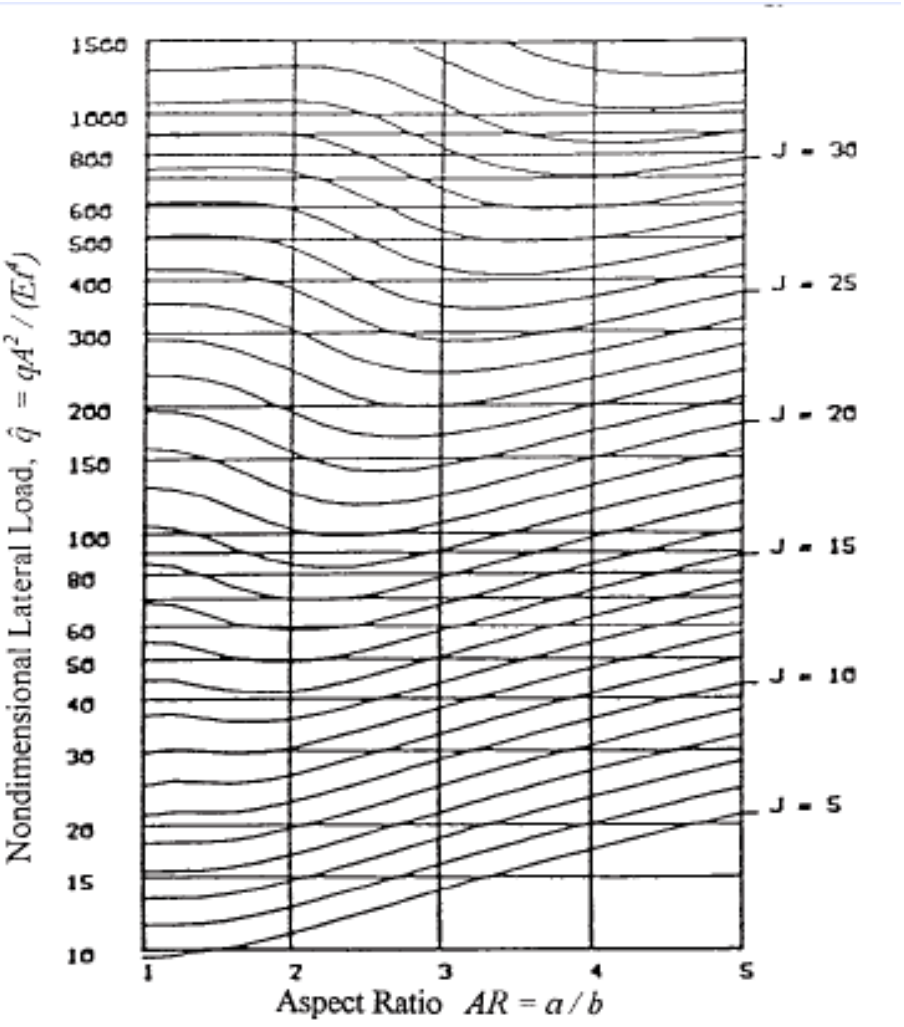


**Figure 4.11: Chart used for determining the stress distribution J from the aspect ratio and non-dimensional lateral load (Beason and Morgan 1984)**

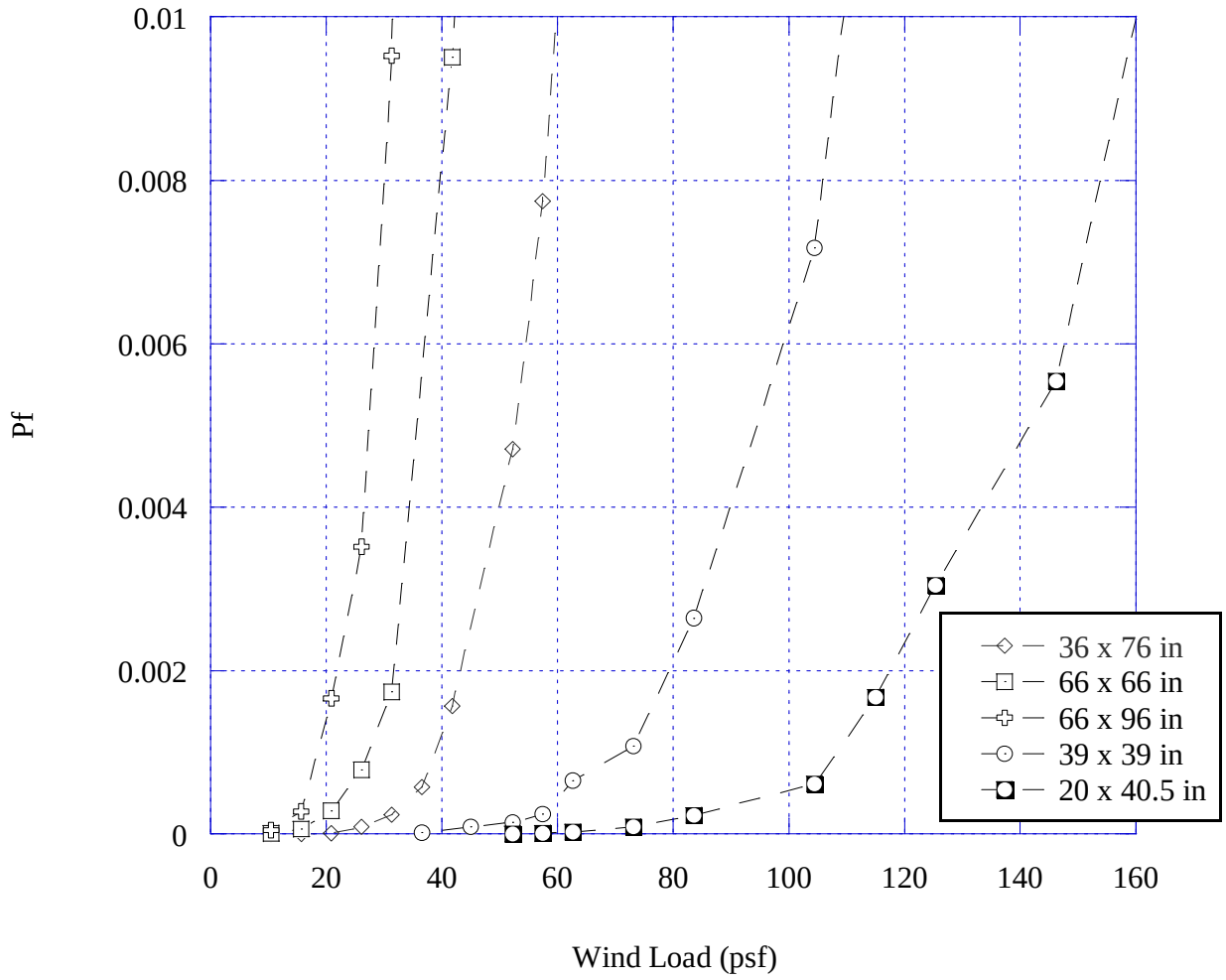


**Figure 4.12: Fragility Curve ($P_f$ = 0.008) of laminated glass using the GFPM**

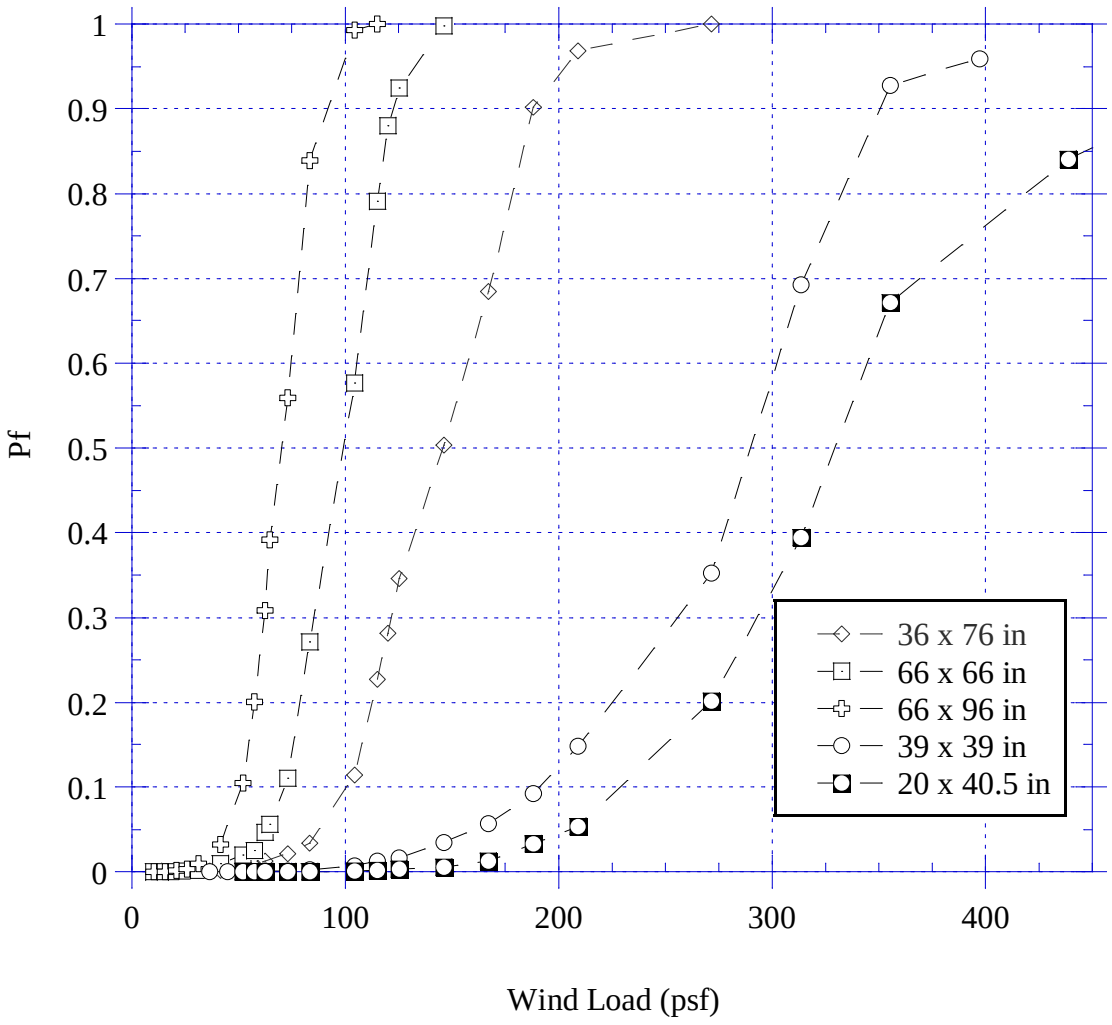


**Figure 4.13: Fragility Curve ($P_f$ = 0.5) of laminated glass using the GFPM**

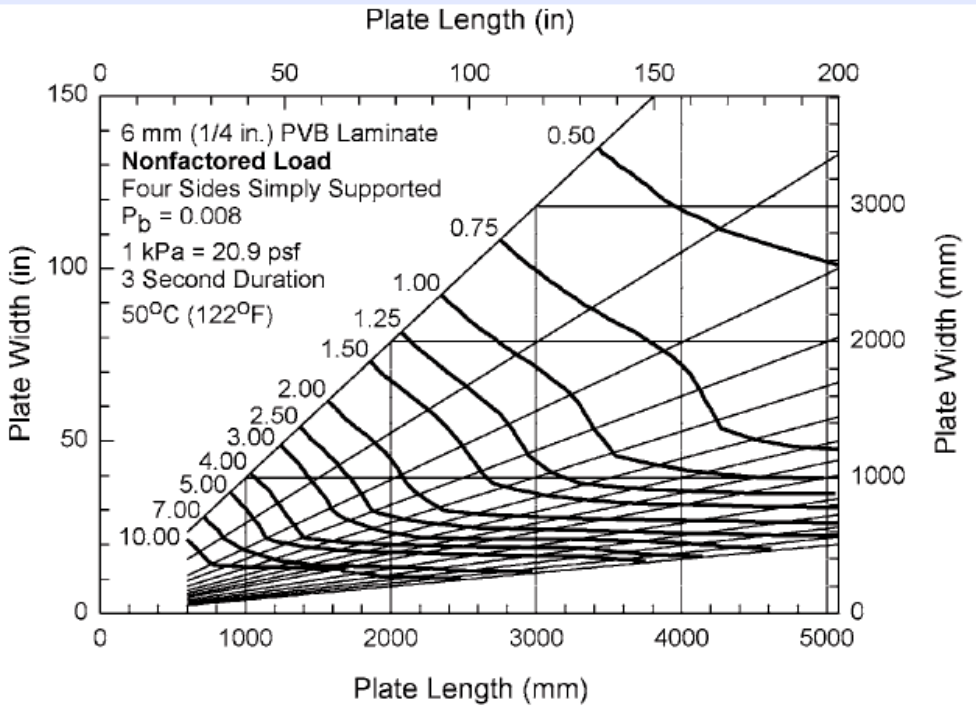


**Figure 4.14: ASTM E1300 design chart for 6 mm laminated glass (ASTM 2009)**

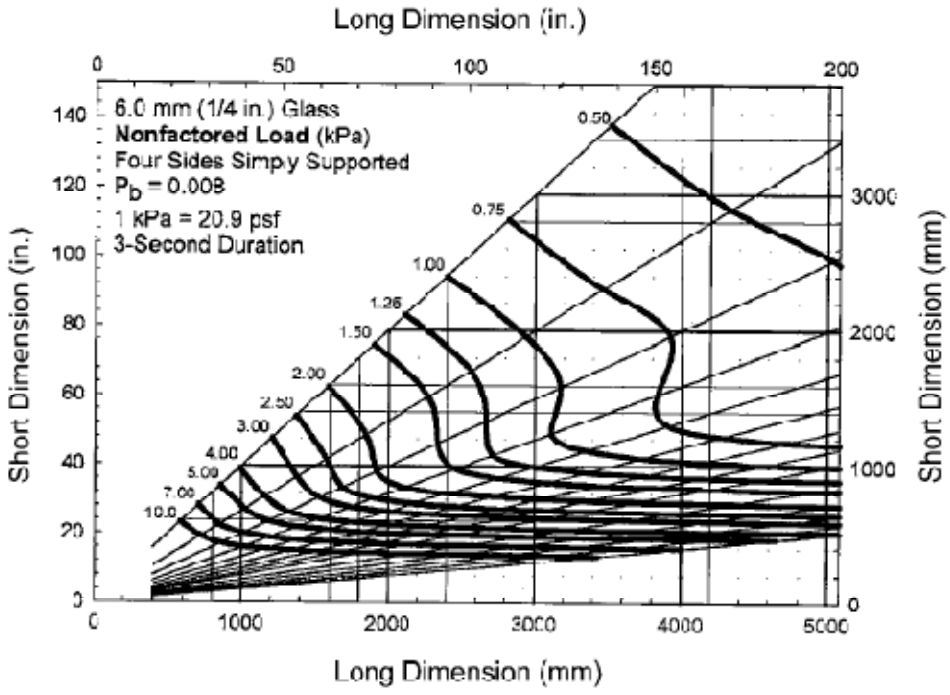


**Figure 4.15: ASTM E1300 design chart for 6 mm annealed glass (ASTM 2009)**

# CHAPTER 5: DOWNBURST DESIGN PRESSURE AND TFPV LOAD RESISTANCE

Thus far in Chapter 3 the design velocity pressures associated with the downbursts in the WBMA were determined for building façade elements located at 33 ft above the ground, and for three different possible strike factors respectively. In Chapter 4 the fragility curves were determined for five cases with different sized TFPV panels using two 3-mm thick annealed glass lites (see Figure 4.12 and 4.13). It is now possible to compare each of these results to their respective existing design standards, as well as compare these two results with each other to create a failure prediction model.

## 5.1 ASCE 7-05 AND DOWNBURST DESIGN WIND LOADS

Before comparing the downburst design wind loads with that of the BIPV panel probability of failure curves, it is relevant to first compare the current design wind speeds in the WBMA and the predicted design wind speeds from downbursts using the model in this research. If the predicted wind speed from the downbursts is lower than that of the current design wind speed, it seems reasonable to believe there is limited concern of needing additional design considerations for downburst winds in the WBMA. However if the design wind speeds predicted by the downburst model are above that of existing design wind speeds, it is reasonable to consider addition recommendations for downburst winds be included in future ASCE 7 standards.

The 50-year design wind speed specified by ASCE 7-05 for the WBMA is 90 mph (40 m/s) (ASCE 2005). Given the three possible methods of calculating the strike factor for downburst occurrences in the WBMA, the 50-year design wind speeds at 33 ft height were calculated to

range from approximately 80-93 mph (35-40 m/s) (Table 3.8). This range of numbers is approximately the same design wind speed specified for this region. Using the ASCE conversion from wind speed to pressure, this translates to an equivalent uniform wind velocity pressure of approximately 14 - 20 psf (689 - 938 Pa). The 100-year design velocity pressure, sometimes used for the design of buildings, is only slightly higher, at up to 21 psf (988 Pa). Based on the comparison of these two values, it is seen that the ASCE 7-05 design wind values may be sufficient for use in the design of buildings for downburst occurrences without modification.

However, an important difference to note when comparing these two design wind speeds is the difference in the vertical profile of a downburst and that of the ASCE 7-05 profile. According to downburst simulation models created by others (e.g. Kim and Hangan 2007; Woods et al. 2001), the vertical wind profile of a downburst peaks at a certain height that varies with the downburst diameter then begins to decrease. According to downburst simulation models created by Kim and Hangan (2007), the maximum velocity of a downburst wind profile occurs at heights of less than 5% of the initial downburst diameter. Similar models of downburst vertical wind profiles have been created by others based on field and experimental data (e.g. Woods et al. 2001; Ozegura and Bowles 1988). Holmes (2002) found that thunderstorm downbursts produce the extreme winds at 10 m (33 ft) height. Following the results of Kim and Hangan (2007), for a downburst of 500 m and 1 km diameter, the maximum wind velocities would occur at less than 25 - 50 m (82 - 164 ft), then would begin to decrease as height increases.

The vertical wind profile used in the design of buildings per ASCE 7-05, unlike that of a downburst, continually increases with height. Using this wind speed, the ASTM 7-05 design

methodology based on factors such as the size of the building, height, etc. can be followed to create a vertical wind profile of the design pressures for the building cladding and components (see ASCE 7-05 (2005) for a more detailed explanation). This wind profile increases significantly in the first 15 ft (5 m) then continues to slowly increase with height at a rate that varies with the specified exposure level of the building in question.

An example of the comparison of these two different profiles is shown in Figure 5.1. In this figure, $V/V_{max}$ is the normalized wind velocity and $Z/Z_{0.5*Vmax}$ is the height divided by the half-velocity height. These scales are used so that multiple datasets can be compared on one graph. The dotted line represents the atmospheric boundary layer (similar to that of ASCE 7-05) and the other data points are results from multiple studies. From this figure, it is clear that the two wind profiles are different. Thus it is possible that above the height of 33 ft, depending on the size of the downburst, that the downburst wind speed is greater than that of the wind speed predicted by ASCE 7-05. Further analysis and research is needed to confirm this issue.

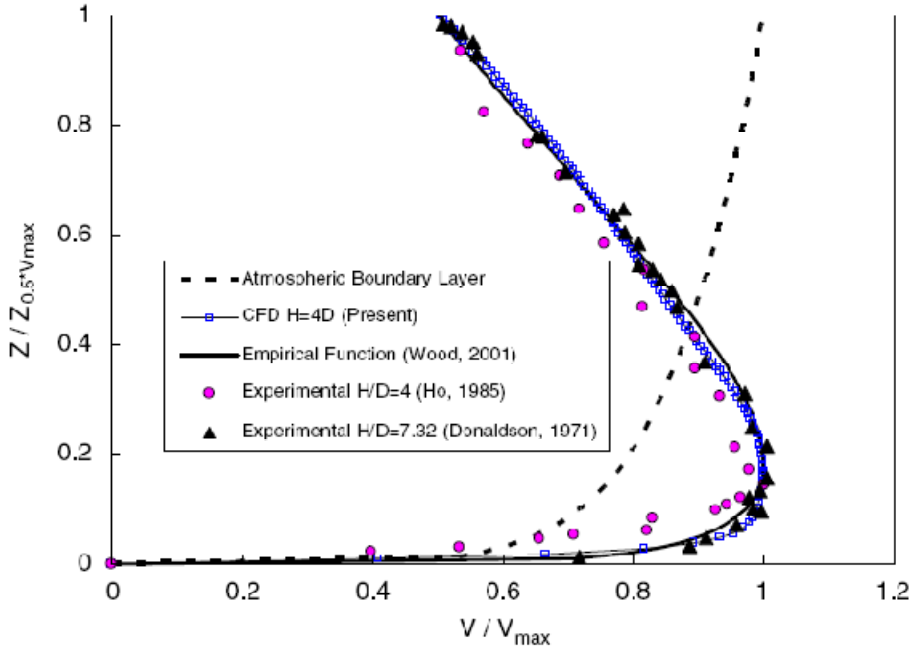


**Figure 5.1: Downburst mean velocity profile: comparison with laboratory experiments, empirical models and with a typical boundary layer profile (Kim and Hangan 2007)**

## 5.2 EUROPEAN IEC 61646 MECHANICAL LOAD REQUIREMENTS AND GFPM PREDICTED LOAD RESISTANCE

It is also relevant to compare the predicted load resistance of the TFPV panels from the model used in this research with that of the loads used to test TFPV panels. Currently one standard test exists that uses standardized test procedures to test and certify TFPV panels. This standard, IEC 61646 – "Thin-film terrestrial photovoltaic (PV) modules – design and qualification and type approval" was developed in 1996 to standardize testing of thin-film PVs such as those used in BIPV applications. A test standard for the United States specifically has not yet been developed. The IEC 61646 standard, recognized throughout much of Europe, tests many different aspects of new TFPVs, including tests such as temperature, performance under different solar conditions,

thermal cycling, damp heat, twisting, and, most important and relevant to this research, mechanical load testing. In comparing the predicted performance of TFPVs with the prescribed load in IEC 61646 a better understanding of the relevance of the standard load can be understood.

Part of the IEC 61646 test requires that both the front and back of the solar panel withstand two cycles of 2400 Pa (50 psf) for 1 hour. As discussed previously, glass behaves differently based on the duration of the load induced on it. The strength of glass predicted in this research is for a 3-second load, thus to translate a 1 hour load (3600 seconds) to a 3-second load, for purposes of comparison, following ASTM E1300, 2400 Pa is divided by a factor of 0.64 (Table X6.1 in ASTM E1300 (2009)), which yields a pressure of 3750 Pa (78.32 psf). For the five sizes used in this research, the probability of failure of the TFPV predicted by the GFPM model used in this research ranges from less than 8:1000, the design value assumed for ASTM E1300 (39 x 39 and 20 x 40.5 inch) to a nearly 70% failure probability (66 x 96 in) (see Figure 4.12). While the 66 x 66 and 66 x 96 inch sizes are significantly larger than most BIPV panels surveyed, it is worth noting their failure probabilities are very large. Table 5.1 lists the failure probabilities for each of the five sizes considered.

The percentages in Table 5.1, particularly those of the 36 x 76 inch, 66 x 66 inch and 66 x 96 inch size BIPVs can be misleading. These sizes are significantly larger than that of the solar panels surveyed. It is likely that if manufacturing solar panels of this size were to be used, that thicker glass would be used for the front and back lites, equating to a greater strength and resistance to the given load.

## 5.3 DOWNBURST DESIGN WIND LOADS AND GFPM PREDICTED LOAD RESISTANCE

Ultimately the design wind loads determined from the probabilistic downbursts wind model are now compared with the probabilistic strength distribution of the BIPVs used in building facades. Based on these, a failure probability model is derived for BIPVs specific to the Washington D.C.-Baltimore metropolitan region.

From Table 5.2 it is shown that only the largest of the five sizes considered had a large enough predicted probability of failure to be recorded. From this it can be concluded that if only the 33 ft design wind pressures are considered, then a building's BIPVs should be able to withstand the downburst occurrences in the WBMA. Further analysis of the vertical profiles of the downburst and ASCE 7-05 specified wind load design curves is needed to compare these two in more detail.

**Table 5.1: Failure Probabilities of Five TFPV BIPV Panels at the Equivalent 3-second Uniform Pressure Specified by IEC61646**

| *36 x 76 in.* | *66 x 66 in.* | *66 x 96 in.* | *39 x 39 in.* | *25 x 40.5 in.* |
|---|---|---|---|---|
| 2.76 % | 19.1 % | 69.9 %* | 0.19 % | 0.02 % |

** This value is very high, however it should be noted that few to none of TFPV are this large in size, regardless if they were they likely would use thicker glass to compensate for the large size*

**Table 5.2: Failure Probabilities of Five TFPV BIPV Panels at the 3-second Uniform Pressure Predicted by the Downburst Wind Pressure in the WBMA**

| *Strike Factor* | *Pressure* | *36 x 76 in.* | *66 x 66 in.* | *66 x 96 in.* | *39 x 39 in.* | *25 x 40.5 in.* |
|---|---|---|---|---|---|---|
| 0.00297 | -- | -- | -- | -- | -- | -- |
| 0.0283 | 14.39 | Negligible | Negligible | 0.028 % | Negligible | Negligible |
| 1 | | Negligible | 0.028 % | 0.17 % | Negligible | Negligible |

*Note: "Negligible" in this chart indicates a failure probability of less than 0.001%*

# CONCLUSIONS AND FUTURE WORK

Thin-film building integrated photovoltaics (BIPVs) are technologies that are being implemented in buildings today, uniquely producing clean energy from the sun's light while simultaneously acting as the building's weather-resistant envelope. Of the many potential causes of failure of these primarily glass solar panels, extreme loading can cause failure of the BIPV panel. Downbursts have the potential to produce extreme winds capable of causing these panels to fail. This research focuses on this issue through a region-specific approach – utilizing the Washington D.C.- Baltimore metropolitan area (WBMA) as the area of analysis.

In this research first a region-specific probabilistic load model of downburst winds has been created for the WBMA. Downburst data was obtained from both the Storm Event Database, available through the National Climactic Data Center and the National Weather Service, and through a search conducted of WBMA news papers, news wires, and other publications. This data was then compiled and modeled using Type I and III extreme value distribution functions. Using a goodness-of-fit test, the Type III distribution is found to fit the dataset best, although it did not provide a satisfactory fit due to lack of sufficient downbursts data in the region. A slightly better fit is found when the dataset is limited only to the downbursts with reported wind speeds, using very similar distribution curve parameters. A stochastic model was adopted to predict the 50-year wind loads that downbursts occurring in the WBMA would subject to the building in this area. Depending on the strike factor assumed in the stochastic model, the 50-year design wind speeds (79 – 93 mph) were both slightly above and below the 50-year design wind speeds specified for the WBMA by ASCE 7-05 standards (90 mph). Using the

methodology of ASCE 7-05, these wind speeds were then converted to velocity pressures for purpose of comparison with the strength of the BIPV panels.

The behavior of BIPVs installed on the facades of buildings subjected to uniform wind loading was next accomplished. Assuming that the thin-film layer (TF) and the transparent conducting oxide (TCO) can be neglected because of their high stiffness and very small thickness, the TFPV panels are modeled with an assumption that their behavior is that of a laminated glass plate. The glass failure prediction model (GFPM) is then used to predict the probability of failure of the BIPV panels under uniform loading, and with simple supports on four sides. In comparing the strength of the BIPV panels to the load effect of the downburst-induced design wind loads in the WBMA, only for large panels (> 66 in) was the probability of failure due to downbursts is measurable, although it was still less than the design 8/1000 probability of failure specified by the current design standards for glass - ASTM E1300. Caution should be exercised in interpreting this since a number of assumptions were made in deriving this. It is also concluded that the downburst loads (14-20 psf) are less than the loads at which they are currently required by IEC 61646 (60 psf equivalent 3-second load), a standard primarily used in Europe for testing of thin-film BIPVs.

In future work it is proposed that the modeling of TF BIPVs as laminated glass be verified through uniform pressure testing. It is also proposed that the probabilistic model created in this research be further expanded to include consideration of the height above the ground on the downburst wind speed as it compares to the TF BIPV panels strength.

# APPENDIX A

## A.1 EXTREME VALUE DISTRIBUTION TYPES

### A.1.1 Type I –Extreme Value Distribution

The Gumbel or Type I extreme value distribution (EVD) has two forms, one based on the smallest extreme and the other based on the large extreme. These are called the minimum and maximum extremes respectively. For this, as for other wind data cases, the maximum form of the Type I EVD is used. The general formula for the probability density function (PDF) of this distribution is:

$$f(x) = \alpha\, e^{-(x-\mu)\alpha} e^{-e^{-(x-\mu)\alpha}}$$

The probability distribution function (i.e. cumulative distribution function (CDF)) is:

$$F(x) = 1 - e^{-e^{(x-\mu)\alpha}}$$

The function is based on two parameters: $\alpha$, the scale parameter, and $\mu$, the location parameter.

### A.1.2 Type III –Extreme Value Distribution

The Weibell or Type III EVD general formula for the PDF of this distribution is:

$$f(x) = \frac{\gamma}{\alpha}\left(\frac{x-\mu}{\alpha}\right)^{(\gamma-1)} e^{-((x-\mu)/\alpha)^{\gamma}}$$

In the case where $\mu = 0$ (location parameter) then the distribution can be reduced to its simpler form called the 2-parameter Type III EVD:

$$f(x) = \frac{\alpha}{\gamma^{\alpha}}\,(\mathrm{x})^{(\alpha-1)} e^{-\left(\frac{x}{\gamma}\right)^{\alpha}}$$

The probability distribution function (i.e. cumulative distribution function, CDF) is:

$$F(x) = 1 - e^{-\left(\frac{x}{\gamma}\right)^{\alpha}}$$

The function is based on two parameters $\alpha$, the scale parameter, and $\gamma$, the shape parameter.

## A.2 DISTRIBUTION PARAMETER ESTIMATION METHODS

### A.2.1 Method of Moments

The method of moments is one of the oldest methods to estimate population parameters. In this method, it is important to examine two moments:

Mean – first moment about the origin

Variance – second moment about the mean

The respective *k*th moment about the origin for a discrete or continuous random variable is:

$$M_k' = \int_{-\infty}^{\infty} x^k f_x(x)dx \quad \text{or} \quad M_k' = \sum x_i^k P_x(x_i)$$

In which *x* is the random variable, $f_x(x)$ is its density function, n is the number of elements in the underlying sample space of *X*, and $P_x(x)$ is the probability density function. The first moment about the origin, where *k=1* in the above equations yields the mean of *X* and is denoted as $\bar{x}$. Because the downburst data is discrete rather than continuous, only the discrete equations will be shown below. The generalized function of this is denoted as:

$$E[g(x)] = \sum_{i=1}^{n} g(x_i)P_x(x_i)$$

To obtain the parameters for the Type I EVD from sample mean $\bar{x}$ and standard deviation $\sigma$ , the following equations are used, as developed from the more generalized equations above $\gamma$ is the Euler-Mascheroni constant $\approx .577$ ) in the method of moments:

$$\sigma = \frac{\pi}{\alpha\sqrt{6}} \quad \text{or} \quad \alpha = \frac{\pi}{\sigma\sqrt{6}}$$

$$\bar{x} = \mu + \frac{\gamma}{\alpha} \quad \text{or} \quad \mu = \bar{x} + \frac{.577}{\alpha}$$

To obtain the parameters of the Type III EVD distribution, the coefficient of variation is first obtained from the equations of the first and second moments and used to calculate $\alpha$:

$$CV = \frac{\sqrt{\Gamma\left[1+\frac{2}{\alpha}\right] - \Gamma^2\left[1+\frac{1}{\alpha}\right]}}{\Gamma^2\left[1+\frac{1}{\alpha}\right]}$$

Then $\sigma$ is calculated:

$$\sigma = \left(\frac{\bar{x}}{\Gamma\left[\frac{1}{\alpha}+1\right]}\right)^{\alpha}$$

### A.2.2 Maximum Likelihood Estimation

Maximum likelihood parameter estimation is based on the principle of calculating values of parameters that maximize the probability of obtaining the particular sample. The likelihood of the sample is the total probability of drawing each item in the sample. The total probability is the product of all the individual item probabilities. This product is then differentiated with respect to the parameters and the resulting derivatives are set to zero to achieve the maximum. Maximum likelihood solutions, however, do not always produce solvable equations.

Given the Type I EVD as an example, the likelihood function, *L*, is defined as:

$$L(\alpha,\beta) = f(y_1,...,y_n \mid \alpha,\sigma) = \prod_{i=1}^{n} f(y_i \mid \alpha,\sigma) = \prod_{i=1}^{n} \sigma \exp\{-\sigma(y_i-\alpha)\}\exp\{-\exp\{-\sigma(y_i-\alpha)\}\} =$$

$$= (\sigma)^n \exp\left\{-\sum_{i=1}^{n}\left[\sigma(y_i-\alpha) + \exp\{-\sigma(y_i-\alpha)\}\right]\right\}$$

Taking the natural log of both sides:

$$l = \ln(L) = -n\ln(\sigma) - \sum_{i=1}^{n}\left[\sigma(y_i-\alpha) + \exp\{-\sigma(y_i-\alpha)\}\right]$$

The partial derivative of the equation must be taken for each variable being estimated, thus:

$$\frac{\partial l}{\partial \alpha} = -\sum_{i=1}^{n}\left[-\sigma + \sigma\exp\{-\sigma(y_i-\alpha)\}\right] = \sigma n - \sigma\sum_{i=1}^{n}\exp\{-\sigma(y_i-\alpha)\}$$

$$\frac{\partial l}{\partial \sigma} = -\frac{n}{\sigma} - \sum_{i=1}^{n}\left[(y_i-\alpha) - (y_i-\alpha)\exp\{-\sigma(y_i-\alpha)\}\right] = -\frac{n}{\sigma} + \sum_{i=1}^{n}(y_i-\alpha) - \sum_{i=1}^{n}(y_i-\alpha)\exp\{-\sigma(y_i-\alpha)\}$$

Setting the two partial differentials to zero for their maxima and solving simultaneously for $\alpha$ and $\sigma$ the MLE can be obtained. The same methodology can be followed for the Type III EVD but is not shown here.

## A.3 GOODNESS-OF-FIT TESTS:

### A.3.1 Anderson-Darling (A-D) Test:

The A-D test is one of several goodness-of-fit techniques, but is only possible to calculate for continuous distribution functions. Its purpose is to decide whether to accept or reject $H_o$, the null hypothesis that states that the sample data follows the given distribution.

It is important to note that the acceptance of $H_o$ for a given level of confidence does not mean that the population in fact is that distribution. It means that $H_o$ cannot be rejected. Thus for a defined confidence level where $H_o$ is accepted, there is not enough evidence to indicate that the data does not follow the given distribution. The A-D distribution is often preferred over the

Komolgorov-Smirnov (K-S) test because it is more sensitive to deviations in the tails of the distribution.

The A-D is defined by:

$H_o$ : The data follow the specified distribution

$H_a$ : The data follow the specified distribution

For Type I and III distributions the following equations are used to determine $A^2$, the test statistic for the A-D test:

$$A^2 = -n - \left(\frac{1}{n}\right)\sum_{i=1}^{n}(2i-1)[\ln(w_i) + \ln(1 - w_{n-i+1})]$$

Where *n* is the sample size and *w* is the cumulative distribution function (CDF) for the distribution under consideration. For small samples $A^2$ is modified using the following equation:

$$A_m^2 = A^2\left(1 + \frac{0.2}{\sqrt{n}}\right)$$

The critical values obtained from the calculation of $A^2$ are the following for different levels of significance ($\alpha$):

**Table A.0.1: Critical Values for Anderson-Darling Test (D'Agostino and Stephens 1986)**

| **Statistic** | **Values** | | | |
|---|---|---|---|---|
| $\alpha$ | 0.1 | 0.05 | 0.025 | 0.01 |
| $\boldsymbol{A^2}$ | 0.637 | 0.757 | 0.877 | 1.038 |

The A-D method is often preferred over the K-S test for the following reasons:

- The K-S test tends to be more sensitive near the center of the distribution than the tails, while A-D gives more weight to the tails.

- The K-S is not valid if the PDF and CDF parameters are estimated from the data, while A-D can be used for this application.
- The A-D is more sensitive to the lack of fit of the Type III EVD than the K-S test (Evans et al. 1989).

### A.3.2 Kolmogorov-Smirnov (K-S) Test

The K-S test (Kolmogovro 1933) is an alternative to the A-D test, but serves the same purpose of determining the acceptance or rejection of $H_o$, the null hypothesis that states that the sample data follows the given distribution.

The K-S is defined by:

$H_o$ : The data follow the specified distribution

$H_a$ : The data does not follow the specified distribution

Given *n* ordered data points (smallest to largest), $Y_1$, $Y_2$… $Y_n$, the empirical distribution function (ECDF) is defined as:

$$E_n = \frac{N(i)}{n}$$

Where N(i) is the number of data points less than $Y_i$.

The test statistic D, the maximum absolute difference between the values of the cumulative probability distribution of the sample size n and the specified cumulative probability distribution function, can be determined by the following equation:

$$D = \max_{1 \le i \le n} \left( F(Y_i) - \frac{i-1}{n}, \frac{i}{n} - F(Y_i) \right)$$

Where F is the CDF being evaluated.

## A.4 POISSON PULSE PROCESS AND UPCROSS RATE:

This process involves the use of three random variables - $\lambda$ - occurrence rate of downbursts (number of downbursts/year), $d_i$ – duration of the "i"th downburst (with a mean values of $\mu_d$), $W_i$ – intensity (mph) of the "i"th downburst with a probability distribution function (a.k.a cumulative probability distribution) of $F_{db}(w)$. A diagram of this process is shown below. Each square wave represents one downburst with a duration d and an intensity w. The subscript "i" represents the "i"th downburst over a given period of time.

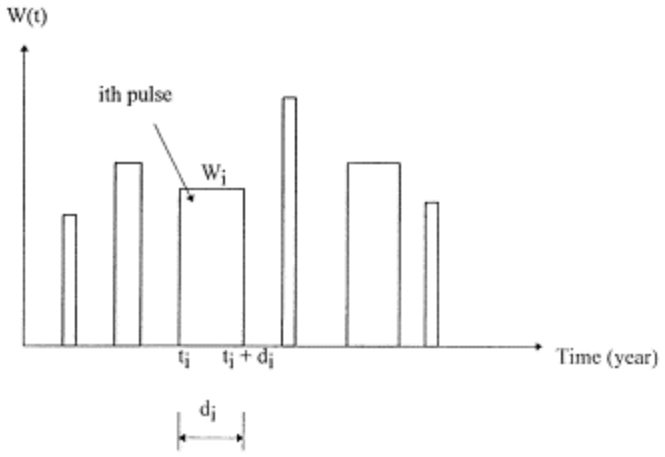


**Figure A.1: Poisson Pulse Process (Li 2000)**

To obtain the probability of exceedence of a given wind speed for a given time period for downbursts, the probability is first defined by an upcross rate – or the rate at which the wind speed measured will exceed a threshold or barrier level value *a(t)* sometime in the structure's design life time from t=0 to T. This is explained using the following equation:

$$p(t) = \int_0^t v(\tau)d\tau$$

In this equation *p(0)* is the probability that wind at a given location exceeds the threshold wind speed at the beginning of the evaluation period *t=0* – this value is considered to be zero. $v(\tau)$ is the upcross rate as described above. The evaluation of this integral is obtained through the following process as outlined in Structural Reliability Analysis and Predictions by Melchers (1987).

A process having rectangular pulses of intensity $W_i$ and length $d_i$ are described as:

$$W(\lambda, d, t, t_i, ) = W_i, \quad \text{when the downburst occurs}$$

$$= 0, \quad \text{at all other times}$$

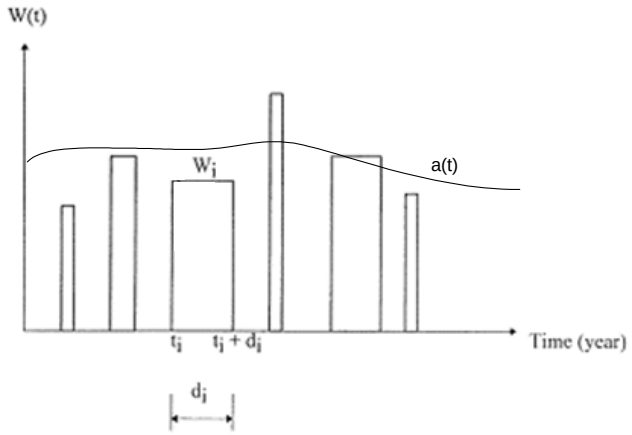


**Figure A.1: Poisson Pulse Process Diagram Modified to Include *a(t)* – Generalized Threshold Value as a Function of Time**

The level of the upcross rate $v_a^+(t)$ of the pulses above the threshold value can be obtained directly from the limit as duration, $d \longrightarrow 0$. The probability that *W(t)* starts out below the threshold value a(t) or $[W(t) \leq a(t)]$ then by the end of the duration, has crossed it so that $W(t + \Delta t)$ is greater than a(t) or $[W(t + \Delta t) > a(t)]$ is equal to:

$$P\{[W(t) \leq a(t)] \cap [W(t+\Delta t) > a(t)]\}$$

Taking the limit of this expression, multiplied by $\lambda$ or the occurrence rate of these downburst wind events, the following expression is created:

$$v_a^+(t) = \lim_{\Delta t \to 0} \left\{ \frac{1}{\Delta t} [P(upcrossing\ in\ \Delta t)] \lambda \right\}$$

$$= \lim_{\Delta t \to 0} \left\{ \frac{1}{\Delta t} [P\{[W(t) \leq a(t)] \cap [W(t+\Delta t) > a(t)]\} \lambda \right\}$$

To simplify the following equation into one that can be more easily evaluated the following things are considered. First in this case, *a(t)* represents the threshold value of the wind speed, or the design wind speed which is constant throughout time t called $V_d$. This is substituted in the equation:

$$v_a^+(t) = \lim_{\Delta t \to 0} \left\{ \frac{1}{\Delta t} [P\{[W(t) \leq V_d] \cap [W(t+\Delta t) > V_d]\} \gamma \right\}$$

Second, the union of two statistically independent events such as those given above is equal to the multiplication of the probabilities of each of the events (i.e. $P(A \cap B) = P(A)P(B)$ where A represents $[W(t) \leq a(t)]$ and B represents $[W(t+\Delta t) > a(t)]$. Additionally, based on the definition of a generalized cumulative distribution function *F(x)* being the probability of a density function $f(s)$ less than a given value *x*:

$$F(x) = P(X \leq x) = \int_{-\infty}^{x} f(s) ds$$

Translated into the terms used in this paper where $V_d$ is the wind speed threshold value:

$$F_{db}(V_d) = P(W_i(t) \leq V_d) = \int_{-\infty}^{V_d} v(\tau) d\tau$$

The probability that *W(t)* will be less than *a(t)* as time approaches zero is equal to the cumulative probability function of that density function $F_{db}(a(t))$. Also based on this same definition, the probability that $W(t + \Delta t)$ will be larger than *a(t)* is equal to one minus that cumulative density function:

$$G(x) = P(X > x) = 1 - \mathrm{F}(x)$$

Translated into the terms used in this paper:

$$G_{db}(V_d) = P(W_i(t + \Delta t) > V_d) = 1 - F_{db}(V_d)$$

Substituting these into the original equation, the final equation obtained is:

$$v(t) = F_{db}(V_d)G_{db}(V_d)\lambda$$

When $V_d$ is large and constant, as is the case in this equation, then $F_{db}(V_d) \approx 1$ because the wind values almost always are below the threshold value except in rare cases, the expression for the upcross rate then becomes a much more usable equation:

$$v(t) = G_{db}(V_d)\lambda$$

The exceedence probability of a given set of wind data due to downbursts over the threshold value $V_d$ is then found by multiplying the upcross rate by time *t* to get the probability over a give time.

$$p(t) = vt = G_{db}(V_d)\lambda t$$

# REFERENCES


Abiassi, J. J. (1981). The strength of weathered window glass using surface characteristics. Institute for Disaster Research, Texas Tech University, Lubbock, Tex.

AGC Solar. (2010). “Thin Film CIGS.” < http://www.agc-solar.com/solar-technologies/solar-photovoltaics/thin-film-cigs.html>. (November 4, 2010).

AIS Glass (AIS). (2010). *PVB Laminated Glass.* <http://www.aisglass.com/pvb_laminated.asp>. (October 29, 2010).

American Architectural Manufacturers Association (AAMA). (1984). *Curtain Wall Manual #12 – Structural Properties of Glass.* Schaumburg, IL.

American Society of Civil Engineers (ASCE). (2005). “Wind Loads.” *Minimum Design Loads for Buildings and Other Structures.* ASCE 7-05.

American Society of Testing and Materials (ASTM). (2004). “Standard specification for heat-treated flat glass.” ASTM C1048.

American Society of Testing and Materials (ASTM). (2009). “Standard practice for determining load resistance of glass in buildings.” ASTM E1300.

Arnold, C. (2009). “Building Envelope Design Guide – Introduction.” Whole Building Design Guide. National Institute of Building Sciences. <http://www.wbdg.org/design/env_introduction.php#evol>. (September 17, 2010).

AstroEnergy. (2010). “Thin-film solar panels”. <http://www.astronergy.com/products.php>. (September 23, 2010).

Atkins, N.T., and Wakimoto, R.M. (1991). “Wet Microburst Activity Over the Southeast United States Implications for Forecasting.” *Weather and Forecasting*, 6 (4), 470-482.

Avancis. (2010). “Avancis Powermax.” <http://www.avancis.de/en/products/powermaxr/>. (September 24, 2010).

B. Sopori, “Thin-film silicon solar cells.” In: *Handbook of Photovoltaic Science and Engineering*, Wiley-VCH, Weinheim. 320.

Beason, W. L. (1980). "A failure prediction model for window glass," PhD dissertation, Texas Tech University, Lubbock, Tex.

Beason, W. L., and Morgan, J. R. (1984). "Glass failure prediction model." *J. Struct. Engrg.*, ASCE, 110(2), 197-212.

Beason, W. L., and Norville, S. H. (1989). "Development of a new glass thickness selection procedure." *Proc., 6th U.S. Nat. Conf. on Wind Engrg.*, Vol. II, University of Houston, Houston, Tex.

Beason, W.L., Kohutek, T.L., and Bracci, J.M. (1998). "Basis for ASTM E1300 Annealed Glass Thickness Selection Charts". *J. Struct. Engrg. 124* (2), 215-221.

Behr, R. A., Minor, J. E., and Linden, M. P. (1986). "Load duration and interlayer thickness effects on laminated glass." *J. Struct. Engrg.*, ASCE, 112(6), 1441-1453.

Behr, R. A., Minor, J. E., Linden, M. P., and Vallabhan, C. V. G. (1985). ''Laminated glass units under uniform lateral pressure.'' *J. Struct. Engrg.*, 111(5), 1037–1050.

Bennisson, S. J., et al. (2005). "Strength and Deformation Behavior of Laminated Glass." *Proc. Glass Proc. Days Conf.*, Tampere, Finland.

Bonnet D, Ed, *Int. J. Solar Energy*, 12, Harwood Academic Publishers, Reading, U.K. (1992).

Brock, F.V., and Govind, P.K. (1977). "Portable Automated Mesonet in Operation" J. Appl. Meteor., 16, 299-310.

Brooks, H., Doswell, C.A. and Kay, M.P. (2003). "Climatological estimates of local daily tornado probability for the United States." *Wea. Forecasting*, 18, 626–640.

Brown, J.M., Knupp, K.R., and Caracena, F. (1982). "Destructive winds from shallow high-based cumulonimbi." *Preprints, Twelfth Conference on Severe Local Storms.* American Meteorological Society, Boston, 272-275.

Button, D., and Pye, B. (1993). *Glass in Buildings.* Butterworth Architecture, Reed International Books, Oxford, U.K.

Caracena, F., and Flueck, J.A. (1988). "Classifying and predicting microburst activity in the Denver, Colorado, Area." *J. of Aircraft*, 25, 525-530.

Caracena, F., McCarthy, J., and Fluck, J. (1983). "Forcasting the Likelihood of microbursts along the front range of Colorado." *Preprints. 13th Conf. on Severe Local Storms*, Tulsa, Amer. Meteor. Soc., 261-264.

Carlson, D. E. (1977). U.S. Patent No. 4,064,521.

Chapin, D., Fuller, C., and Pearson, G. (1954). “A New Silicon p-n Junction Photocell for Converting Solar Radiation Into Electrical Power.” *Journal of Applied Physics*, 25, 676-677.

Chen J *et al*., *Thin Solid Films* 219, 183–192 (1992).

Cheyney, T. (2010). “CIGS PV module conversion efficiency contest heats up, as MiaSole hits 13.8%, Solibro reaches 13%” PV-tech. <http://www.pvtech.org/news/_a/cigs_module_conversion_efficiency_contest_heats_up_as_miasole_hits_13.8_and/>. (September 7, 2010).

Chittick, R. C., Alexander, J. H., and Sterling, H. F. (1969). *J. Electrochem.* Soc. 116, 77

Chuwieduk, D. (2003). “Towards Sustainable-Energy Buildings.” *Applied Energy*, 76 (1-3), 211-217.

Contreras M *et al*. (1999). *Prog. Photovolt.* 7, 311–316.

Cook, N.J. (1982). “Towards Better Estimation of Extreme Winds.” J*ournal of Wind Engr. and Indus. Aerodyn.*, 9(3), 295-323.

D'Agostino, R.B. and Stephens, M.A. (1986). *Goodness-of-Fit Techniques,* Marcel Dekker, Inc., New York, 146.

De Nobel, D. (1959). *Philips Res. Rpts* 14, 361–399 and 430–492.

Doswell, C. A. (1994). “Extreme Convective Windstorms: Current Understanding and Research.” *Proc. U.S.-Spain Workshop on Natr. Haz.*, Barcelona, Spain, 44-55.

Doswell, C.A., Brooks, H.E., and Kay, M.p. (2005). “Climatology Estimates of Daily Local Nontornadic Severe Thunderstorm Probability for the United States.” *Weather and Forecasting*, 20(4), 577-595.

Dougherty, B. P., Fanney, A. H., and Davis, M. W. (2005). “Measured Performance of Building Integrated Photovoltaic Panels. Round 2.” *Journal of Solar Energy Engineering*, 127, 314-323.

Edel, M. T. (1997). ‘‘The effect of temperature on the bending of laminated glass beams,’’ MS thesis, Department of Civil Engineering, Texas A&M University, College Station, Tex.

Ellrod, G. P., Nelson, J. P., Witiw, M. R., Bottos, L., and Roeder, W. P. (2000). “Experimental GOES sounder products for the assessment of downburst potential.” *Wea. Forecasting*, 15, 527–542.

ENF.cn. (2010). *Solar Panel PV Modules Company Directory.* Surrey, U.K. <http://www.enf.cn/database/panels.html>. (September 7, 2010).

Environmental Protection Agency. (2009). "Buildings and Their Impacts on the Environment: A Statistical Summary." <http://www.epa.gov/greenbuilding/pubs/gbstats.pdf>. (September 17, 2010).

EPV Solar. (2010). "EPV Solar EPV-4X, EPV-5X Solar Module Spec Sheet" <http://www.epv.net/productspecs.pdf>. (September 1, 2010).

Evans, J.W., Johnson, R.A., and Green, D.W. (1989) "Two and three parameter weibull goodness-of-fit tests." *Forest Products Laboratory Research Paper FPL-RP-493*. United States Department of Agriculture (USDA).

Evans, J.W., Johnson, R.A., and Green, D.W. (1989)."Two and three parameter Weibull goodness of fit tests." *Research Paper FPL-RP-493,* U.S. Department of Agriculture, Forest Service, Forest Products Laboratory.

Federal Highway Administration (FHA). (2002). "FHWA Route Log and Finder List." <http://www.fhwa.dot.gov/reports/routefinder/table2.cfm>. (October 6, 2010).

First Solar. (2010). "Cadmium Telluride". <http://www.firstsolar.com/en/CdTe.php>. (September 23, 2010).

Flocker, F.W., and Dharani, L.R. (1996). "Stress in laminated glass subject to low velocity impact." *Engineering Structures.* 19(10), 851-856.

Foss, R. V. (1994). ''LAMe hybrid system for glazing design.'' Hybrid neural network and expert systems, L. R. Medsker, ed., Kluwer Academic, Norwell, Mass.

Frerichs, R. (1947) *Phys. Rev.* 72, 594–601.

Freund, L. B., and Suresh, S., (2003). "Thin film materials." Cambridge University Press, 96.

Fritts. C. (1883). "On the Fritts Selenium Cells and Batteries." *Proceedings of the American Association for the Advancement of Science*. 33, 97.

Fujita, T. T. (1976). "Spearhead Echo and Downburst Near the Approach End of a John F. Kermedy Airport Runway." *SMRP Res. Project Research Paper 137*. New York City, Dept. of Geophysical Sciences, Univ. of Chicago.

Fujita, T. T. (1985). "The downburst, microburst, and macroburst." *SMRP Res. Paper No. 210, NTIS No. PB85-148880*, Univ. of Chicago, 122.

Fujita, T. T., and Byers, H. (1977). "Spearhead Echo and Downburst in the Crash of an Airliner." *Monthly Weather Review*, 105, 129-146.

Fujita, T.T. (1978). “Manual of downburst identification for Project Nimrod.” *SMRP Research Paper No. 156*, University of Chicago.

Fujita, T.T. (1983). “Microburst wind shear at New Orleans International Airport, Kenner, Louisiana, on July 9, 1982.” *SMRP Res. Paper No. 199*, Univ. of Chicago, 39.

Fujita, T.T. (1985). “The downburst, microburst, and macroburst.” *SMRP Res. Paper No. 210 [NTIS No. PB85-148880]*, Univ. of Chicago, 122.

Fujita, T.T. (1985). The Downburst. *Report of Projects NIMROD and JAWS*, University of Chicago.

Gast, K. D., and Schroeder J. L. (2003). “Supercell Rear-Flank Downdraft as Sampled in the 2002 Thunderstorm Outflow Experiment,” *Proceedings, Eleventh International Conference on Wind Engineering*, Lubbock, Texas, 2233-2240.

Geerts, B. (2001). “Estimating downburst-related maximum surface wind speeds by means of proximity soundings in New South Wales, Australia.” *Wea. Forecasting,* 16, 261–269.

Gessert, T. A. “Review of Photovoltaic Energy Production Using CdTe Thin-Film Modules” *National Renewable Energy Laboratory, NREL/AB-520-44128.*

Glass Association of North America (GANA). (2008). “GANA Glazing Manual”.

Gleskova, H.; Wagner, S.; Suo, Z. (1999). “Failure Resistance of Amorphous Silicon Transistors Under Extreme in-plan strain.” *Applied Physics Letters.* 75 (19), 3011-3013.

Green, M. A. (1995). *Silicon Solar Cells: Advanced Principles and Practice.* Bridge Printery, Sydney.

Greentech Media Research (GTM). (2010). *Building-Integrated Photovoltaics: An Emerging Market.* <http://www.gtmresearch.com/report/building-integrated-photovoltaics-an-emerging-market>. (October 24, 2010).

Griffith, A.A. (1921). “The Phenomenon and Rupture of Flow in Solids” Philosophical Transactions of the Royal Society of London, 221, 163-198.

Gross, J. L., Main, J. A., Phan, L.T., Sadek, F.H., Cauffman, S.A., and Jorgensen, D.P. (2010). “Final Report on the Collapse of the Dallas Coyboys Indoor Practice Facility, May 2, 2009.” *NISTIR 7661*. National Institute of Standards and Technology (NIST).

Guardian Industries Corp. (2010). “Guardian SunGuard Technical Information.” <http://www.sunguardglass.com/>. (July 1, 2010).

Hahn, H. et al. (1953). *Z. Anorg. Allg. Chem.* 271, 153–170.

Hegedus, S., and Luque, A. (2002). “Status, Trends, Challenges and the Bright Future of Solar Electricity from Photovoltaics.” 11-15.

Hershey, R L., and Higgins, T. H. (1973). "Statistical prediction model for glass breakage from nominal sonic boom loads." Rep. No. FAARD- 73-79, Booz-Allen Applied Research, Inc., Bethesda, MD.

Hess, R. (2004). “Material Glass.” *Structural Engineering International*, 14(2), 76-80.

Hjelmfelt, M.R. (1988). “Structure and life cycle of microburst outflows observed in Colorado.” *J. Appl. Met.* 27, 900–927.

Holmes, J.D. (1999). “Modeling of extreme thunderstorm winds for wind loading of structures and risk assessment.” Wind Engineering into the 21st Century. *Proceedings of Tenth International Conference on Wind Engineering* Larsen, A., Larose, G.L., Livesey, F.M., eds., Denmark.

Holmes, J.D. (2002). “A re-analysis of recorded extreme wind speeds in region A,” *Australian Journal of Structural Engineering, 4,* 29–40.

Holmes, J.D. (2002). “A Re-analysis of record extreme wind speeds in region.” *A. Aust. J. Struct. Eng.* 4(1).

Holmes, J.D., and Moriarty, W.W. (1999). “Application of the generalized Pareto distribution to extreme value analysis in wind engineering,” *J. Wind Eng. Ind. Aerodyn.*, 83, 1–10.

Hooper, J. A. (1973). ‘‘On the bending of architectural laminated glass.’ Int. J. Mech. Sci., 15, 309–323.

Hsu, S. (1987). “Comparison of window glass sample strength estimates: full scale vs concentric ring.” M. Thesis, Texas Tech University. 60.

International Electrotechnical Commission (IEC). (2008). “Thin-film terrestrial photovoltaic (PV) modules – Design qualification and type approval.” IEC 61646.

Jenny, D., and Bube, R. (1954). *Phys. Rev.* 96, 1190–1191.

Kaltschmitt. M., and Streicher, W. (2007). *Renewable Energy: Technology, Economics and Environment*. Springer, New York, 251.

Kanabolo, D. C , and Norville, H. S. (1985). "The strength of new window glass plates using surface characteristics." NTIS Accession No. PB86-140100, Glass Res.and Testing Lab., Texas Tech Univ., Lubbock, Tex., Jul.

Kazmerski, L., White, F., Morgan, G. (1976). *Appl. Phys. Lett.* 29, 268, 269.

Kelly, D.L., Schaefer, J.T., and Doswell, C.A. (1985). "Climatology of Nontornadic Severe Thunderstorm Events in the United States." *Mon. Wea. Rev*, 113, 1997-2014.

Kelly, D.L., Schaefer, J.T., NcNulty, R.P., Doswell, C.A., and Abbey, R.F. (1978). "An Augmented Tornado Climatology." *Mon. Wea. Rev*., 106, 1172-1183.

Kim, J., and Hangan, H. (2007). "Numerical Simulations of Impinging Jets with Applications to Downbursts" *J. of Wind Engr. and Indus. Aerody,* 95 (4), 279-298.

Kim, J.D., and Hangan, H. (2007). "Numerical simulations of impinging jets with application to downbursts," *Journal of Wind Engineering and Industrial Aerodynamics*, 95, 9–298.

King, K.W. (1996). "The Effect of Interlayer Thickness on Laminated Glass Strength." M. Thesis, Texas Tech University, TX.

King, N. J., and King, B. J. (2004) "Creating Incentives for Sustainable Buildings: A Comparative Law Approach Featuring the United States and the European Union." *Va. Envtl. L.J.*, 23, 397-399.

Kolmogorov, A. (1933). "Grundbegriffe der Wahrscheinlichkeitsrechnung. *Ergbnisse der Mathematick un ihrer Grenzgebiete*, 2(3).

Krall, W. R, Siskos, W. R, Stewart, R. A., and Spindler, R. G. (1981). "The behavior of float glass under uniform wind loading." 4th U.S. Nat. Conf. on Wind Engrg. Res., University of Washington, Seattle, Wash.

Kruger, F., de Nobel, D. (1955). *J. Electron.* 1, 190–202.

Li, C.Q. (2000). "A Stochastic Model of Severe Thunderstorms for Transmission Line Design." *Prob. Engineering Mech.,* 15(4), 359-364.

Linden, M. P., Minor, J. E., and Vallabhan, C. V. G. (1984). "Evaluation of laterally loaded laminated glass units by theory and experiment, supplemental report No. 1." NTIS Accession No. PB85-1U532, Glass Res. and Testing Lab., Texas Tech Univ., Lubbock, Tex., Jul.

Lindmayer, J., and Allsion, J. "The violet cell: An improved silicon solar cell." *COMSAT Technical Review*, 3, 1–22.

Loferski, J. “Theoretical considerations governing the choice of the optimum semiconductor for photovoltaic solar energy conversion.” *Journal of Applied Physics*. 27, 777–784.

Madou, M. J. (2002). *Fundamentals of microfabrication: the science of miniaturization.* CRC Press, 298.

McCann, D. W. (1994). “Windex – A new index for forecasting microburst potential.” *Wea. Forecasting,* 9, 532-541.

McCarthy, J., Wilson, J.W., and Fujita, T.T. (1982). “The Joint Airport Weather Studies (JAWS) Project.” *Bull. Amer. Meteor. Soc.,* 63, 15–22.

McDonald, J.R, and Abbey, R.F. (1979). “Comparison of the NSSFC and DAPPLE Tornado Data Tapes.” *Preprints 11th Conf. on Severe Local Storms,* Amer. Meteor. Soc., Boston, MA, 235-240.

McGuire, G. E. (1988). *Semiconductor Materials and Process Technology Handbook.* William Andrew Publishing, Noyes.

McMahon, S. (2008). “NREL boots CIGS thin-film solar cell efficiency to record 19.9%.” PV-Tech. <http://www.pvtech.org/news/_a/nrel_boosts_cigs_thin_film_solar_cell_ efficiency_to_ record_199_percent/>. (September 7, 2010).

Melcheres, R.E. (1999). *Structural Reliability Analysis and Prediction,* 2nd ed. John Wiley & Sons, Chichester (reprinted June 2001).

Michael, H., and Seaman, K. (2009). “The Climate and Weather of Delaware, Maryland and Washington D.C.” *Weatherwise.*

Mimilya-Arroyo, J., Marfaing, Y., Cohen-Solal ,G., and Triboulet, R., (1979). *Sol. EnergyMater.* 1, 171.

Minor, J.E., and Reznik, P.L. (1990). “Failure Strengths of Laminated Glass.” J. Structural Engineering. 116(4), 1030-1039.

Mitchell K, Fahrenbruch A, Bube R, *J. Appl. Phys.* 48, 829–830 (1977).

Morel, D. J., Jhosh, A. K., Feng, F., Stogryn, G. L., Purwin, P. E., Shaw, R. S., and Fishman, C. (1978). *Appl. Phys. Lett.* 32, 495.

Naess, A. (1998). “Estimation of long return period design values for wind speeds.” *Journal of Engineering Mechanics,*124, 252-9.

Nakazawa T, Takamizawa K, Ito K, *Appl. Phys. Lett.* 50, 279–280 (1987).

Nanosolar. (2010). “Nanosolar Utility Panel Data Sheet.” <http://www.nanosolar.com/sites/default/files/Nanosolar_Utility_Panel_Data_Sheet_r2.0.pdf>. (August 1, 2010).

National Climactic Data Center (NCDC). (2010). “Storm Event Database.” National Oceanic and Aviation Administration (NOAA). <http://www4.ncdc.noaa.gov/cgi-win/wwcgi.dll?wwEvent~Storms>. (September 17, 2010).

National Weather Service (NWS). (1995). *NWS Operations Manual, Chapter C-40*, Silver Spring, MD, 61.

National Weather Service (NWS). (2010). “Downburst.” NWS Forecast Office, Columbia, SC. <http://www.erh.noaa.gov/cae/svrwx/downburst.htm>. (September 17, 2010).

National Weather Service (NWS). *Weather Forecasting Office Baltimore/Washington.* < http://www.erh.noaa.gov/er/lwx/>. (September 17, 2010).

National Weather Service. (2010). “NWS CWFA Areal Coverage Sorted by Area.” <http://www.weather.gov/mirs/public/prods/reports/pdf/office_facility/cwfa_sq_mi.pdf>. (September 21, 2010).

Nitkin, K. (2007) “States’ Green Building Laws “Lead By Example.” The Pew, Center on the States. <http://www.stateline.org/live/details/story?contentId=257232>. (September 17, 2010).

Norville, H. S., King, K. W., and Swofford, J. L. (1998). ‘‘Behavior and strength of laminated glass.’’ J. Engrg. Mech., ASCE, 124(1), 46–53.

Norville, S. H., and Minor, J. E. (1985). "Strength of weathered window glass." Am. Ceramics Soc. Bull., 64(11), 1467-1470.

Oliver, S.E, Moriarty, W.W. and Holmes, J.D. (2000). “A Risk Model for Design of Transmission Line Systems Against Thunderstorm Downburst Winds.” *Engineering Structures*, 22, 1173-1179.

Orr, L. (1957). "Engineering properties of glass." Publ. 478, Build. Res. Inst., Nat. Acad. of Sci., National Research Council, Washington, D.C.

Oseguera, R.M., and Bowles, R.L. (1988). “A simple, analytic 3-dimensional downburst model based on boundary layer stagnation flow.” *N.A.S.A. Technical Memorandum 100632*.

Pandey, M.D., Van Gelder, A.J.M., and Vrijling, J.K. (2003). “Bootstrap simulations for evaluating the uncertainty associated with peaks-over-threshold estimates of extreme wind velocity.” *Environmetrics*, 14, 27–43.

Peterka, J.A. and Shahid, S. (1998). “Design Gust Wind Speeds in the United States.” *J. of Struc. Engrg.* , 124(2), 207-214.

Phillips, J., Birkmire, R., and Lasswell, P. (1982). "Stability of Thin-Film $Cu_2S$-Based Solar Cells at $V_{oc}$ Under Continuous Illumination," *Proc. 16th IEEE Photovoltaic Specialist Conf.*, 719–722.

Pilkington. (2010). “Glass Strength” <http://www.pilkington.com/europe/norway/norwegian/building+products/pilkington4architects/about+glass/mechanicalfunctionsofglass/glass+strength.htm>. (October 17, 2010).

Ponpon J, Siffert P, *Rev. Phys. Appl.* 12, 427–431 (1977).

PPG glass thickness recommendations to meet architects' specified 1minute wind load. (1979). Tech. ServicesJFlat Glass Div., PPG Industries, Pittsburgh, PA.

Prince, M. (1955). “Silicon Solar Energy Converters.” *Journal of Applied Physics,* 26, 534–540.

Pryor (2009). – Personal communication on “Downburst Climatology for the Eastern United States 2001-2003.”

Pryor, K. L., Ellrod, G. P., and Bailey, A. A. (2002). “Convective downburst potential using GOES sounder derived products.” N*ational Weather Association Electronic Journal of Operational Meteorology*, EJ1.

Pryor, K. L., Ellrod, G. P., and Bailey, A. A. (2003). “Recent Improvements to the GOES Wind Index.” *National Weather Association Electronic Journal of Operational Meteorology*, EJ1.

Q-cell. (2010). “CIGS Technology: For the best performance and design.” <http://www.q-cells.com/en/solar_modules/module_portfolio/qsmart/ cigs_technology/index.html>. (September 23, 2010).

Rajabi, M.R., and Modarres, R. (2008). “Extreme Value Frequency Analysis of Wind Data from Isfahan, Iran.” *J. Wind Engr. and Indust. Aerodyn.,* 96(1), 78-82.

Reynolds, D., Leies, G., Antes, L., and Marburger. R. (1954). “Photovoltaic effect in cadmium sulfide” *Physics Review*. 96, 533, 534.

Reznik, P. L., and Minor, J. E. (1986). "Failure strengths of laminated glass units." NTIS Accession No. PB87-118873, Glass Res. and Testing Lab., Texas Tech Univ., Lubbock, Tex., Oct.

Rinehart, R.E., DiStefano, J.T., and Wolfson, M.M. (1987). “Preliminary Memphis FAA/Lincoln Laboratory Operational Weather Studies Results.” Project Report ATC-141, Lincoln Laboratory, Massachusetts Institute of Technology.

Roger Edwards. (2006). "The Online Tornado FAQ". National Weather Service. National Oceanic and Atmospheric Administration. <http://www.spc.ncep.noaa.gov/faq/tornado/>. (September 9, 2010).

Romeo, A., Khrypunov, G., Kurdesau, F., Batzner, D.L., Zogg, H., and Tiwari, A.N. (2005). "High-efficiency flexible CdTe solar cells on polymer substrates."*14th Intl. Photovolt. Sci. and Egr. Conf.*, 90(18-19), 304-3415.

Rose, M. (2010). "Downbursts." National Weather Service (NWS). <http://www.srh.noaa.gov/ohx/?n=downbursts>. (September 17, 2010).

Runyon, R. (2010). "BIPV Market Gaining Traction." *Renewable Energy World.* <http://www.renewableenergyworld.com/rea/news/article/2010/08/bipv-market-gaining-traction>. (September 16, 2010).

Savory, E., Park, G.A.R., Zeinoddini, M., Toy, N., and Disney, P. (2001). "Modeling of tornado and microburst-induced wind loading and failure of a lattice transmission tower." *Engineering Structures*, 23, 365–375.

Schaefer, J.T., and Edwards, R. (1999). "The SPC Tornado/Severe Thunderstorm Database." *11th Conf. Applied Climatology*, Dallas, TX.

Schaefer, J.T., Kelly, D.L., and Abbey, R.F. (1986). "A Minimum Assumption Tornado-Hazard Probability Model." *J. Climate Appl. Meteor.*, 25, 1934-1945.

Schott Solar. (2010). "BIPV- Building Integrated Photovoltaics with Schott ASI Solar Modules." <http://www.us.schott.com/2009_architecture/english/products/bipv/asiglass.html>. (September 1, 2010).

Sedlack, R. (1968). "Tensile fatigue strength of brittle materials." Stanford Research Inst.

Shay, J., Wernick, J. (1974). *Ternary Chalcopyrite Semiconductors: Growth, Electronic Properties, and*

Shaybani, Reza. (2010). "Building Integrated Photovoltaics (BIPV)." Scheuten Solar Glass. <http://www.sesam-uae.com/greenbuilding/presantation/SOLARDAYS_PPP.pdf> (September 10, 2010).

Shockley, W., and Queisser, H. (1961). *J. Appl. Phys.* 32, 510–519.

Simiu, E., and Heckert, N.A. (1996). "Extreme Wind Distribution Tails: A Peaks over Threshold Approach." *J. Struct. Engrg.*, 122(5), 539-547.

Simiu, E., Heckert, N.A., and Filliben, J.J. (1999). “Comparisons of wind loading estimates based on extreme speeds and on square of extreme speeds.” *Proceedings, 13th ASCE Eng. Mechs. Div. Conference,* Baltimore, MD.

Simiu, E., Heckert, N.A., Filliben, J.J., and Johnson, S.K. (2001). “Extreme wind load estimates based on the Gumbel distribution of dynamic pressures: an assessment.” *Structural Safety,* 23(3), 221-229.

Stephens, M. A. (1974). “EDF Statistics for Goodness of Fit and Some Comparisons.” *Journal of the American Statistical Association*, 69, 730-737.

Stephens, M.A. (1974). EDF Statistics for Goodness of Fit and Some Comparisons, *Journal of the American Statistical Association,* 69, 730-737.

Strong, S., (1996). “World Overview of Building-Integrated Photovoltaics” *Proceedings of 25th IEEE Photovoltaic Specialist Conference,* 1197–1202.

Stuar, B. “Researchers announce 20.3 percent world record CIGS solar cell efficiency.” PV Magazine. <http://www.pv-magazine.com/news/details/beitrag/researchers-announce-new-203-percent-world-record-cigs-solar-cell-efficiency_100000748/>. (November 4, 2010).

Suri, D., Nagpal K, Chadha G, *J. Appl. Cystallogr.* 22, 578 (1989) (JCPDS 40-1487).

The National Weather Service (NWS). (2006). “NWS CWFA areal coverage sorted by area.” <http://www.weather.gov/mirs/public/prods/reports/pdf/office_facility/cwfa_sq_mi.pdf>. (October 6, 2010).

Thom, H.C.S. (1963). “Tornado Probabilities.” *Mon. Wea. Rev*., 91, 730-736.

Topbas, A. (2008). “An Overview of State-of-the-Art Report for Glass Structures.” *Proc. AEI Bld. Integ. Solns.* Architectural Engineering Institute (AEI), Denver, CO.

Tsai, C. R., and Stewart, R. A. (1976). "Stress analysis of large deflection of glass plates by the finite-element method." J. Am. Ceramic Soc., 59(9-10),445-448.

Turner, C., and Frankel, M. (2008). “Energy Performance of LEED for New Construction Buildings: Final Report.” New Buildings Institute. <http://www.usgbc.org/ ShowFile.aspx?DocumentID=3930>. (September 17, 2010), 2.

Twisdale, L.A., and Dunn, W.L. (1983). “Probabilistic analysis of tornado wind risks.” *J. Struct. Div.,* 109, 468-488.

United States Army Corp of Engineers (USACE). (2010). “Buildings and Structures: Causes and Characteristics of Hurricane Damage.” *USACE National Hurricane Study Program.*

<http://chps.sam.usace.army.mil/ushesdata/Assessments/alicia/buildings_damage.htm>. (September 17, 2010).

Vallabhan, C. V. G., and Wang, B. Y.-T. (1981). "Nonlinear analysis of rectangular glass plates by finite difference method." Inst. for Disaster Res., Texas Tech University, Lubbock, Tex.

Van Duser, A., Jagota, A, and Bennison, S.J. (1999). "Analysis of Glass/Polyvinal Butyral Laminates Subjected to Uniform Pressure." J. Engrg. Mech. 125(4), 435-442.

Vink T, Somers M, Daams J, Dirks A, *J. Appl. Phys.* 70, 4301–4308 (1991).

Wakimoto, R.M. (1985). "Forecasting dry microburst activity over the high plains." *Monthly Weather Rev.,* 113, 1131-1143.

Walter, J.C. (2007). "A new climatology of 25-year, 50-year, and 100-year microburst winds." *22nd Conference on Weather Analysis and Forecasting*, 5a.6.

Webb, J. (2010). "Thin specialty glass for thin-film reliability." European Photovoltaic Solar Energy Conference, Valencia.

Weibull, W. (1939). A statistical theory of the strength of materials. Ingeniorsvetenskapsakademiens, Handlinger, NR 151, Stockholm, Sweden.

Wesoff, E. "CIGS: Will technology be revealed before funding dries up?" Seeking Alpha. <http://seekingalpha.com/article/139444-cigs-will-technology-be-revealed-before-funding-dries-up>. (September 7, 2010).

Wilson, J.W., Moore, J.A., Brant Foote, G., Martner, B., Rodi, A.R., Uttal, T., Wilczak, J.M. "Convective Initiation and Downburst Experiment (CINDE)." Bulletin of the American Meteorologoical Society, 69(11), 1328-1348.

Wilson, J.W., Roberts, R.D., Kessinger, C., and McCarthy, J. (1984). "Microburst wind structure and evaluation of Doppler radar for airport wind shear detection." *J. Climate Appl. Meteor.,* 23, 898-915.

Wolfson, M. (1983). "Doppler Radar Observations of an Oklahoma Downburst." *Preprints, 21 Conf. Radar Meteorology*, Edmonton, Amer. Meteor. Soc., 590-595.

Wood, G.S., Kwok, K.C.S., Motteram, N.A. and Fletcher, D.F. (2001) "Physical and numerical modeling of thunderstorm downbursts." *Journal of Wind Engineering and Industrial Aerodynamics* 89, 535–552.

Wysocki, J., and Rappaport, P. "Effect of temperature on photovoltaic solar energy conversion." *Journal of Applied Physics*, 31, 571–578.

Xie, J., Uchida, S., Rand, B. P., and Forrest, S. R. (2004). “4.2% efficient organic photovoltaic cell with low series resistances” *Appl. Phys. Lett.* 84, 3012.

Yamaguchi K, Matsumoto H, Nakayama N, Ikegami S, *Jpn. J. Appl. Phys.* 16, 1203–1211

Yuh-Lang, L. (2007). *Mesoscale Dynamics.* The Cambridge University Press, Cambridge U.K., 275-276.